Dissecting the role of the major cleft gene, IRF6, in primary palatal epithelia

Monica T Parada Sanchez

A dissertation

submitted in partial fulfillment of the

requirements for the degree of

Doctor of Philosophy in Oral Biology

University of Washington

2012

Reading Committee:

Timothy Cox, Chair
Michael Cunningham
Richard Presland
Sue Herring

Program Authorized to offer Degree:
Oral Health Sciences

University of Washington

Abstract

Dissecting the role of the major cleft gene, IRF6, in primary palatal epithelia

Monica T Parada Sanchez

Chair of the Supervisory Committee:
Associated Professor Timothy Cox
Department of Pediatrics

Mutations and common polymorphisms in Interferon Regulatory Factor 6 (IRF6) are associated with cleft lip/palate (CLP). IRF6 is expressed in the epithelium that mediates the outgrowth and contact of the embryonic tissue masses that fuse to form the upper lip and primary palate as well as in the epithelium that mediates fusion of the palatal shelves to form the secondary palate. Unfortunately, mice deficient in Irf6 display only secondary palatal clefts and abnormal intraoral adhesions but not classic CLP. To provide insights into the role of IRF6 in the pathogenesis of CLP, yeast two hybrid screens were performed to identify IRF6 protein interactors. Using this approach, NME2 was identified and confirmed as a *bona fide* IRF6 partner protein and this interaction is regulated by serine phosphorylation at the C-terminus of IRF6. *In vivo* studies revealed that NME2 co-localizes with IRF6 in the cytoplasm of primary palatal epithelial cells. Furthermore, NME1, the member of the NME family most closely related to NME2, heteromultimerizes with NME2 to form part of the same complex. Notably, NME

proteins are NDP kinases that have been implicated in regulation of epithelial cell adhesion and E-cadherin endocytosis. The lack of a suitable IRF6 CLP model prompted the development of an *in ovo* electroporation protocol to facilitate use of the chick as an alternative model system. The application of a dominant negative form of IRF6 and shRNA constructs using this technique reproduced the phenotype seen in humans, demonstrating that IRF6 is required in epithelial cells to promote outgrowth and fusion of the facial prominences, with secondary effects on the differentiation of the underlying mesenchyme. It is proposed that localization and interactions of NME proteins with other factors may provide clues as to the cellular pathways in which IRF6 is involved, and therefore an explanation of the cellular etiology of the CLP. The data generated during this study have opened new directions not only for future studies on IRF6 itself, but in particular on the possible role of NME proteins in governing the behavior of facial epithelia during fusion of the primary palate and hence susceptibility to CLP.

TABLE OF CONTENTS

LIST OF FIGURES

LIST OF TABLES

ABBREVIATIONS

A_{260}: absorbance at 260nm

A_{600}: absorbance at 600nm

bp: base pairs

BSA: bovine serum albumin

cDNA: complementary DNA

DMEM: Dulbecco's minimal essential medium

DMSO: dimethylsulfoxide

DNA: deoxyribonucleic acid

dNTP: deoxyribonucleoside triphosphate

dsDNA: double-stranded DNA

DTT: dithiothreitol

EDTA: ethylene-diamine-tetra-acetic acid

EMT: Epithelia-to-mesenchyme transition

EST: Expressed Sequence Tag

EtOH: ethanol

FBS: Fetal bovine serum

GFP: green fluorescent protein

HH: Hamburger Hamilton

H&E: Hematoxylin And Eosin

HRP: Horseradish peroxidase

hrs: hours

IHC: Immunohistochemistry

kb: kilobase pairs

kDa: kilo Daltons

LB: Luria Broth

MeOH: methanol

min: minutes

mRNA: messenger RNA

OD: optical density

ORF: open reading frame

PBS: phosphate buffered saline

PCR: polymerase chain reaction

PFA: paraformaldehyde

rpm: revolutions per minute

SDS: sodium dodecyl sulphate

Sec: Seconds

shRNA: Short hairpin RNA

RNAi: RNA interference

TAE: tris-acetate-EDTA buffer

TBS: Tris buffered solution

TE: tris-EDTA buffer

U: units

UV: ultraviolet light

v/v: volume per volume

V: volts

w/v: weight per volume

ACKNOWLEDGMENTS

Foremost, I would like to express my sincere gratitude to my advisor Dr. Timothy Cox, for the opportunity to complete an interesting, challenging and worthwhile project during my time in his laboratory. I also would like to acknowledge his guidance, patience, help, understanding, and endless support over these years.

I would like to thank the other members of my supervisory committee Drs. Richard Presland, Sue Herring, Michael Cunningham and Anne-Marie Bollen for their helpful suggestions.

I also would like to thank all the members of the Cox laboratory. I have special words to Liza Cox for her valuable collaboration, advice, teaching and support throughout my graduate school career, and to Yongzhao Huang for her friendship, for sharing her considerable skills very generously, teaching me many techniques, and troubleshooting with me whenever necessary.

I would like to thank the students and staff of the department of Oral Health Sciences for their friendships and assistance.

Lastly, I would like to acknowledge the love, encouragement and support that parents have always given me. Thank you for being there.

Dedication

I would like to dedicate this achievement to my husband, Juan Carlos, whose love, encouragement and unconditional support allowed me to finish this journey; and to our children for being the force that drives my motivation to continue, never give up and succeed.

CHAPTER I. INTRODUCTION

Collectively, craniofacial malformations are the most common birth defects that occur in humans. Cleft lip with or without cleft palate (CLP), which is the most frequent of the specific craniofacial defects, affects approximately 1 per 700 newborn children worldwide (Nixon et al., 2011). Besides the considerable cost of this anomaly in terms of morbidity and health care (Boulyjenkov et al., 2004), the impact of such a defect on daily life is pronounced, and sadly does not just come from the medical/dental sequelae. Even from the social perspective the impact can be striking when one appreciates how facial appearance can influence the perception and acceptance by others, which in some cultures can often include acceptance by family members.

The following sections present an overview of our current understanding of the cellular and developmental mechanisms responsible for the proper assembly of the primary palate as well as our current understanding of IRF6 function. An introduction to the genetic technologies that underpin this dissertation is also presented to demonstrate the power of these approaches for understanding the role of IRF6 in craniofacial morphogenesis and cleft susceptibility.

Overview of Upper Lip and Primary Palate Morphogenesis

The complex development of the vertebrate face initiates with the proliferation and migration of cranial neural crest cells to form a single, bilateral pair of protrusions known as the first branchial or pharyngeal arches on the ventral surface of the embryo (Cox,

2004; Sperber, 2001). These first outgrowths continue to undergo enlargement and consolidation to give rise to the mandibular processes that gradually join at the midline to form the lower lip and jaw. In addition, a pair of protrusions, known as the maxillary processes arises from a separate condensation and immediately rostral to the mandibular processes. These tissue buds will ultimately generate the lateral aspects of the upper jaw (Sperber, 2001; Cox, 2004; Jiang et al, 2006). Above these structures lies the midline frontonasal prominence. Bilateral invaginations within this central mass generate the medial nasal and lateral nasal processes (Jiang et al. 2006). The frontonasal tissue lateral to each invagination (the lateral nasal processes) merges with the growing maxillary processes. In contrast, the tissue positioned medial to the nasal pits (the medial nasal process) represents freely projecting growth. These medial processes expand ventrally and then finally laterally to make contact with the paired maxillary processes allowing for the creation of the nasal openings and the correct assembly of the primary palate and upper lip (Cox, 2004; Jiang et al, 2006). The primary palate extends just anterior to the incisive foramen (immediately behind the incisor teeth), and corresponds to only a small portion of the adult hard palate. In contrast, the secondary palate, which fuses later in development extends posteriorly from the incisive foramen, and represents the primordia of the hard and soft palates (Jiang et al, 2006).

Active Role of Embryonic Facial Epithelia During Primary Palatal Formation

The process of lip and palate fusion requires the convergence of the three paired tissue protrusions: the lateral and medial nasal processes and the maxillary processes. Each of these structures is populated by mesenchymal cells derived principally from the

neural crest, and is surrounded by an epithelia of ectodermal origin (Cox, 2004; Jiang et al, 2006). The facial epithelia play the principal role in these morphogenetic processes not only coordinating their directed outgrowth but also, critically, the fusion of these freely projecting tissue masses. Experiments involving ectopic transplantation of the frontonasal ectoderm clearly show that it is signals provided by the ectoderm that drive the directional proliferation and differentiation of the underlying neural crest mesenchyme to ultimately sculpt the face (Hu et al, 2003). And then as the facial primordia begin to approximate, it is the facial ectoderm that specifically enables the contact and their dispersion that permits subsequent consolidation of the fusion between the medial nasal and maxillary processes that is required to form the primary palate (Cox, 2004). These ‘pre-fusion contact zone’ epithelia are remarkable in that they not only continue to support proliferation of the underlying mesenchyme that is required for convergent growth of the medial nasal and maxillary processes, but also undergo cellular changes distinct from the rest of the facial epithelia that are believed to facilitate and restrict the adherence to the tips of the converging processes (Cox, 2004). These pre-fusion contact zones are first demarcated by the presence of a significant proportion of epithelial cells that undergo apoptosis, with these dying cells thought to be apically extruded via actin and myosin contractions. The remaining epithelia begin to bulge due to the weakening of cell contacts, reflecting a change in adhesive properties, and send out cellular extensions that probably promote the subsequent formation of the epithelial seam (Cox, 2004). During fusion, tight epithelial junctional complexes are formed to establish the epithelial seam (Gong and Guo, 2003). Finally, primary palatal fusion requires the dispersion and elimination of the seam epithelia that line the opposing

processes. This is believed to occur through a combination of apoptosis, epithelial-to-mesenchymal transition (EMT), and cell migration (Jiang et al. 2006) and allows the formation of a mesenchymal bridge (Sun et al. 2000; Gong and Guo, 2003; Cox, 2004).

Pathogenesis of Cleft Lip And Palate

Failure of appropriate growth, contact, or merging of the nasal and maxillary processes at one or both sides prevents the formation of a whole face with structural integrity and functional unity (Young et al., 2000), and results in a unilateral or bilateral cleft lip / primary palate, respectively. Often this defect is accompanied by clefting of the secondary palate (CLP). In contrast, failure of fusion between the secondary palatal shelves later in embryogenesis generates cleft palate only (CP) (Jiang et al. 2006). While formation of the primary and secondary palates share many similarities, there are also numerous differences, including timing of fusion and the contribution of genetic factors. Furthermore, CP can also occur secondarily to multiple other abnormalities (eg. enlarged or poorly positioned tongue, small lower jaw, a failure to elevate the palatal shelves above the tongue) and therefore from quite distinct developmental processes. Clefting of the lip / primary palate, but not of the secondary palate, is the focus of the body of work presented in this thesis.

CLP is seen as an isolated feature associated with only mild changes in mid-facial shape in 70-90% of all cases (Cox, 2004). However, CLP can also be seen in association with a wider spectrum of anomalies that define various syndromes. Linkage analysis and association studies have been employed to identify candidate genes contributing to the genesis of CLP. Similarly to IRF6, mutations and/or polymorphisms in

other genes, such as p63, MID1 and PVRL1 are also associated with syndromic and non-syndromic forms of orofacial clefting.

The IRF6 Family and Its Function

IRF6 belongs to the Interferon Regulatory Factor (IRF) family that consists of nine transcription factors, well known for their transcriptional roles in many biological processes. Arguably the best characterized of these roles is in innate immunity in which these factors function through toll-like receptor signaling to modulate the activation of type I interferons and to participate in NF-κB activation and signaling in response to pathogenic stimuli (Tsujimura et al., 2004). In addition to this role, IRFs have also been linked to cellular growth regulation and apoptosis, tumor suppression, hematopoietic and embryonic development (Mamane et al., 1999; Ozato et al., 2007, Tamura et al., 2008).

IRF proteins have two conserved functional domains. The amino terminus contains a DNA binding domain (DBD) that is characterized by the presence of five tryptophan residues (Fujii et al., 1999; Tanaka et al., 1993) and consists of a winged-type helix-turn-helix motif that recognizes the consensus DNA sequence, 5' A/GNGAAANNGAAACT-3' known as the IFN-stimulated response element (ISRE) (Darnell et al., 2004). In contrast, the carboxy-terminal region of IRFs, with the exception of IRF1 and IRF2, contains the Interferon Association Domain (IAD) that is responsible for homomeric and heteromeric interactions with other family members or other transcription factors (Mamane et al., 1999, Taniguchi et al., 2001).

Among the members of the IRF family for whom protein-protein interactions involving the IAD have been shown, most of these interactions are regulated through phosphorylation of one or multiple serine residues present within the serine-rich region near the carboxy-terminus (Qin et al., 2003). Moreover, the IAD shows structural similarity to the C-terminal domain found in the SMAD family of transcription factors. In the SMAD family, the equivalent domain similarly mediates protein-protein interactions but in response to cytokines of the Transforming Growth Factor beta family (TGFβ) (Takahasi et al. 2003; Qin et al., 2005).

Of note, the IAD domain in IRF family members, specifically IRF3, IRF4, IRF5 and IRF7 is flanked by two segments that coordinately act in an auto inhibitory manner to block specific regions of the IAD domain required for protein interaction blocking also their transactivation functions (Lin et al, 1999, Eroshkin and Mushegian, 1999; Barnes et al, 2002, Takahasi et al., 2003). However, this autoinhibitory association can be relieved through phosphorylation of multiple serine residues in the serine-rich region. Upon phosphorylation, the IAD mediates protein-protein interactions, including homo- and heterodimerization among the IRF family members, as well as with other transcriptional co-modulators and members of the Stat family, Stat1 and Stat2 (Lau et 14 al., 2000; Meraro et al., 1999; Suhara et al., 2002).

Molecular Biology of Interferon Regulatory Factor 6

IRF6, the least studied member of the IRF family, seems to have completely different functions to the other IRF members in that it does not have a role in innate immunity. Nevertheless, it still possesses the two key IRF functional domains, the DBD, which

binds specifically and with high affinity to the consensus sequence AACCGAAACC/T in vitro (Little et al., 2009), and the IAD (Kondo et al., 2002). The chick IRF6 gene encodes a 460 amino-acid protein that displays 86% identity with murine IRF6 and 85% identity with human IRF6. The sequence conservation is highest in the DBD, where the chick and mammalian sequences exhibit 93% identity. The IAD region is also highly conserved with the chicken and mammalian orthologues displaying 85% identity (Knight et al., 2006).

IRF6 and Cleft Lip And Palate

Recent studies have linked mutations in IRF6 to two distinct genetic disorders: Van der Woude's syndrome (VWS) and popliteal pterygium syndrome (PPS) (Kondo et al., 2002). VWS is the most common form of syndromic clefting, accounting for 2 per cent of all cleft lip/palate (CLP). This syndrome is characterized by cleft lip and/or palate with associated pits of the lower lip mucosa, and occasional hypodontia (Rizos and Spyropoulos, 2004). PPS presents with a similar orofacial phenotype but also includes various genital (hypoplasia of the labia majora or genitals and cryptorchidism) and skin abnormalities, including syndactyly between fingers, and pterygium (webbed skin) of the lower limbs (Froster-Iskenius, 1990).

VWS is caused by missense mutations evenly distributed amongst the DBD and IAD regions, and are thought to result in loss of either DNA binding or protein binding functions. In contrast, most missense mutations that cause PPS are found in the DBD, destroying DNA binding ability while leaving protein-binding activity intact (Kondo et al., 2002). It is still unclear as to what distinguishes the mutations in the DBD that cause

VWS and PPS. In addition to these known mutations, there is strong evidence showing that common single nucleotide polymorphisms (SNPs) in IRF6 contribute to the risk of non-syndromic CL/P in populations with ancestry in Asia, Europe and South America (Zucchero et al., 2004, Scapoli et al., 2005). It has been estimated that these common variants account for ~12% of the genetic contribution to the risk of CLP, thus indicating the significant role of IRF6 in the susceptibility to this birth defect.

Our Current Understanding About IRF6 Function

IRF6 expression has been studied in mouse and chick embryos and reported in epithelial-derived tissues such as keratinocytes (Ingraham et al. 2006), the medial edge epithelium of the fusing secondary palate (Knight at al., 2006), and in the epithelium covering the facial primordia around the time of their fusion to form the primary palate (Washbourne and Cox, 2006). Despite appropriate expression of the time of primary palate development and its major role in CLP, the only information on IRF6 function comes from studies of skin, mammary gland tissue and the secondary palate. IRF6-deficient mice have a hyper-proliferative epidermis that fails to undergo terminal differentiation, resulting in soft tissue fusions that affect development of not only the skin but also limb and craniofacial morphogenesis (Richardson et al, 2006). In the skin, IRF6 appears to act as a key regulator of the switch from keratinocyte proliferation to differentiation (Ingraham et al., 2006). Although these studies provide insights into IRF6 function early in development, its role in primary palatal epithelia has not been investigated.

IRF6 Role During Development of the Secondary Palate

Similar to IRF6, the CLP-associated p63 gene, a member of the p53 family, is expressed in embryonic ectoderm. Indeed, in the developing mouse and chick embryos, p63 is highly expressed in the ectoderm of the limb buds, in the maxillary and branchial arch epithelia and epidermal appendages (Yang et al. 1999; Yasue et al., 2001). Later, in the adult, p63 is expressed in the basal regenerative layer of many epithelial tissues such as skin (Yang et al., 1998), where it is essential for maintaining the proliferative potential of basal keratinocytes. Mutations in the p63 gene are responsible for three cleft lip with or without cleft palate associated syndromes, ectrodactyly-ectodermal dysplasia-clefting syndrome (EEC), (Celli et al. 1999) ankyloblepharon-ectodermal dysplasia-clefting syndrome (AEC) (McGrath et al. 2001) and Rapp-Hodgkin syndrome (RHS) (Rinne et al., 2007). Common variants in p63 have also recently been associated with non-syndromic cleft lip/palate (Leoyklang, 2006). p63 deficient mice exhibit severe limb truncations, craniofacial anomalies and lack all squamous epithelia and their derivatives, indicating a requirement for normal development of all these tissues (Yang et al., 1999; Mills et al., 1999). Interestingly, IRF6 mutant mice show p63 positive cells in the suprabasal layers of the epidermis. Although it is unclear if this is a primary or secondary effect, ectopic or deregulated expression of p63 results in hyper-proliferation and inhibition of terminal differentiation (Richardson et al, 2006). Subsequent research established a relationship between these two transcription factors; IRF6 and p63 function epistatically during the development of the secondary palate (Thomason et al., 2010). In fact, IRF6 is a target of p63 in the midface; p63 binds directly to an upstream enhancer element in the IRF6 locus to activate its transcription. This, in turns, results in

p63 degradation via an unknown mechanism (Moretti et al., 2010; Thomason et al., 2010). Other findings demonstrated that IRF6 is essential for oral epithelial differentiation and plays a role in the formation and maintenance of integrity of the oral periderm, an embryonic layer that is required for proper adhesion of the secondary palate. This function is mediated through the Jagged2-Notch1 pathway (Richardson et al., 2009).

IRF6 and Maspin in Mammary Gland Epithelia

A recent study reported that IRF6 interacts with Maspin (Mammary Serine Protease Inhibitor) through the protein interaction domain. Notably, binding of Maspin was inhibited by prior phosphatase treatment of IRF6, suggesting that the interaction was regulated by IRF6 phosphorylation (Bailey et al., 2005). Maspin is an atypical member of the Serpin protein family and although is widely expressed in almost all epithelia, it has been well studied during breast development (Zang et al., 1999), where its expression profile is similar to that of *IRF6* (Bailey et al., 2005; 2009). Other studies demonstrated that Maspin, recognized as a tumor suppressor in the breast, functions mainly by inhibiting cell invasion and metastasis, but also has been reported as having pro-apoptotic and anti-angiogenic effects (Zou et al., 1994). Similar to Maspin, IRF6 expression is reduced or lost in breast carcinomas linking IRF6 with tumor suppressive properties (Bailey et al., 2005). More importantly, these studies suggest that IRF6 functions in coordination with Maspin to promote differentiation of the mammary epithelial cell by facilitating entry into the G_0 phase of the cell cycle (Bailey et al., 2005, 2008, 2009). These findings have provided some insights into the role of IRF6 in normal

mammary development and breast cancer that could resemble its role during the development of primary palate.

The Chick as an Experimental Model for Studying Embryonic Development

Molecular studies in animal models such as the mouse and chick have significantly contributed to the understanding of normal lip and palate development (Jiang et al., 2006). The chick embryo has been a remarkable experimental animal model in the field of developmental biology because it is easily accessible for manipulation during all stages of craniofacial morphogenesis at a low cost (Young et al., 2000). Chick embryos, unlike rodents, have a relatively flat midface at the time of primary palatal fusion comparable to that seen in developing humans. Indeed, facial morphogenesis is notably similar between the two species. Although the medial nasal process is more square in the embryonic chicken face (Jiang et al., 2006), fusion still occurs with its neighboring maxillary processes to form the lip externally and the primary palate internally (Sun et al., 2000). Chicks are also susceptible to developing facial clefts; in fact, a recessive chicken mutation known as cleft primary palate (cpp) that causes complete truncation of the upper beak with normal development of the lower beak has been employed to study mechanisms of facial outgrowth (MacDonald et al., 2004). Therefore, the chick model is an attractive system for studies of facial development, and may be a better model than rodents for studying primary palatal development, particularly those relating to mechanisms of lip and palate fusion.

Electroporation as a Tool for the Transient Transfection of DNA Into the Chick Embryo

An understanding of the biological role of any gene is gained only after observing the phenotypic consequences of altering the levels and/or the function of that gene in a cell or organism (Paddison et al., 2002). In the last decade, the use of chick embryos as a model system has been made more powerful by the development of *in ovo* electroporation as a gene transfer method. In ovo electroporation has been used successfully to introduce genes not only into the CNS but also somites, limb mesenchyme, lens and surface ectoderm (Itasaki et al., 1999). This method has been the most effective for ectopic or over-expression of gene products in the chick embryo, an approach somewhat similar to the use of a tissue specific promoter to express particular genes in the transgenic mouse (Chen et al., 2004). Recently, *in ovo* electroporation has also been used for loss of function experiments. In these studies, constructs expressing inhibitor RNAs such as small interfering or small hairpin RNAs (siRNAs or shRNAs) (Katahira and Nakamura, 2003), morpholinos (antisense oligos) that block translation or splicing (Kos et al., 2001; Basch et al., 2006), or dominant-negative constructs that act as competitive inhibitors (Renzi et al., 2000; Suzuki-Hirano et al., 2005; Barembaum and Bronner-Fraser, 2007) have been used. These methods allow investigators to disrupt protein signaling or knockdown protein levels in a transient manner thus potentially answering questions within days or weeks, compared with the creation of gene knockouts in mice which can take up to nine months (Dai et al., 2005).

Short Hairpin RNAs (shRNAs)

RNA interference (RNAi) has emerged as a powerful tool to silence gene expression.

This system operates through an evolutionarily conserved pathway in which introduced double-stranded RNA (dsRNA) molecules can trigger the assembly of a nuclease complex that targets homologous RNAs for degradation (Hannon, 2002). Chick cells can be transfected with plasmids encoding short hairpin dsRNA (shRNA), which is subsequently processed via the endogenous chick RNAi machinery to form the active small interfering RNA (siRNA). These siRNAs then bind to and degrade the targeted mRNA (in this case, for IRF6). This method of vector-based RNAi has demonstrated efficacy in the chick model system (Katahira and Nakamura, 2003; Chesnutt and Niswander, 2004). Furthermore it has been demonstrated that both human H1 and U6 Pol III promoters can be used to drive shRNA for silencing chicken target genes (Dai et al., 2005). It has been shown that silencing of the target gene can be detected by 4h after application of synthesized siRNA to cultured cells (Byrom et al., 2002). However, effects of shRNA have been detected after 6h and up until 48h after electroporation of live chick embryos (Katahira and Nakamura, 2003).

Dominant –Negative Constructs

Most dominant-negative constructs express truncated or variant forms of proteins that act as competitive inhibitors of the corresponding wild-type forms, disrupting the function of the endogenous proteins when co-expressed in the same cells. Dominant-negative mutants of transcription factors often have intact DNA binding domains, allowing them to compete with the wild-type forms for the binding site within the chromatin (Sauka-Spengler and Barembaum, 2008). Such an approach has recently been successfully used to begin to address the role of IRF6 in primitive epithelia of early

blastula stage *Danio rerio* (zebrafish) and *Xenopus laevis* (African clawed frog) embryos. Injection of RNA encoding a putative dominant negative IRF6 that encodes only the amino-terminal -115 amino acids, corresponding to the DNA binding domain (IRF6DBD), caused arrest of epiboly, loss of gene expression characteristic of the primitive epithelia, and rupture of the embryo at late gastrula stage. A fraction of embryos injected with a lower dose of IRF6DBD mRNA survived gastrulation and at 3 days post fertilization (dpf) displayed short pectoral fins and blistered skin (Sabel et al., 2009). In these embryos, cartilage elements of the craniofacial skeleton were present but reduced in size and variably disorganized. These phenotypes are reminiscent of the truncated forelimbs, abnormal skin, and shorten craniofacial skeleton of mice deficient for IRF6 (Ingraham et al., 2006; Richardson et al., 2006).

Significance and Specific Aims

The formation of the midface is tightly regulated by a series of evolutionarily conserved mechanisms that are required to facilitate the appropriate outgrowth of the facial primordia and their subsequent fusion. Disruption of any aspect of this controlled morphogenetic process can result in the presentation of a facial cleft. Cleft lip and cleft palate is one of the most common craniofacial birth defects in humans and has caused suffering to many patients due to the associated functional and esthetic problems that typically require multiple cycles of surgery, speech therapy and orthodontics. While both genetic factors and nutritional deficiencies are recognized risk factors in the susceptibility to CLP, there is little known about the molecular mechanisms involved or indeed how these genes and nutritional factors interact. The overarching goal of this

dissertation work was to provide a better understanding of the molecular pathways underlying CLP. With this in mind, the research focused on the IRF6 gene as arguably the most important clefting gene identified to date. Variation in the IRF6 gene has been found to be the major genetic contributor to CLP susceptibility in most populations, yet the failure of IRF6 deficient mouse lines to reproduce the CLP phenotype seen in patients has hampered progress on understanding the molecular mechanisms controlling primary palatal development and the discovery and development of possible new treatments and prevention strategies in humans.

IRF6 expression is restricted to the epithelia of the embryonic tissue masses that fuse to form the upper lip and primary palate as well as the secondary palate later in development (Washbourne and Cox, 2006). Therefore, the objective of this dissertation work was to identify the possible mechanism(s) by which perturbation of IRF6 function modifies primary palatal epithelial morphogenesis and leads to cleft lip and palate. The overarching hypothesis was that IRF6 plays an important role in maintaining the pre-fusion primary epithelial cell phenotype, such that the polarity, adhesion and proliferation of the epithelia are tightly coordinated with the outgrowth of the facial primordia and their ultimate fusion to form the intact lip and primary palate. This hypothesis was addressed with three specific aims:

Specific Aim 1: To Identify developmentally relevant protein interactors of IRF6 that might provide insight into the cellular process and molecular pathways in orofacial epithelia in which IRF6 is involved.

Specific Aim 2: To establish an *in ovo* electroporation system targeting the facial

epithelia to enable investigation of the role of IRF6 during primary palate development.

Specific Aim 3: To determine whether decreased IRF6 activity alters the behavior and/or cellular phenotype of primary palatal epithelia in the chick system.

This dissertation will address the hypothesis and the three specific aims as follows. Aim 1 is presented in Chapter 3 and 4. Aim 2, the facial epithelia *in ovo* electroporation system is presented in Chapter 5. Aim 3 is presented in Chapter 6. Conclusions and implications for all studies are summarized in Chapter 7.

CHAPTER II. MATERIALS AND METHODS

This chapter describes in detail general material and methods that were utilized routinely across this dissertation. Specific material and methods were included accordingly in each following chapter.

Preparation of Frozen Chemically Competent Top 10 E. Coli

4ml of overnight culture was inoculated into 400ml of LB media in a 2 liters flask. Cells were grown at 30°C the first 4hrs, and then were incubated at 37°C until they reached OD_{600} 0.2 (approximately 2 hours later). At which point, cells were transferred into 8 ice cold 50 ml Falcon tubes, and incubated for 10min. The cells were pelleted by centrifugation at 4°C, 3500 rpm for 10min. Media was decanted, and tubes were kept in an inverted position for 1min. Then, pellets were resuspended, by gently vortexing, in 6ml of RF1 cold solution per tube. (RF1 solution contains 100mM KCL, 50mM $MnCl_2$-$4H_20$, 30mM KAcetate, $CaCl_2$-$2H_20$, 15% Glycerol, pH 5.8 with acetic acid, filter steriled and stored at -20°C), incubated on ice for 10min., and pellet by centrifugation at 4°C, 2500rpm for 5min. Media was decanted, tubes were kept inverted for 1min., and pellets were resuspended, by gentle pipetting, in 2ml of RF2 ice cold solution per tube (RF2 solution contains 10mM MOPS, 10mM KCL, 75mM $CaCl_2$,-$2H_20$, 15% Glycerol, pH 7.0 with KOH, filter steriled, and stored at -20°C). Cells were aliquoted in ice cold sterile 1.5ml Eppendorf tube, and stored at -80°C.

Transformation of Chemically Competent *Escherichia Coli* (*E. Coli*) Cells

For heat-shock transformation, 1µl of (10pg to 100ng) plasmid DNA, or 2-3µl from ligation or recombination reaction were added and mixed gently to chemically competent TOP10 E. coli cells (Invitrogen or homemade). Cells were incubated on ice for 15min before being heat-shocked at 42°C for 30sec. Then, the cells were placed back on ice for 2min. 250µl of S.O.C Medium was added to transformed cells, which were then incubated on a horizontal shaker (200rpm) at 37°C for 1hr. Using a sterile glass spreader, transformed cells were plated onto pre-warmed (37°C) LB Agar plates containing either 50µg/ml kanamycin, 100µg/ml ampicillin or 10µg/ml gentamycin. Plates were incubated overnight at 37°C upside down in a sealed plastic bag.

Plasmid DNA Preparation

Small-scale preparations of purified DNA were isolated using the QIAprep Spin Miniprep Kit (Qiagen) or GeneJET Plasmid Miniprep Kit (Fermentas) from 2ml overnight bacterial cultures in LB Broth containing the appropriate selective antibiotic. DNA was eluted using 30µl of Elution Buffer. Large-scale preparations of highly purified DNA were isolated using either the QIAprep Spin Midiprep or Maxiprep Kits (Qiagen) from 50ml or 100ml overnight bacterial cultures respectively. DNA was diluted in 100µl to 200µl TE buffer. In all instances, preparations were performed according to the manufacturers' protocols. Plasmids were analyzed for appropriate size and purity on an agarose gel.

Determination of DNA Concentration

For accurate determination of DNA concentration, UV absorbance at 260nm was measured and quantified with a NanoDrop ND-1000 UV-Vis Spectrophotometer (NanoDrop Technologies), using 2µl of neat or diluted DNA solutions. Alternatively, in situations where precision was not an issue, concentrations of DNA samples were approximated by comparison to bands of known concentration and size on an agarose gel.

Ethanol Precipitation of Nucleic Acids

Samples were adjusted to 0.3MNaAc pH5.2 using a 3M stock solution. 2.5 volumes of 100%(v/v) EtOH was then added, mixed thoroughly and incubated at room temperature for 20min. The precipitated nucleic acid was then pelleted by centrifugation at 13000rpm for 20min. The supernatant was carefully removed and the pellet then washed in 70% (v/v) EtOH by centrifugation at 13000rpm for 10min and the supernatant was again carefully discarded. Samples were dried either at room temperature or in a 37°C heat block. Resuspension of the pellet was performed using 1xTris (Elution Buffer from miniprep kits) or 1xTE as necessary.

Agarose Gel Electrophoresis of DNA

UltraPure Agarose (Invitrogen) was melted in 1XTAE Buffer or Na_2Norate Buffer to final concentrations of 0,7%, 1%, 1.5% or 2% (w/v) to which 0.5µg/ml Ethidium Bromide Solution (Invitrogen) was added. The melted agarose was poured into a gel casting tray with a fine toothed plastic comb inserted to form wells, and upon setting at room

temperature was submerged in an electrophoresis tank containing 1X TAE or NaBorate buffer. Typically, DNA samples were mixed with 6X Loading Buffer, and volumes dependent on the application were pipetted into the wells. The gel was run at a constant voltage of 80-100 until the dye within the loading buffer had migrated the required distance. Following cessation of electrophoresis, DNA was visualized under an ultraviolet transilluminator to determine its fragment size via comparison with a standard ladder. Two types of nucleic acid molecular weight markers were employed in gel analyses: the 1Kb Plus DNA Ladder (Invitrogen), and in some instances, the 100bp DNA Ladder (Invitrogen) were used for comparison of smaller-sized fragments. 300ng of the selected molecular marker was used every time.

Gel Extraction of DNA Fragments

Following agarose gel electrophoresis of DNA fragments on an appropriate percentage agarose gel, bands of interest were directly excised from the agarose gel with a scalpel, under long wavelength UV light to aid DNA visualization. The DNA was extracted and purified from the gel using the QIAquick Gel Extraction Kit (Qiagen) in accordance with the manufacturer's protocol. One tenth of the eluted DNA was typically verified on another agarose gel to ensure purity and to determine concentration.

Automated Sequencing of DNA Plasmids

For automated sequencing analysis at the Biochemistry DNA Sequencing Facility, University of Washington, Seattle, WA; reactions comprised of 2µl BigDye Terminator Premix Version 3.1 (Applied Biosystems), ~500ng template DNA (usually 2µl from a miniprep), 4pmol primer, 5µl 5X Better Buffer (The Gel Company) and dH_2O to a final

volume of 10µl. PCR cycles were completed on a PTC-200 Peltier Thermal Cycler (MJ Research) with the following parameters: initial denaturation 96°C for 1min, and a 25 cycle-repeat of 96°C for 30s, 50°C for 15s, and 60°C for 4min. Samples were cleaned-up using Dye-Ex 2.0 spin kit (Qiagen), and dried using a vacuum. shRNA plasmids were treated differently compared to regular plasmid DNA. Although the same sequencing reaction was performed, more DNA was used (usually 3µl to 4µl from a miniprep). Samples were cleaned up but not dried up. Automated sequencing was performed in the Department of Pediatrics at the University of Washington including an extra heat step of the plate at 95°C for 2 minutes before processing the samples. For sequencing analysis using the SimpleSeq^{TM} DNA sequencing service (Eurofins (mwg|operon; Fisher Scientific), 10µl of DNA samples were submitted at a concentration of 200ng/µl.

Restriction Endonuclease Digestions

Restriction endonuclease digests were typically performed in 15µl to 20µl volumes, using ~1µg purified DNA template (usually 2µl from a 30µl miniprep preparation), 1-5U of the desired restriction enzyme with the appropriate buffer according to enzyme manufacturer specifications. Reactions were incubated at 37°C and allowed to proceed for 1.5 hrs, before being evaluated on an agarose gel. In restricted occasions, reactions were heated up in the microwave 4 times for 10seconds, leaving the samples 2 minutes in between at room temperature, giving the same results as the traditional method. Restriction enzymes were obtained from New England Biolabs, Invitrogen, Fermentas and Promega, for which reactions were supplemented with 1mg/mL Bovine Serum Albumin. When performing reactions with two enzymes, Supper Dupper Buffer was used in cases where the same buffer was not compatible for both enzymes.

Polymerase Chain Reactions (PCR)

PCR amplifications were performed in 50µl volumes using Primer Start DNA Polymerase (Takara) along with its appropriate buffer. The amount of DNA template used per reaction varied, and was generally dependent on the quality and source of the DNA (e.g. cloned, genomic or library templates). All amplifications were completed on a PTC-200 Peltier Thermal Cycler (MJ Research), with cycling parameters varying according to primer pair melting temperatures (Tm) and DNA template size. When preparing (A-tailing) PCR products for PCR8/Topo reactions (Invitogen), they were incubated at 72°C for 10minutes with 0,25µl of GoTag Flexi DNA Polymerase (Promega) immediately after the PCR reaction.

LR Recombinase Reactions

8 µl reactions were performed using 50ng of PCR8/Topo entry vector and 150ng of the selected Gateway compatible destination vector following manufacturer's instructions. Half reactions were also performed in some instances, adjusting concentration/volume of the reagents accordingly.

Ligation of DNA

10µl reactions were performed using a 3:1 molar ratio of vector:insert DNA, 0.3 µl -0.5µl of T4Ligase (3U/µl, Promega) and 50ng of vector The insert mass in ng was calculated using the following equation: ((ng of vector × bp size of insert)/ bp size of vector) x molar ratio of insert. Reactions were incubated either 16hrs. at room temperature or overnight at 4°C.

Protein Concentration Determination (Bradford Assay)

Lysate samples were diluted 1:10 in MQ Water. A 50:1 (10000 µl: 20 µl) Bradford reagent/diluted sample volume ratio was used for the assay, and the absorbance at 590nm was measured using a Nanrop ND-100 Spectrophotometer. A BSA protein standard curve was created using 7 concentrations (2, 1.5, 1, 0.75, 0.5, 0.25, 0.125 mg/ml) of BSA (BSA Standard, 2 mg/ml, BioRad). For diluent the same buffer as in the samples was used (M-PER Mammalian Protein Extraction Reagent, Thermo Scientific). All assays were completed in duplicates and the mean result was determined.

Preparation of Yeast Media and Plates

Synthetic Defined 2- and 3- amino acid dropout media including SD-Leu-Trp, SD-Leu-Trp-Ura and SD-Leu-Trp-His (Sunrise Science Products) was used to prepare SD-media or SD-agar plates. For SD-agar plates, 10gr of Bacto-Agar (Fisher) and the content of each 0.5L pouch were added to 500ml of MQ H_2O. pH was adjusted to 5.9 using 10N NaOH, and solution was autoclaved 15min. For SD-Leu-Trp-His containing 3AT (Sunrise Science Products), 1M 3AT solution was prepared in MQ H_2O, filter sterilized and stored at 4°C for about a month, covered with foil. 3AT was added to autoclaved agar that had been cooled down to around 50°C so that the final concentrations of 3AT were 10mM, 25mM, 50mM, 75mM and 100mM.

For YPAD plates, 25.09gr of YPAD broth powder (Sunrise Science Products), and 10gr. of Bacto-Agar (Fisher) were added to 500ml of MQ H_2O. pH was adjusted to 6.0 using 1M HCL, and solution was autoclaved 15min.

CHAPTER III. IRF6 DOES NOT BIND MASPIN

Introduction

IRF6 is the gene mutated in two allelic autosomal dominant CLP disorders, Van der Woude syndrome (VWS) and Popliteal Pterygium syndrome (PPS), and its common variations represent the greatest genetic contribution (12%) to the isolated form of CLP (Kondo et al, 2002; Zucchero et al., 2004, Scapoli et al., 2005). As a consequence it is generally considered to be the most significant CLP locus identified to date. Despite this, the molecular pathway and cellular processes in which IRF6 functions within the developing primary palate remain largely unknown.

Protein-protein interactions are required for the regulation of essentially all biological processes in a living cell. Upon interaction, such proteins can be subjected to several events including protein modification, transport, folding or signaling in order to ensure their proper function within the cell. The other members of the IRF family have been suggested to function as dimers through interactions mediated via the IAD located near the C-terminal end of the protein, and to cooperate with other transcription factors to express target genes. Therefore, identifying developmentally relevant protein interactors of IRF6 is likely to provide clues as to the cellular process in which it is involved during the development of the primary palate.

Bailey et al. (2005), initially using a yeast two-hybrid approach, reported that IRF6 protein interacts with Maspin in mammary epithelial cells via the IRF protein interaction domain. The possibility of a role for the IRF6:Maspin interaction complex in regulating

primary palatal epithelia was of interest since Maspin, a tumor suppressor protein widely expressed in almost all epithelia (Zou et al., 1994, Bailey et al., 2006b), has been shown to regulate cell movements and apoptotic events in the breast. Furthermore, the tumor suppressive properties of Maspin also include roles in growth control and cellular differentiation (Bailey et al., 2005; 2009), all critical events during primary palate morphogenesis.

Under normal conditions**,** the pre-fusion epithelia covering the facial primordia undergo a remarkable series of cellular changes that includes proliferation, cell migration, apoptosis, changes in polarity, and differentiation to tightly coordinate outgrowth of the facial primordia and their ultimate fusion (Cox, 2004). IRF6 is expressed in, and restricted to, the epithelia that cover the facial processes around the time of their fusion and its expression decreases during the fusion and formation of the primary palate (Washbourne and Cox, 2006). This reduced expression occurs at a time when the epithelia must alter their adhesive properties and disperse to allow the mesenchymal bridge to form. As the expression of IRF6, like Maspin, is also reduced or lost during cancer progression to a metastatic disease, a process in which epithelial cells lose adhesive properties and adopt more mesenchymal-like properties (Bailey et al., 2005; 2009), it was hypothesized that the IRF6:Maspin interaction could also function to regulate and maintain the primary palatal epithelial cell phenotype. As the first step in investigating this possibility, it was important to verify the IRF6:Maspin interaction in the chick system. However, in contrast to the published results, a direct interaction of Maspin with IRF6 could not be confirmed regardless of whether the chick or human proteins (as used by Bailey et al, 2005) were employed in our yeast two-hybrid system.

Rather, our results suggest that each full-length protein has the capacity to self-activate in this assay system and therefore the Maspin-IRF6 interaction reported by Bailey and colleagues (2005) may not be true. However, further validation may be warranted.

Materials and Methods

Assembly of Chick/Human IRF6 Full-Length/Deletions and Chick/Human Maspin cDNA Sequences

Given that full-length chick IRF6 cDNA was not immediately available, full-length chick IRF6 sequence was assembled from a previously isolated partial cDNA (Washbourne B.J. and Cox T.C., 2006) and an amplified product from a chick genomic DNA preparation. Overlapping PCR products from the cDNA (1230 bp) and genomic DNA (150 bp) were combined in a single reaction along with the primers designed to the most 5' and 3' ends respectively. This reaction generated a full-length cDNA of 1383 bp that encodes a 460 amino-acid protein (Figure 3.1). Full-length human IRF6 and human/chick Maspin EST clones were purchased from Invitrogen, and cDNAs were amplified by PCR using several 5' and 3' primer-end combinations (listed in Table 3.1) to enable cloning into the appropriate expression vectors.

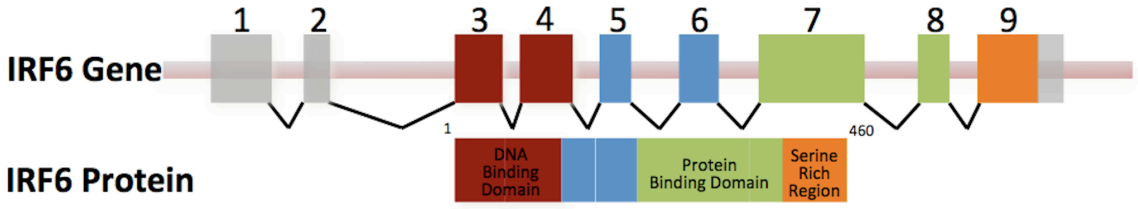

Figure 3.1. The chick IRF6 gene structure. Exons 3 through 9 encode a transcription factor that belongs to the Interferon Regulatory Factor (IRF) family characterized by the presence of two conserved functional domains. The N-terminal DNA Binding Domain (DBD) is encoded by Exons 3 and 4 while the IRF Protein Interaction Domain (IAD) is encoded by Exons 7 and 8. The C-terminal region of IRF6 contains the Serine Rich Region that in other IRF proteins is required for phosphorylation.

Table 3.1. Primer sequence combinations employed for amplification of the human/chick IRF6/Maspin cDNAs

Amplified Region	Forward Primer (5'-3')	Reverse Primer (5'-3')
cIRF6 Exons 3-9	CAGACGATGGCGTTACACCC	GAATCACTGCGCAGGCAGTGGCTGTG
cIRF6 Exons 3-8	CAGACGATGGCGTTACACCC	TCACTGAACCACGATCAGCTTTCTCTCC
cIRF6 Exons 3-7	CAGACGATGGCGTTACACCC	TCAACTTAGAAACGTTTCCAAACAG
cIRF6 Exon 7	ATGACAGACCTAGAAATCAAGTTTG	TCAACTTAGAAACGTTTCCAAACAG
cIRF6 Exons 7-8	ATGACAGACCTAGAAATCAAGTTTG	TCACTGAACCACGATCAGCTTTCTCTCC
cIRF6 Exon 7-9	ATGACAGACCTAGAAATCAAGTTTG	GAATCACTGCGCAGGCAGTGGCTGTG
cIRF6 Exons 5-9	ATGCCAGGGTCCACTGGCTCAGCTC	GAATCACTGCGCAGGCAGTGGCTGTG
cIRF6 Exons 5-8	ATGCCAGGGTCCACTGGCTCAGCTC	CACAATTACTGGGGAGGCAG
hIRF6 Exons 3-9	CATATCATGGCCCTCCACC	CACAATTACTGGGGAGGCAG
hIRF6 Exons 3-8	CATATCATGGCCCTCCACC	TCACTGAACCAAGATGAGTTTCC
hIRF6 Exon 7-9	ATGACTGACCTGGACATCAAGTTTC	CACAATTACTGGGGAGGCAG
hIRF6 Exons 7-8	ATGACTGACCTGGACATCAAGTTTC	TCACTGAACCAAGATGAGTTTCC
hIRF6 Exon 5-9	ATGCCAGGATCCACAGGGTCTGCTC	CACAATTACTGGGGAGGCAG
hIRF6 Exons 5-8	ATGCCAGGATCCACAGGGTCTGCTC	TCACTGAACCAAGATGAGTTTCC
cMaspin-Full-length	AGGAATTCCATGACGATGGATGCTCTGCAAC	GCTATGCATTTATGGGGAACAGAATCTGCCTG
hMaspin-Full length	CCCGCAATGGATGCCCTGCAACT	CACTTAAGGAGAACAGAATTTG

Generation of IRF6 and Maspin Constructs for Yeast-Two Hybrid Analysis

Yeast two hybrid experiments were performed using the ProQuest™ Two-Hybrid System (Invitrogen). This system uses pDEST22 as the prey vector and pDEST32 as the bait vector, both of which are low copy number vectors and therefore avoid issues associated with excessive ectopic expression of proteins. Full-length/deletion mutant IRF6 and full-length Maspin bait/prey constructs were generated by cloning independently amplified cDNAs into the pCR8-TOPO entry vector and then performing the Gateway LR recombinase reaction using both pDEST32 and pDEST22 Gateway compatible destination vectors (Invitrogen). The resultant pDEST22 constructs contained the Gal4 Activation Domain (AD) as an N-terminal fusion with the various IRF and Maspin sequences, while the resultant pDEST32 constructs contained the Gal4 DNA Binding Domain (DBD) as an N-terminal fusion with the respective IRF/Maspin sequences. All plasmid constructs were sequence verified using the DNA Sequencing Center at the University of Washington before transforming into yeast cells.

Two-Hybrid Screening Assays

For co-transformation of bait and prey constructs, competent MAV203 yeast cells were prepared following the Frozen-EZ Yeast Transformation II Kit protocol (Zymo Research). Briefly, bait and prey plasmids were added to competent cells in the presence of the Frozen-EZ solution III (Polyethyleneglycol, PEG, 3350), incubated for 40 minutes at 30°C and plated onto SD-Leu-Trp plates. These plates select for the presence of both the pDEST22 and pDEST32 vectors, which contain the TRP and LEU genes respectively. Therefore, transformed yeast cells with both constructs will grow on yeast media lacking Trp and Leu. Prey and bait co-transformations were then

incubated overnight at 30°C in selective media. Optical density (OD) from liquid cultures was measured, and 3µl with an OD_{600} of 0.100 from each culture was used to spot, and assay on SD-Leu-Trp-His+3AT and SD-Leu-Trp-Ura selection plates 48hours later. The SD-Leu-Trp-His+3AT plates select for the activity of the HIS3 reporter via growth in the presence of 3-amino-1,2,4-triazole (3AT). 3AT competitively inhibits imidazole glycerol phosphate dehydratase, a histidine biosynthetic enzyme (Hilton et al., 1965; Klopotowski and Wiater, 1965; Wiater et al., 1971) and therefore can limit histidine biosynthesis and thus growth. Background levels of activity due to self-activation by singly transfected IRF6/Maspin-GAL4DBD fusions is first balanced by an appropriate concentration of 3-amino-1,2,4-triazole (3AT). A successful two-hybrid interaction results in higher expression of the HIS3 reporter and thus overcoming the growth-inhibitory effect of 3AT in the medium. Therefore, in addition to the URA reporter, the use of 3AT and the HIS3 reporter represent a positive selection for successful two-hybrid interactions.

Negative and positive controls provided from the manufacturer were included on each plate to verify its correct preparation and allow comparison to be drawn with the strength of interaction of the test proteins as they represent varying interaction strengths. These controls included: Control A (pPC97 and pPC86, no interaction); control B (pPC97-RB and pPC86-E2F1; weak interaction); control C (pPC97-CYH2^{S}-dDP; moderately strong interaction); control D (pPC97-Fos and pPC86-Jun; strong interaction) and control E (pCL1 and pPC86, very strong interaction).

Results and Discussion

Failure to Validate MASPIN as an IRF6 Interacting Protein Partner

In order to assist the understanding of the role of IRF6 during primary palate, it was first important to replicate and delineate the nature of the IRF6:Maspin interaction in the chick system. Full-length/deletion mutant IRF6 constructs and full-length Maspin constructs were generated and tested in both orientations in our yeast system. IRF6-prey fused protein and Maspin-bait fused protein did not show any evidence of interaction either on SD-leu-Trp-Ura or SD-Leu-Trp-His+10mM 3AT selection plates regardless of whether the human or chick clones were used (Figure 3.2).

To determine whether the lack of detectable interaction might be due to the specific N-terminal fusion to each protein, the interaction was tested following swapping of the Gal4 domains: Gal4DBD-IRF6 and Gal4AD-Maspin. In this direction, the IRF6 fusion constructs that contain Exons 3-9 and Exons 5-9 encoded sequence showed significant self-activation of the reporters, ie. in the absence of Maspin (Figure 3.3) even at the highest 3AT concentrations (data not shown). This level of self-activation therefore precluded testing of the interaction with Maspin in this combination. Notably, self-activation by bait proteins can be observed if a transcriptional activation domain is present as is often the case if the bait protein is a transcription factor (Ma and Ptashne, 1987; Ruden et al., 1991; Ruden, 1992). Like the other members of the Interferon Regulatory (IRF) family, IRF6 is thought to function as a transcriptional regulator based on the presence of both DNA-binding and transactivation domains. C-terminal sequence alignments of human IRF members initially suggested that IRF6 has a transcriptional

activation domain that contains the protein interaction domain (Qin et al., 2003), but there was not evidence that IRF6 would function in a similar manner to the other IRFs until later research. Little at al. in 2009 used a GAL4-DBD luciferase reporter system to asses the ability of a series of IRF6 C-terminal deletions to activate transcription. The N-terminal deletion construct containing Exon 5-9 encoded sequence resulted in a 4-fold increase in transcriptional activation compared to the activation of the reporter plasmid alone, while the N-terminal deletion construct containing Exons 7-9 resulted in the greatest activation. In line with these observations, results from the two-hybrid assays described here clearly show that the self-activation occurs with the presence of the sequence encoded by Exons 5-9.

The best way to overcome the self-activation is to try to remove the activating domain by creating specific deletions within the gene and retesting the deletion constructs for activation without eliminating the interacting domain (Matchmaker™ GAL4 Two-Hybrid System 3 & Libraries User Manual, Clontech, 2007). According to Bailey et al. (2005), the IRF6:Maspin interaction occurs through the conserved IRF Protein Interaction Domain that is encoded by Exons 7-8. Additionally, it was claimed that growth was observed on selective plates when using constructs containing Exon 3-8 and Exon 5-8 encoded sequence and that inclusion of Exon 9 encoded sequence in their constructs effectively abrogated the growth response in the two-hybrid system. This latter result, however, is contradictory to the two-hybrid data reported in this chapter and the transactivation assays reported by Little et al, 2009. To investigate this apparent discrepancy further, the same Exon 3-8 and Exon 5-8 deletion constructs used by Bailey et al (2005) were then tested in our ProQuest two-hybrid system. Consistent with

our initial data, the IRF6 deletion constructs missing Exon 9 encoded sequence were sufficient to overcome the self-activation. However, there was still no evidence supporting interaction of IRF6 with Maspin.

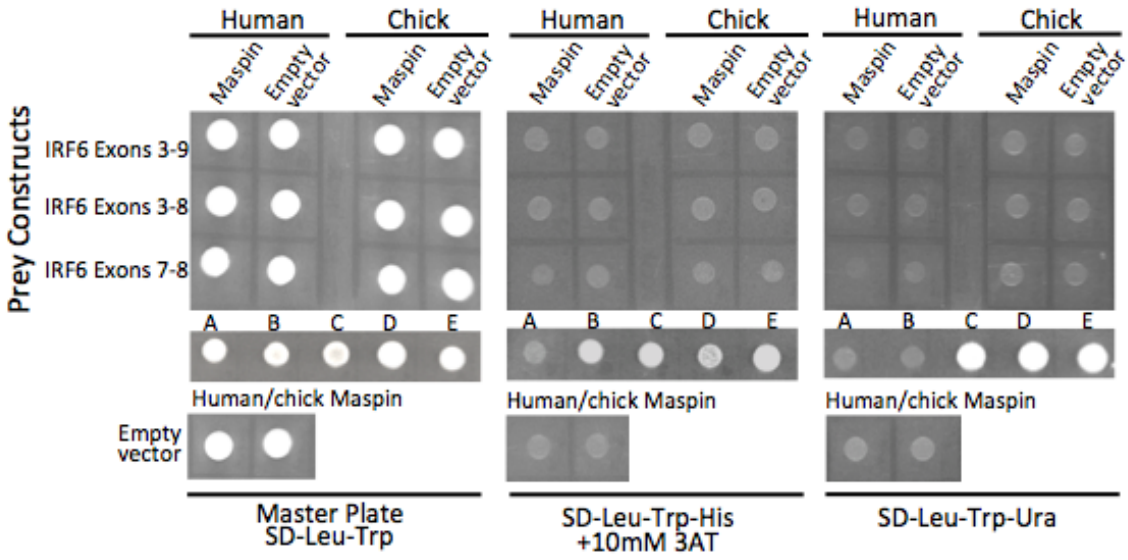

Figure 3.2. Yeast two-hybrid assay testing Maspin-bait and IRF6-prey interaction. Yeast agar SD-Leu-Trp master plate shows growth expected for the presence of both pDEST22 and pDEST32 constructs. However when transferred to each of the selection plates (SD-Leu-Trp-His+ 10mM 3AT and SD-Leu-Trp-Ura) no growth was seen for any IRF6-Maspin combination. The positive and negative control two-hybrid combinations showed the expected response on each plate.

Two more constructs, containing Exon 3-7 and only Exon 7 encoded sequence, were then tested in case part of the Exon 8-encoded sequence was preventing this interaction. Similar to the previous results, these deletion constructs overcame the self-activation, but again no growth on the selection plates was observed. Taken together, these findings confirm that the self-activation was conferred by exon 9 encoded sequence, but was dependent on the presence of Exon 5/6 encoded sequence. These

regions correspond to the N- and C-terminal flanking sequences of the IRF protein interaction domain, respectively, and that removal of at least one of these flanking regions was necessary to overcome the self-activation seen with the IRF6-bait constructs.

Notably, studies on IRF3 and IRF5 crystal structures suggest that the analogous regions in these proteins contain auto-inhibitory sequences. These auto-inhibitory sequences have been proposed to maintain these factors in an inactive form in the cytoplasm, but once activated by phosphorylation of serine residues in the C-terminal flanking sequence, conformational changes occur that alleviate the auto-inhibition and allow translocation into the nucleus and the initiation of transcription (Qin et al., 2003; Chen et al., 2008). In the heterologous yeast system where these fusion proteins are forced into the nucleus, the presence of these regions may interact with endogenous factors to activate transcription. In this case, their removal would be required to return transcription to its basal or background state and also permit evaluation of protein-protein interactions mediated by the IAD, as described in Chapter IV. It is therefore unclear why we could not reproduce the results of Bailey et al (2005) with either the chick or human IRF6 and Maspin clones. One possibility is that Bailey and colleagues did not conduct the appropriate self-activation controls and the growth they interpreted as an interaction between Maspin and IRF6 was in fact self-activation by the specific IRF6 constructs. This would fit with the conflicting consequences of removal of Exon 9 encoded sequence in the two yeast two-hybrid systems. Alternatively, the discrepancy in results may be due to the different attributes of the yeast vectors used. The vectors of the Clontech system employed by Bailey and colleagues (2005) are high copy number

vectors whereas the pDEST vectors of the ProQuest system are low copy number vectors optimized for detection of strong and arguably more likely *bona fide* interactions.

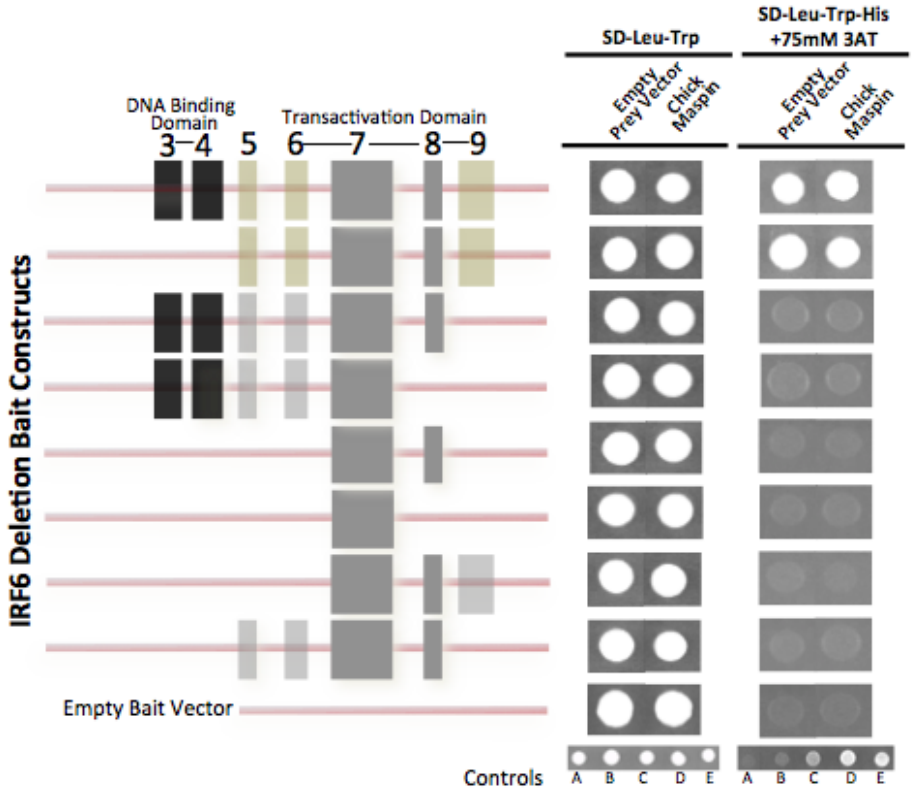

Figure 3.3. Yeast two-hybrid assay testing IRF6-bait and Maspin-prey interaction. The yeast agar plate SD-Leu-Trp shows growth of full-length chick IRF6 and seven chick IRF6 deletion mutant constructs expressed as bait and co-transformed with chick Maspin (prey). The selection plate SD-Leu-Trp-His+ 75mM 3AT shows growth of two IRF6-bait and Maspin-prey combinations due to self-activation of the bait, along with growth for positive control two-hybrid combinations and no growth for negative controls. The diagram on the left represents the different IRF6-bait constructs generated for this screen and highlights that self-activation of IRF6 was dependent on the presence of both exon 5/6 and exon 9 encoded sequences. Same results were obtained with human clones.

CHAPTER IV. INSIGHTS INTO THE NOVEL IRF6 INTERACTION WITH NME2

Introduction

The initial work to aid understanding of the role of IRF6 in CLP was focused on a reported interactor of IRF6, called MASPIN (Bailey et al, 2005). As described in Chapter III, extensive experimentation does not support the previously published data and suggests that IRF6 and MASPIN may not in fact directly interact. Consequently, it was decided to perform an unbiased screen for IRF6 interactors using the yeast two-hybrid system and a developmental stage-appropriate cDNA library as prey. From this screen, we identified the Nme2 protein and subsequently validated it as a *bona fide* IRF6 binding protein. The results from this work are described in this chapter.

NME2 belongs to a large family of highly conserved proteins from bacteria to humans (Desvignes et al, 2009) that were first discovered for their involvement in metastasis, thus the name 'NME', for non-metastatic (Steeg et al, 1988). Later, the NME1/2 proteins were identified as NDP kinases (Gilles et al, 1991), an activity that previous studies had related exclusively to the synthesis of nucleoside triphosphates, and the maintenance of the nucleotide pool (Postel, 1998; Postel at al, 2002). However, further research has proven that these small proteins are involved in a fascinating variety of cellular functions including proliferation, adhesion, differentiation and apoptosis, depending on the cellular context (Lacombe et al, 2000; Lombardi et al, 2000; Kimura et al, 2000; Fournier et al, 2003; Aktary et al, 2010), In epithelia, a primary role for NME1/2 has been the

regulation of epithelial adhesion. Consistent with this, as IRF6, NME2 is described here as being expressed during primary palatal development

The IRF6:NME2 protein interaction may be critical for primary palate development and key to the pathogenesis of CLP. This chapter provides some insights into the regulation of the IRF6:NME2 interaction via IRF phosphorylation, and supports the notion that the interaction with NME2 serves to sequester IRF6 and regulate its function by controlling IRF6 translocation to the nucleus using similar mechanisms to other IRF members and factors like beta-catenin and ZO-1 that also have dual roles in adhesion and transcriptional regulation.

Materials and Methods

Plasmid Construction

Chick IRF6

Single and double amino-acid substitutions (S401A, S401D, S418A and S418D) were introduced into constructs using PCR mutagenesis using the following primers in combination with forward and reverse primers binding to the very 5' and 3' ends of IRF6 open reading frame: S401A forward: 5'-GATATATGAGATGTTTGCCGGTGACTTCACGCGCTC-3' and S401A reverse 5'-CGTGAAGTCACCGGCAAACATCTCATATATCATCC-3'; S401D forward 5'-GATATATGAGATGTTTGACGGTGACTTCACGCGCTC-3' and S401D Reverse 5'-CGTGAAGTCACCGTCAAACATCTCATATATCATCC-3'; S418A forward 5'-GGCTCCAGATCGCTACTCCTGACATCAAGGAC-3' and S418A reverse 5'-

GATGTCAGGAGTAGCGATCTGGAGCCGCACACTG-3'; S418D forward 5'-GGCTCCAGATCGATACTCCTGACATCAAGGAC-3' and S418D reverse 5'-GATGTCAGGAGTATCGATCTGGAGCCGCACACTG-3'. The underlined nucleotides indicate those that are different from the wild type sequence. After cloning into the pCR8-TOPO entry vector, the Gateway LR recombinase reaction was performed using the Gateway compatible expression vectors pDEST32 and pDEST-myc (Invitrogen) for yeast two hybrid assays and mammalian cell expression studies, respectively. Similarly, the IRF6 cDNA sequence corresponding to the DNA binding domain (DBD, amino acids 1-128) was amplified using the following primers: forward 5'-CAGACGATGGCGTTACACCC-3' and reverse 5'-TTGCAGAGCAGTCGGAGGCATCTC-3'. IRF6 DBD and the other IRF6 deletion products generated previously for the Maspin two hybrid studies (Chapter III) were cloned into pDEST-myc.

Chick NME2

Full-length chick NME2 cDNA was obtained from University of Delaware Chick EST database, amplified by PCR using the following primers: start (forward) 5'-CAGATCTCGAGCATGGCTGCCAACTGCGAG-3' and stop (reverse) 5'-CATCGGTACCTCACTCATAGACCCAGTCATG-3', and ligated into the KpnI and XhoI sites of the expression vector pEGFP-C2 (Clontech) downstream of, and in-frame with, the GFP reporter gene. Full-length cDNA was also cloned into pDEST-c-myc and pcDNA3.2/V5 vectors using Gateway technology for additional immunoprecipitation studies.

To generate a kinase-dead form of NME2, the catalytic histidine residue in the ATP-

binding domain was changed to Phenylalanine (H118F) by PCR mutagenesis using the following primers: start primer for NME2 (described above) and reverse 5'-CTACAGAGTCGCTGCCAAAGATGATGTTTCTTCCCAC-3', as well as forward 5-GAAGAAACATCATCTTTGGCAGCGACTCTGTAGAAAGC-3' and the stop primer for NME2 (as above). The amplified overlapped product was ligated into pEGFP-C2 as described for the wild type.

Chick NME1

Full-length chick NME1 was amplified by PCR from an embryonic day 4 (E4) chick cDNA library (Cox laboratory) using the following primers: forward 5'-ACCATGGCTTCCATCTCAGAGC-3' and reverse 5'-GTTCTACTCGTAGATCCATTCG-3', and cloned using the Gateway technology into the yeast expression vector pDEST22, and into pcDNA-DEST53 for expression as a GFP fusion protein and for immunoprecipitation studies. All constructs were sequenced and purified by large-scale plasmid DNA preparation.

Yeast-Two Hybrid Screens

Overview

Three truncated human IRF6 proteins were used as bait to screen a murine embryonic day 10.5 (whole embryo) cDNA library (ProQuest ^{TM} yeast two-hybrid library, Invitrogen). The first and second screens used IRF6 Exon 5-8 and IRF6 Exon 3-8 encoded sequences as bait, respectively. These truncated proteins contain the protein binding domain, but not the serine rich region present in Exon 9 encoded sequence. The third screen used IRF6 Exon 7-9 encoded sequence as bait. This bait contains both

the protein binding domain and the serine rich region.

Screens

To screen for possible interactors of IRF6, more than $1x10^7$ cDNAs (in the cDNA library) were co-transfected with the corresponding bait and plated on twenty five 15 cm diameter agar plates containing synthetic complete medium lacking histidine (SD-Leu-Trp-His+75mM 3AT). 75mM 3AT in the –His medium was shown to be sufficient to inhibit the background HIS3 expression induced by each of the bait constructs. Yeast colonies that grew strongly under these conditions were selected and streaked on SD-Leu-Trp master plates along with the five-control yeast strains (provided by the manufacturer) for stock cultures. The relevance of including these controls on the screens was described in Chapter III. Selected colonies as well as controls were grown up in SD-Leu-Trp media overnight at 30°C. As the number of cells transfected onto the selection plates can affect the quantification of the assay (i.e background growth), optical density was measured for each of the cell cultures, and 3µl with an optical density of 0.100 were used for spotting onto the selection plates to test for the activation of the three endogenous reporter genes: His3, Ura and LacZ respectively. For confirmation of HIS3 activity, colonies were spotted on SD-Leu-Trp-His+75mM 3AT media plates for 48 hours at 30°C. For URA3, colonies were spotted on SD-Leu-Trp-Ura media plates for 48 hours at 30°C. For LacZ, individual colony cultures were spotted on a nylon membrane placed on a YPAD media plate. After overnight growth, the colonies on the membrane were lysed with liquid nitrogen and incubated with Z buffer solution overnight at 37°C. Colonies demonstrating activity of at least two of the reporter genes were deemed as containing cDNA clones encoding potential interactors.

Positive colonies were regrown in liquid cultures overnight, and DNA was extracted using the Qiagen MiniPrep kit after treatment with Zymolase (Cat No. 786-036; Biosciences). Five microliters of DNA extracted from yeast were transformed into competent Top10 *E.coli* cells and grown overnight at 37°C on Ampicillin selective media. DNA was extracted using the Qiagen MiniPrep kit and prepared for sequencing using the GAL4AD primer. Sequencing was performed by the University of Washington Department of Biochemistry Sequencing Facility. Obtained sequences were searched against the NCBI murine nucleotide database, and verified as being in frame with the N-terminal GAL4 tag.

Verifying Interactions

DNA from in-frame plasmid sequences was re-transformed into yeast along with human pDEST32-IRF6. These plasmids were also re-transformed with the empty pDEST32 vector as a negative control. Transformants were assessed for HIS3, URA3 and LacZ activity as described above. Transformants recapitulating the interaction detected by the initial Yeast Two-Hybrid screens were designated as containing putative positive interactor cDNAs.

Computer-Assisted Detection of Serine Phosphorylation Sites

Analysis of putative consensus serine phosphorylation sites in IRF6 was performed using NetPhos version 2.0 [http://www.cbs.dtu.dk/services/Netphos/]

Immunoprecipitation Studies

Human embryonic kidney (HEK) 293T cells were maintained in Dulbecco's modified Eagle's medium (DMEM; Thermo Scientific) medium supplemented with 10% fetal bovine serum (FBS) and 1% Glutamax in a humidified atmosphere containing 5% CO_2 at 37°C. HEK 293T cells were seeded in 100 mm dishes so that they were 70-80% confluent at the moment of transfection with c-myc-IRF6 wild type, deletion and phosphorylation sites constructs, GFP-NME2 and GFP-NME1 constructs independently. Twenty-four hours after transfection, cells were washed with TBS and lysed on iced cold M-PER Mammalian Protein Extraction Reagent (Pierce) containing a cocktail of protease inhibitors (Product No. 87785; Thermo Scientific). Cells were scraped from the plate, and lysates were centrifuged for 20 min. at 16,000g. The resulting supernatants were separated from the pellets. Protein determination was performed using Bradford assays according to the manufacturer's instructions. 1000 µg of total cellular protein from each transfection was combined and immunoprecipitated with myc-agarose (Pierce) overnight at 4°C. Protein complexes were washed with TBS-T (0.1% tween 20), eluted with 2X non-reducing sample buffer, separated on 8-12% SDS-PAGE along with loading controls and transferred onto PVDF membranes (Millipore) using a semi-dry transfer apparatus (Owl). Membranes were blocked with 5% non-fat milk in TBS-T, except when probed with phosphoserine antibody, in which case it was blocked with 3% BSA in TBS-T. Then, the membranes were incubated with the appropriate primary antibody, washed with TBS-T, incubated with the appropriate HRP-conjugated secondary antibody and washed again with TBS-T. Detection was carried out using Super Signal West Pico Chemiluminescent Substrate (Thermo Scientific) as per the

manufacturer's instructions. Antibodies used in western blot analyses included rabbit polyclonal anti-GFP antibody (1:5000; ab290, Abcam), mouse monoclonal anti-c-myc antibody (1;1000; 9E10), mouse monoclonal anti-phosphoserine antibody (1:500; ab17465, Abcam), mouse monoclonal anti-Nme2 (1:1000; ab6062, abcam) and Goat HRP conjugated anti-rabbit and anti-mouse IgG secondary antibodies (1:10000; Sigma).

Immunofluorescent Analysis of Cultured Cells

MDCK cells were maintained in the same conditions as 293T cells. The cells were plated on coverglass (Fisher) pre-coated with 0.1% (w/v) poly-L-Lysine (Cat No. P4707; Sigma). Twenty-four hours after co-transfection, cells were washed once with warm PBS and fixed with 4% PFA/1% Sucrose for 10 min at RT. After fixation, cells were washed with PBS, permeabilized in 0.2% Triton X-100 in 1% BSA/PBS for 15 min., washed and blocked in 10% normal goat serum/1% BSA/PBS for 1h at RT. Cells were stained with the appropriate primary and secondary antibodies for one hour each. Before and after each antibody incubation, cells were washed three times for 5 min each in 1% BSA/PBS. Primary antibodies and fluorescent secondary antibodies were diluted to optimized concentration in 1% BSA/PBS. After staining, the coverglass was inverted and mounted onto super frost plus glass microscope slides (Fisher) with Vectashield mounting medium with DAPI (Vector Laboratories) for visualization of nuclei using a Leica SP5 confocal microscope. The following primary and secondary antibodies were used: mouse monoclonal anti-myc (1:1000; 9E10) and rabbit polyclonal anti-GFP (1:500 Abcam), Alexa Fluor goat anti-mouse 568, goat anti-mouse 488 and

goat anti-rabbit 568 (Invitrogen) and FITC goat anti-rabbit (Abcam). Secondary antibodies were used at 1:300 dilution.

NME2 Wholemount Immunohistochemistry

Following fixation with 4% PFA/4% sucrose/PBS for 2.5 hours at 4°C, chick heads were washed four times with PBST (0.1% Tween 20) 5 minutes each at room temperature, and incubated in blocking solution (10% (v/v) normal goat serum in PBST) overnight at 4°C. The heads were then incubated with mouse monoclonal anti-NME2 antibody (1:500, Abcam) diluted in blocking solution overnight at 4°C, followed by 5 gentle washes with PBST for 5 minutes each. After these washes, heads were incubated with an Alexa Fluor 568 goat anti-mouse secondary antibody (1:300, Invitrogen) diluted in blocking solution overnight at 4°C, and washed 4 times in PBST, 5 minutes each the following day. NME2 expression was visualized using a dissecting fluorescent microscope (Leica, MZ8).

Results

Yeast Two-Hybrid Screens Identify Nme2 as a Novel IRF6 Binding Partner

Yeast two-hybrid screens were conducted in order to identify potential IRF6 interacting proteins and provide clues as to the cellular processes with which this transcription factor is involved. Given the high level of amino acid identity between human and mouse IRF6 proteins (97.2%) and between mouse and chick IRF6 proteins (85%) it was reasoned that human and chick IRF6 proteins would function in an identical manner to the mouse protein with respect to interactions with other murine protein partners (Figure

4.1). And, since self-activation was observed with pDest32-full-length human IRF6 in previous studies (Chapter III), three truncated IRF6 proteins, all containing the predicted protein binding domain, and just one including the C-terminal serine rich region, were used as a bait to screen a 10.5 embryonic mouse cDNA library (Figure 4.2A). This library has been used successfully in the laboratory previously to identify protein interactors with cross-species probes (Short et al, 2002). Furthermore, this stage library was selected because it represents the profile of gene expression at the point of primary palatal fusion and therefore maximizes the likehood of detecting functionally relevant interactors of IRF6 as its expression in mice is maximal in the orofacial epithelia at this stage (Knight et al, 2006). Potential interacting clones were selected based on the activation of at least two of the endogenous reporter genes (His, LacZ, and Ura).

Analysis from recovered cDNA sequences from screens 1 and 2 (which utilized N- and C-terminally truncated IRF6 proteins) were either out of frame with respect to the GAL4 domain or were in-frame GAL4 fused proteins, but failed to interact with IRF6 when re-transformed back into yeast. These were therefore reclassified as false positives. In contrast, the latter screen (which used as a bait the N-terminally truncated IRF6 protein but retaining both the protein interaction domain and the serine rich region) identified multiple in-frame putative IRF6 interactors. Database searches identified two clones as encoding Nme2. By comparison with the published murine Nme2 sequence, the clones were judged as being full-length. The other clones were identified as encoding Ccl27, Wac, IK and Sertad1. Single isolates were recovered for each of these putative interactors. While Sertad1 and Ccl27 represented full-length coding sequences, Wac

and IK represented partial full-lengths encoding more than half of the protein sequence (Figure 4.3).

To confirm that these interactions were not an artifact of the independent GAL4 activation domain and DNA binding domain fusion events, prey recovered plasmids were co-transformed with IRF6 back into yeast, along with negative controls. Both His and LacZ reporter genes were activated after co-transformation of IRF6 and prey vectors, but were not activated after transformation of the corresponding empty vectors. IRF6 interactions were scored as moderate to strong as compared to the level of activation of the interacting control proteins (Figure 4.2B). Nme2 was selected for further studies in the chick system for several reasons. Although Sertad1 and Ccl27 are conserved proteins across species, the chick sequences were not available. Similarly, there was only a predicted chick sequence for the WAC protein. Although chick IK was available, IRF6 interaction with Ik was not as strong as with Nme2. Furthermore, this protein is a cytokine, which has been mostly studied for its role in immune response (Willers et al, 2001; Willers et al, 2001b). Nme2 therefore represented the best candidate for further investigation in the context of the development of primary palate not only because its chick sequence was available but, more importantly because of its roles in epithelial morphogenesis (Hsu, 2011) as well as its involment in a variety of cellular functions including proliferation, adhesion, differentiation and apoptosis (Lacombe et al, 2000; Lombardi et al, 2000; Kimura et al, 2000; Fournier et al, 2003; Aktary et al, 2010).

Figure 4.1. Alignment of the amino acid sequences of the IRF6 human, mouse and chick proteins. The blue line indicates the sequence of the DNA Binding Domain. The dashed red lines represent the autoinhibitory sequences, while the solid red line represents the Interferon Association domain (IAD). The serine rich region, which resides within the C-terminal most auto-inhibitory region, is delimited by putative and conserved serines (highlighted in yellow) at positions 401 and 418 in the chick sequence.

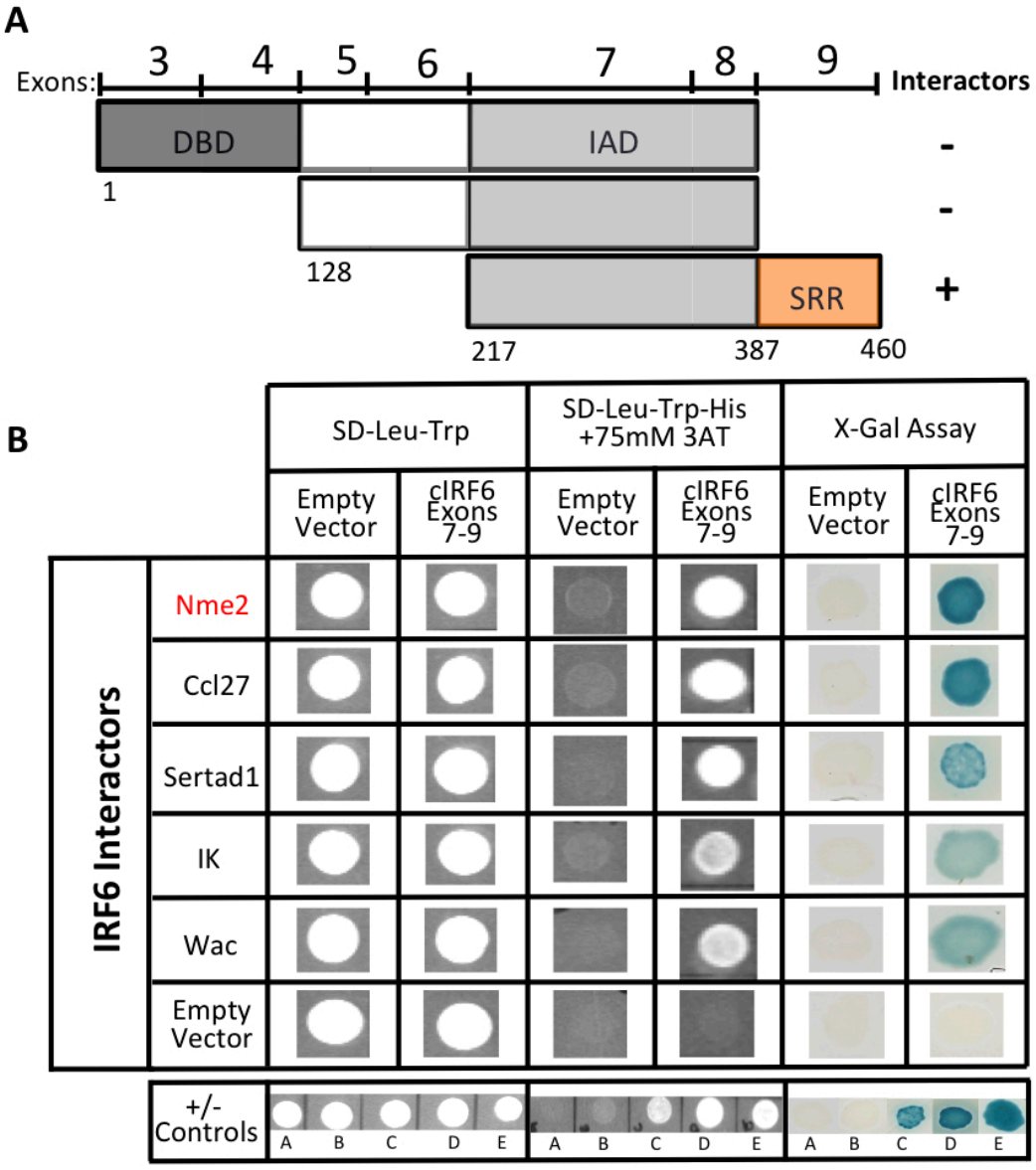

Figure 4.2. Nme2 was detected from truncated IRF6-bait yeast two-hybrid screens. A. IRF6 constructs that did not exhibit any self-activation were utilized in the yeast two-hybrid screens for identification of putative interactors. Only one of them contained the serine rich region at the C-terminus of the protein. (-) indicates that no validated putative interactors were recovered from the screen, whereas (+) indicates that positive colonies represent in-frame sequences that interact with IRF6 when tested back into yeast cells. **B**. Five putative interactors were identified using IRF6 exons 7-9 coding sequence. These IRF6 interactions each activated two reporter genes, HIS and LacZ, in our yeast two-hybrid system (Invitrogen). Self-activation controls for all proteins as well as positive (+) and negative (-) controls that come with the system were included in order to verify the accurate preparation of the plates and, to compare the strength of the interactions. Co-transformation of IRF6 and Nme2 into MaV203 cells gave similar levels of growth on 3AT and intensity/color of X-Gal activation comparable to the strongest interacting control proteins (Control E). DBD (DNA Binding Domain); IAD (Interferon Association Domain); SRR (Serine Rich Region).

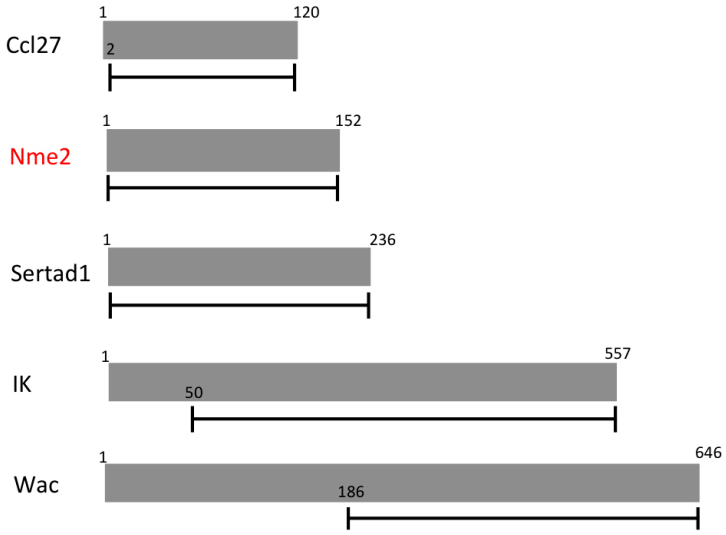

Figure 4.3. Positive clones identified in the yeast two-hybrid screen. Black lines highlight the extent of the clones retrieved for each protein interactor relative to their full-length, which are shown in gray boxes. Numbers represent amino acid positions.

Further Validation of The IRF6:NME2 Interaction in the Chick

The predicted chick NME2 protein encodes a protein of 153 amino acids and shares 93% identity with mouse Nme2, which encodes a protein of 152 amino acids. (Figure 4.4A). The yeast two-hybrid assay showed a physical interaction between human IRF6 and mouse Nme2. To provide further support for the validity of this interaction, an interaction between full-length chick IRF6 and chick NME2 was tested by co-immunoprecipitation following ectopic expression of tagged versions of each, c-myc-IRF6 and GFP-NME2, in HEK293T cells. This human cell line only expresses low levels of endogenous IRF6 (data not shown). Cell lysates were incubated with anti-c-myc agarose, and immunoprecipitation reactions were analyzed by immunoblotting with a GFP-specific polyclonal antibody. This approach clearly supported the interaction between the two orthologous chick proteins (Figure 4.4B).

An important consideration for pursuing the role of any given IRF6 protein interactor is that the interactor is also expressed appropriately in the orofacial epithelia at the time of primary palate development. To this end, NME2 wholemount immunofluorescence staining of chick heads at stages HH23, HH24 and HH25 was performed. This demonstrated that chick NME2 is indeed expressed in the facial epithelia, and also at a lower level in the mesenchyme both before and during contact of the maxillary and lateral/medial nasal processes. Furthermore, NME2 expression appears to increase at the point of fusion of these processes at HH25 (Figure 4.4C). These two findings support the conclusion that NME2 is a physiologically relevant interactor of IRF6 and confirms the appropriateness of the chick system as a model for further studies into the cellular and developmental roles of IRF6-NME2 function.

NME2 Binds to IRF6 via the IAD, but Its Interaction is Enhanced by the C-Terminal Serine Rich Region

Given that Nme2 was identified as a putative interactor using only the construct incorporating the Exon 9-encoded C-terminal serine rich region of the protein, this suggested that the interaction between Nme2 and IRF6 was dependent on the presence of this region. To test this, four truncated IRF6 proteins, including those utilized in the initial two screens were tested for their ability to bind NME2 in both direct yeast two-hybrid assays and co-immunoprecipitation assays. Results from these approaches clearly indicated that the interaction between these proteins occurs through the IRF6 IAD (Interferon Association Domain) (encoded by exons 7 and 8) but requires the presence of the C-terminus of the protein (Figure 4.5).

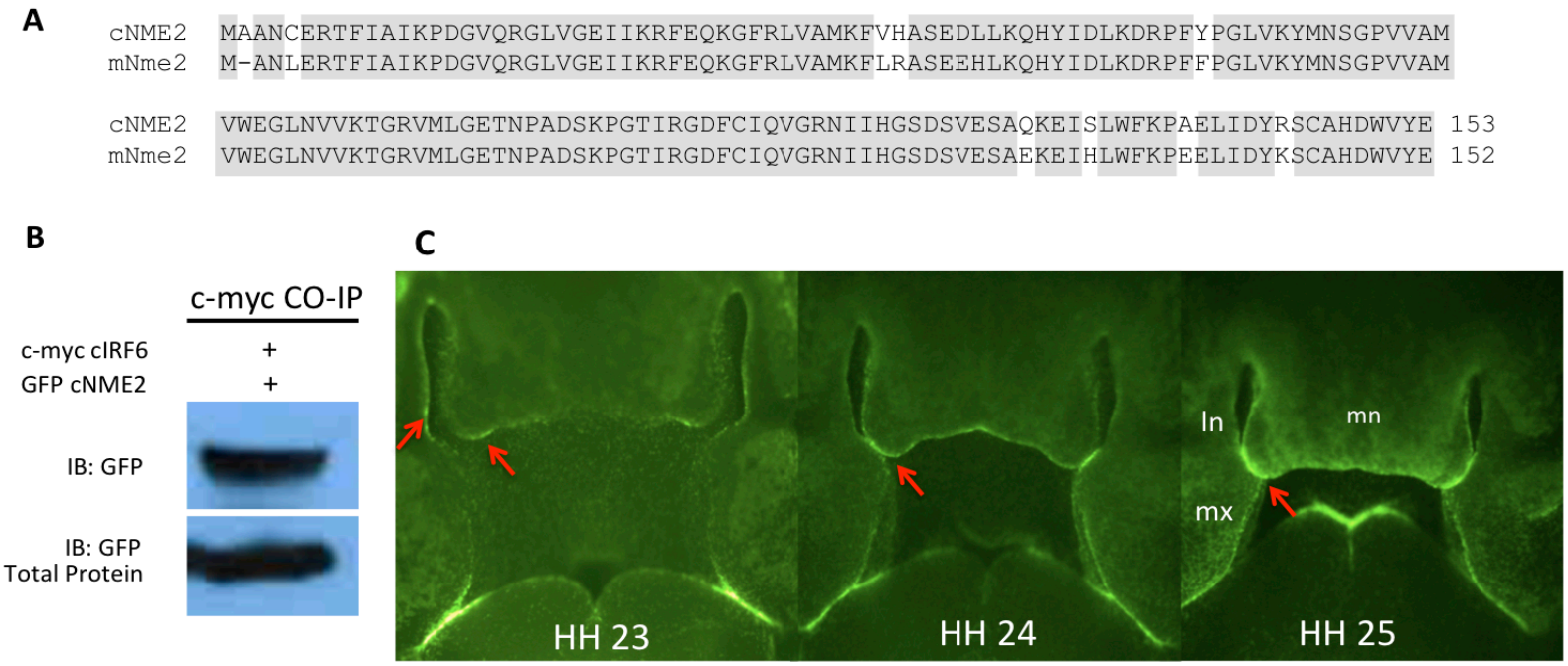

Figure 4.4. IRF6 interacts with NME2, a conserved protein that shares similar expression during primary palate development in the chick. A. Chick NME2 encodes a 153 amino acid protein that displays 93% identity with murine Nme2. Gray boxes represent amino acids that are identical in both proteins. **B**. Co-immunoprecipitation of chick IRF6 and chick NME2. HEK293T cells were transfected with c-myc-IRF6 and GFP-NME2. Samples were immunoprecipitated with anti-c-myc antibody agarose beads, separated on 8-12% SDS polyacrylamide gel, transferred to a PDVF membrane and blotted with anti-GFP antibody to detect the co-precipitated NME2 protein. **C.** Expression of NME2 during development of the primary palate in the chick. Anti-NME2 wholemount immunohistochemistry of chick head embryos was performed between HH23 and HH25. Red arrows indicate strong expression of NME2 in the tips of the facial processes immediately prior to fusion as well as at the site of fusion between them. ln, lateral nasal process; mn, medial nasal process; mx, maxillary process; HH, Hamburger Hamilton stages.

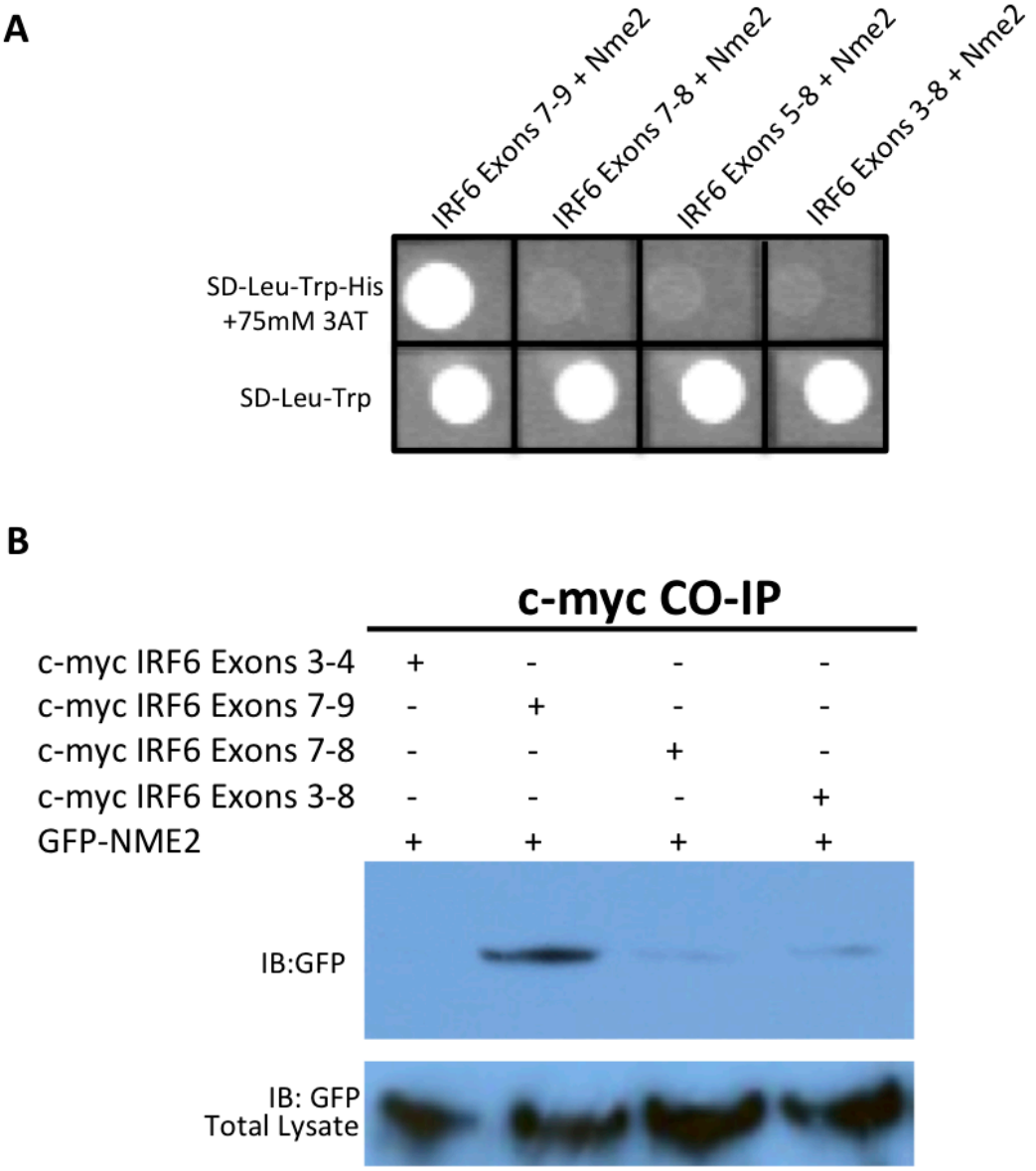

Figure 4.5. The IRF6 C-terminal serine-rich region significantly enhances its interaction with NME2 through the protein-binding domain (IAD). A. Direct yeast hybrid assays and **B.** c-myc co-immunoprecipitation studies were performed using several deletion IRF6 constructs to delineate the region responsible for the binding to NME2. Presence of the sequence encoded by exon 9 results in marked growth of transformed yeast cell on the selective plate, SD-Leu-Trp-His containing 75mM 3AT (**A**), and more co-precipitated GFP-NME2 (**B, compare lane 2 with lanes 3 and 4**).

IRF6 is Phosphorylated on C-Terminal Serine Residues

Phosphorylation of some members of the IRF family has been reported to occur in the serine-rich cluster of amino acids (serine rich region) located in their respective C-termini. In each case, serine phosphorylation appears to play a role in regulating protein-protein interactions through the IAD (Qin et al, 2003; Panne et al, 2007; Chen et al, 2010). Based on the presence of multiple conserved serine residues, it was hypothesized that IRF6 was also a phosphorylated protein, and that perhaps IRF6 serine phosphorylation plays an analogous role in regulating binding of NME2. To explore these possibilities, the NetPhos 2.0 program was initially used to analyze the full-length chick IRF6 sequence for putative protein phosphorylation sites. NetPhos 2.0 uses an output score with values in the range of 0.000-1.000. It assigns serine residues as predicted phosphorylation sites if the score is above the threshold of 0.500. This bioinformatic analysis revealed many possible sites of serine phosphorylation along the protein. However, only two serine residues (S401 and S418) in the C-terminal serine rich region of the protein had a very high predictive score (0.930 and 0.924, respectively) of being phospho-serine sites (Figure 4.6A). To verify the computer prediction experimentally, and assess the contribution of these serines in the phosphorylation events of IRF6, site-directed mutagenesis was performed to replace the serine residues (S401 and S418) with either alanine or aspartic acid. Alanine substitutions replace the serine with a similar sized amino acid that is unable to be phosphorylated, and such substitutions are typically used to mimic the unphosphorylated state. In contrast, aspartic acid (and sometimes glutamic acid) substitutions provide a structure that resembles that of phospho-serine (ie. act as

phosphomimics) and consequently aspartic acid substitutions are frequently employed in situations to mimic a constitutively phosphorylated form of the protein. The prediction was that if phosphorylation of these serine residues was important for the interaction with NME2 that differences in binding strength would be seen in different assay systems. To this end, HEK293T cells were transiently transfected with the various expression constructs containing wild type IRF6, the single (S401A or S418A) or double (S401A+S418A or S401D+S418D) mutated putative phosphorylation sites, and the c-myc-IRF6 tagged proteins immunoprecipitated from protein extracts using an anti-c-myc antibody. The immunoprecipitates were then analyzed by western analysis using an anti-phosphoserine. This analysis resulted in the detection of a band at around 65kDa that was subsequently validated as the signal from the c-myc-IRF6 fusion protein by stripping and re-probing the blot with anti-myc antibody. These results indicate that IRF6 is indeed a serine-phosphorylated protein. Notably, however, all the mutant proteins were also readily detected by the anti-phosphoserine antibody, suggesting that either serine residues other than those at position 401 and 418 are phosphorylated, or that if serines at position 401 and/or 418 are phosphorylated, they are not the only phosphorylated serines in IRF6. The latter possibility would be in line with the predictions by the NetPhos algorithm described above which suggested at least 5 possible phospho-serine sites in the N-terminal half of IRF6.

Although not markedly affecting the overall phosphorylation level of IRF6, the mutation of both serines to alanines significantly affected the serine-phosphorylation status of two other proteins, detected at around 55kDa and 22kDa, and completely abolished the detection of a 15kDa phosphoserine protein that co-precipitated with IRF6. (Figure

4.6B). The identity of these co-precipitated proteins remains un-identified although initial attempts to identify them using MALDI-TOFTOF and LCMS mass-spectroscopy analyses were carried out (Mass Spectrometry Facility, South Lake Union, University of Washington, Seattle, WA). Nevertheless, the results suggest a critical role for these two serine residues (S401 and S418) in regulating either the binding and/or phosphorylation status of three other proteins that form part of a larger complex involving IRF6.

The Phosphorylation Status of Serines 401 and 418 Defines IRF6 Interaction with NME2

To investigate the role of IRF6 C-terminal serine phosphorylation in regulating the IRF6:NME2 interaction, the IRF6 single and double mutated phosphorylation sites were cloned in-frame into the yeast two hybrid bait vector, pDEST32, and co-transformed into MaV203 yeast cells with pPC86-Nme2. Substitution of both serine residues to alanines resulted in no growth on the selection plates suggesting that inhibition of serine phosphorylation at positions 401 and 418 abolished the ability of Nme2 to bind IRF6. Conversely, substitution of both serines to the phosphomimic aspartic acid residues stimulated robust growth of the yeast on the selection plates. As individual substitutions, the S418D substitution had a stronger effect than the S401D mutation in enhancing the interaction, but both substitutions together had an additive effect. Additionally, in contrast to the individual S401A substitution, the S418A substitution was sufficient to abolish the interaction completely (Figure 4.7A). These results were confirmed by western analysis of co-immunoprecipitates of c-myc-IRF6 doubly mutated phosphoserine sites when GFP-NME2 was co-expressed with each mutant form in HEK293T cells (Figure 4.7B). The results presented here support the notion that the

interaction of IRF6 with NME2 is dependent on the phosphorylation status of the C-terminal serines at positions 401 and 418.

Nme2 Kinase Activity is not Required for Its Interaction with IRF6

NME2 is also known as nucleoside diphosphate kinase B (NDPK-B), based on earlier studies of the enzymatic activity prior to identification of the gene encoding this protein (Gilles et al., 1991). This nucleoside diphosphate kinase is classified as a histidine-dependent protein kinase, as its activity relies on the function of a histidine residue (His118) within the catalytic site. As part of the kinase mechanism, NME2/NDPK-B is auto-phosphorylated on His118 in the presence of ATP and then the intermediate phosphate is transferred to other target residues (Webb et al, 1995; Bilitou et al, 2009). Since IRF6 is a phosphorylated protein, it was hypothesized that IRF6 could represent a substrate for the putative protein kinase activity of NME2 and that this activity may be required for their interaction or the interaction of other proteins in the complex. To test this possibility, Histidine 118 was mutated to Phenylalanine (H118F), which has been shown to inactivate the NDP kinase activity (Postel, at al, 2000). The ability of this kinase dead form of NME2 was then tested for its ability to interact with both wild type IRF6 and each of the double serine mutants in co-immunoprecipitation assays. As shown in Figure 4.7, Nme2-H118F behaved similarly to the wild type Nme2 protein in that it was able to bind wild type IRF6 and the S401D+S418D double mutant, but failed to bind the S401A+S418A double mutant. These data suggest that the IRF6-NME2 interaction is independent of the kinase activity of NME2, but dependent on IRF6 phosphorylation on these specific serines (Figure 4.7B).

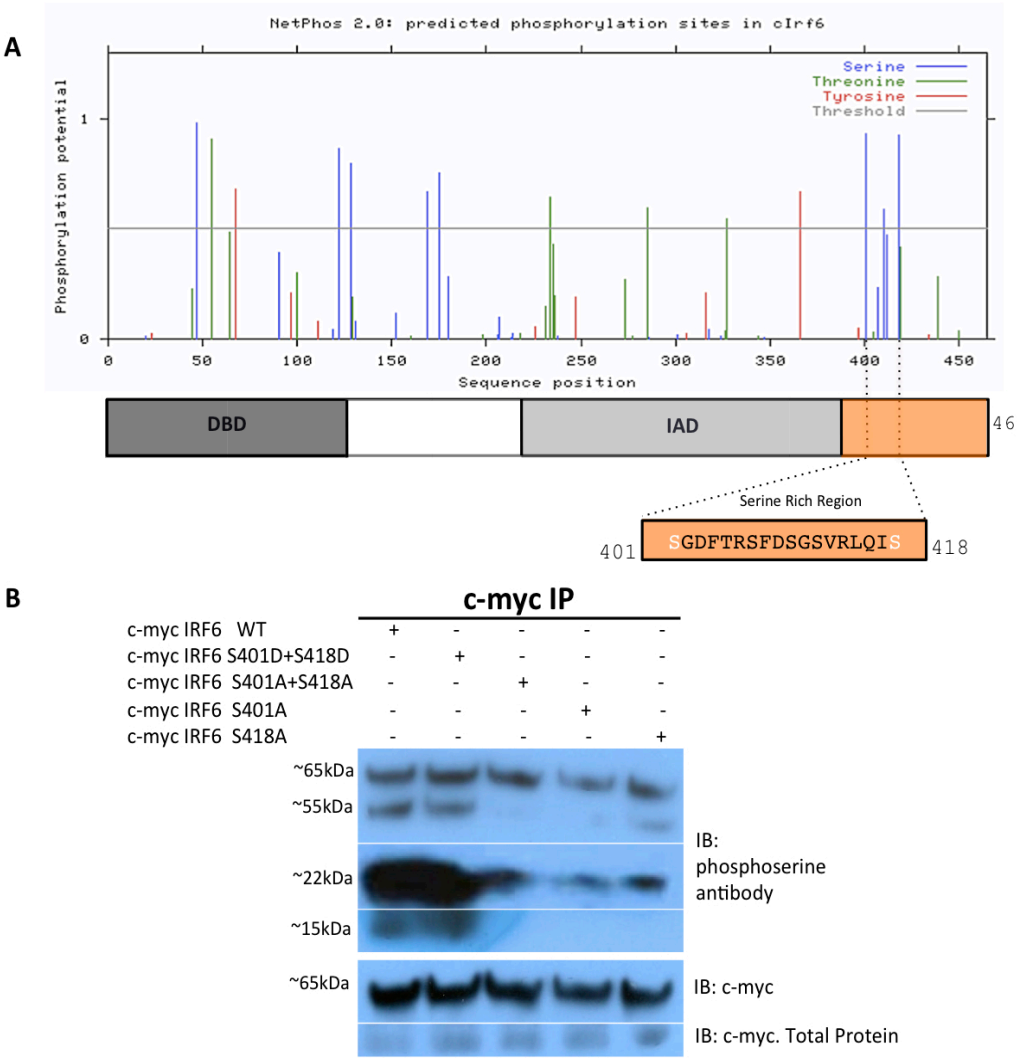

Figure 4.6. IRF6 contains phosphorylated serine residues. A. Computer assisted detection of potential serine phosphorylation sites in IRF6. Two potential serine phosphorylation sites were identified in the IRF6 C-terminus serine rich region, at positions 401 and 418 using NetPhos 2.0 software. **B.** These serines were mutated to alanine (that prevents phosphorylation) and aspartate acid (that mimics phosphorylation). Mutant phosphorylation sites and wild type c-myc IRF6 constructs were transfected into 293T cells, immunoprecipitated with anti-c-myc antibody agarose beads, and analyzed by western blot analysis using an anti-phosphoserine antibody. Protein band at ~65 kDa, which corresponds to c-myc IRF6 (after stripping and blotting with anti c-myc antibody) demonstrated that IRF6 contains phosphoserine residues, and mutation of serines S401 and S418 to either alanine to aspartic acid do not alter the overall phosphorylation state of the protein. However, phosphoserine detection of protein bands at ~55KDa and ~22kDa, and ~15kDa are remarkable affected and inhibited respectively by the presence of the alanine substitutions. DBD (DNA Binding Domain); IAD (Interferon Association Domain).

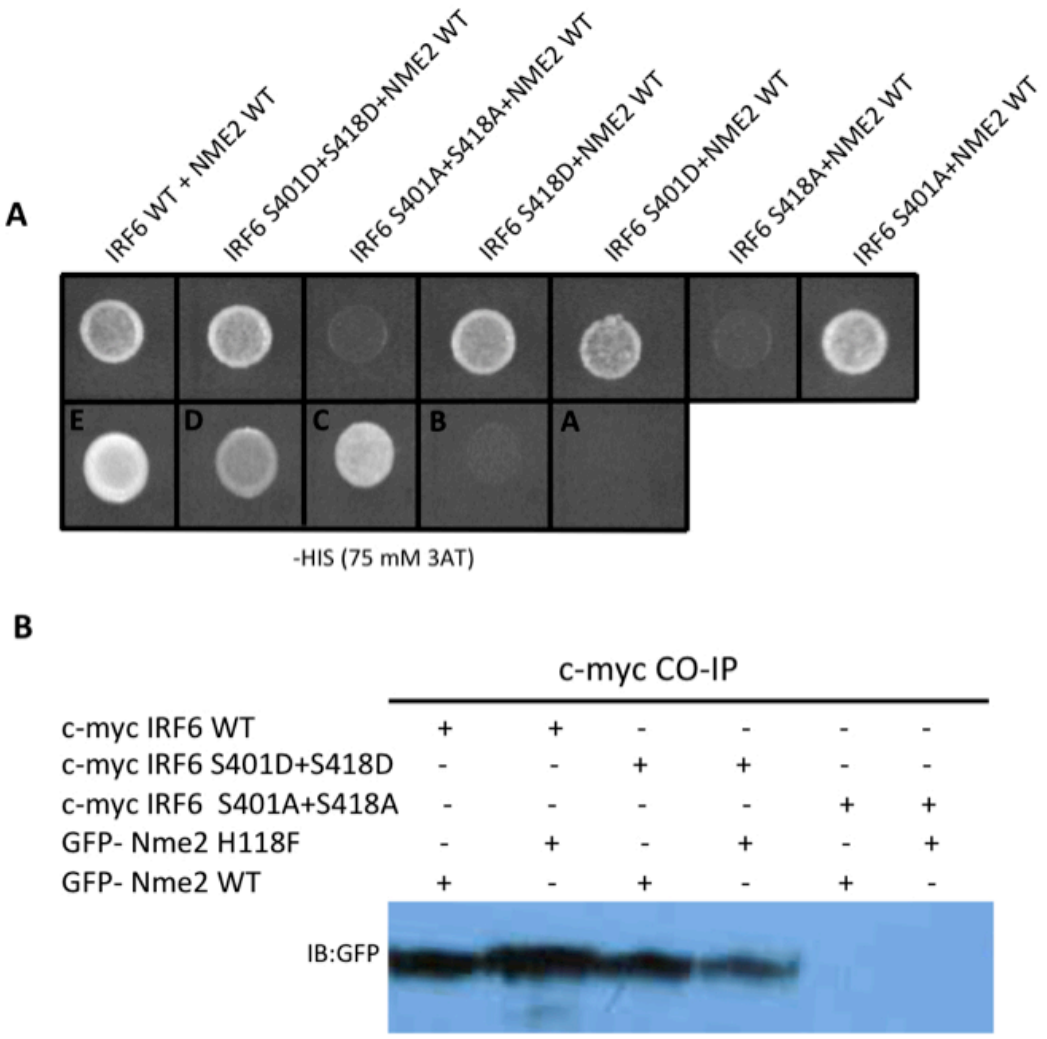

Figure 4.7. The IRF6:NME2 interaction is dependent on IRF6 C-terminal serine phosphorylation but does not require NME2 nucleoside diphosphate kinase activity. A. Direct yeast two-hybrid assays testing interaction between IRF6 mutated phosphorylation sites and NME2. Mutation of both serines S401 and S418 to alanine residues blocked the interaction-dependent growth on selective media. Conversely, substitution of these serine residues to the phosphomimic aspartic acid residues stimulated robust growth. The single mutations S418D and S418A showed a stronger effect in enhancing and inhibiting the growth than S401D and S401A respectively. Positive and negative controls (labeled A, B, C, D, and E) were included on the same yeast selection plate. **B.** c-myc co-immunoprecipitation studies corroborated the yeast two-hybrid observations regarding the effect of double alanine and aspartic acid mutations in influencing NME2 interaction. In addition, co-immunoprecipitated GFP-NME2-H118F was detected following c-myc immunoprecipitated IRF6 WT and S401D+S148D, but not with IRF6 S401A+S148A.

IRF6 Binds to NME2 and Remains in the Cytoplasm of MDCK Epithelial Cells

From studies on other members of the IRF family, serine phosphorylation in the C-terminal region is believed to trigger a conformational rearrangement that leads to homo- or heteromerization of the IRF member, transport into the nucleus and interaction with various transcription factors and co-modulators to activate gene expression (Taniguchi et al. 2001; Honda & Taniguchi 2006, Chen at al, 2008; 2010). In an attempt to investigate if the C-terminal serine phosphorylation status of IRF6 also plays a role in its translocation to the nucleus, Madin-Darby Canine Kidney epithelial cells were transfected with GFP-NME2 and either c-myc-tagged wild type IRF6 or the double phosphoserine mutants (S401A+S418A; S401D+S418D). Analysis by confocal microscopy showed that ectopically expressed wild type IRF6 was primarily found in the cytoplasm with only limited amounts in the nucleus. In contrast, ectopic NME2 could be found equally in both compartments in most cells. These results are consistent with the findings of others (Kraeft et al, 1996; Bosnar et al, 2009). The S401D, S418D double mutant when ectopically expressed showed a similar distribution to wild type IRF6. Importantly, co-expression of NME2 with the double mutants did not have any effect of IRF6 translocation to the nucleus and showed the same localization pattern as shown on Figure 4.8.

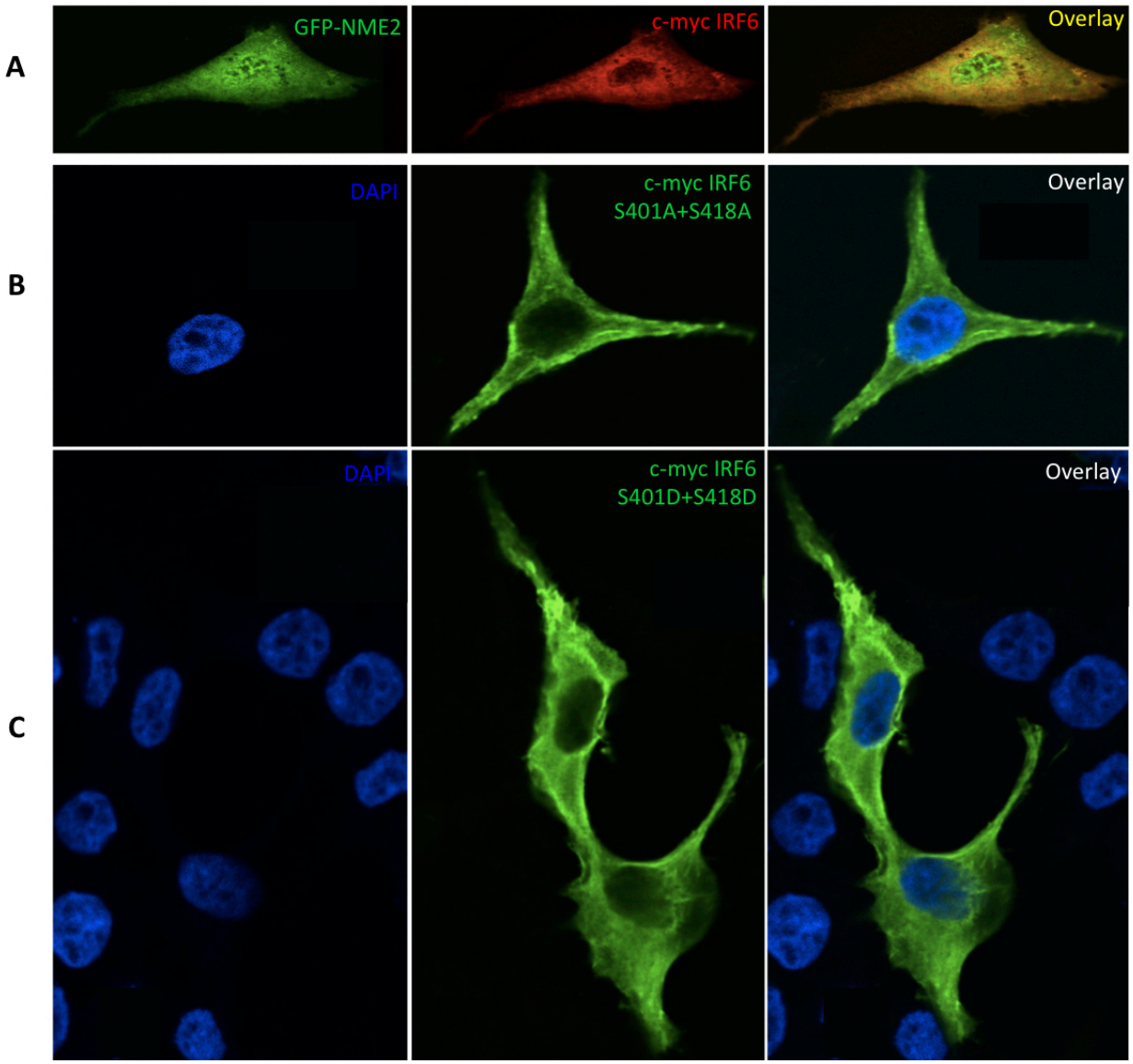

Figure 4.8. Immunofluorescence of ectopically expressed IRF6 and NME2. A. Co-expression of c-myc-IRF6 (red) and GFP-Nme2 (green) in transiently transfected MDCK cells showing that while NME2 is found in both the cytoplasm and nucleus, IRF6 primarily localizes in the cytoplasm. Co-localization in the cytoplasm is shown in the overlay image. **B**. Cytoplasmic expression localization of c-myc IRF6 S401A+S401A (green) and **C.** IRF6 S401D+S401D (green) of transiently transfected MDCK cells. Overlay images also show DAPI stain (blue), which indicates the position of the nucleus.

Specificity of IRF6: NME2 Interaction. IRF6 does not Bind NME1 Directly

Given that NME1 and NME2 share 88% overall amino acid identity (Figure 4.9A), it was considered that IRF6 might also be capable of interacting directly with NME1. To test this, vectors expressing full-length wild type IRF6 and full-length NME1 were transformed into MaV203 yeast for assay using the two-hybrid system. The IRF6:NME2 interaction was used as the positive control. As shown in Figure 4.9B, co-transformation of NME1 with any of the domain-specific deleted IRF6 proteins did not result in any notable growth or X-gal conversion on the respective selection plates, compared to the growth/color of IRF6/NME2 interactors. These findings imply that NME1 does not directly interact with IRF6 despite the high degree of similarity with NME2. Therefore it appears that there is considerable specificity in the interaction of IRF6 with NME2.

NME1 Forms Part of the IRF6:NME2 Complex

Although NME1 does not appear to directly interact with IRF6, it has previously been reported that the NDPK A and B enzymes, encoded by NME1 and NME2 genes, respectively, associate as homo or hetero hexamers to be catalytically active (Pinon et al., 1999). Therefore the possibility that NME1 was still part of the IRF6:NME2 complex via an interaction with NME2 was investigated by co-immunoprecipitation. As the first step, heteromultimerization between NME2 and NME1 was verified by anti-c-myc co-immunoprecipitation from extracts containing c-myc-NME2 and GFP-NME1. As shown in Figure 4.10A, these experiments clearly demonstrated that NME1 and NME2 do indeed heteromultimerize. An anti-c-myc co-immunoprecipitation was then performed using extracts containing c-myc-IRF6, untagged NME2 and GFP-NME1. As shown in

Figure 4.10B, GFP-NME1 co-precipitated with IRF6 when NME2 was also co-expressed, suggesting the existence of an IRF6:NME2:NME1 complex.

A

```
cNME1 MASISERTFIAIKPDGVQRGLVGEIIRRFEQKGFKLVAMKLTHASEDLLREHYIDLKDRPFYAGLVQYMHSGPIVAM
cNME2 MAANCERTFIAIKPDGVQRGLVGEIIKRFEQKGFRLVAMKFVHASEDLLKQHYIDLKDRPFYPGLVKYMNSGPVVAM

cNME1 VWEGLNVIKTGRVMLGETNPMDSKPGTIRGDLCVQVGRNIIHGSDSLESAEAEINLWFSPEELVDYRSCAHEWIYE 153
cNME2 VWEGLNVVKTGRVMLGETNPADSKPGTIRGDFCIQVGRNIIHGSDSVESAQKEISLWFKPAELIDYRSCAHDWVYE 153
```

B

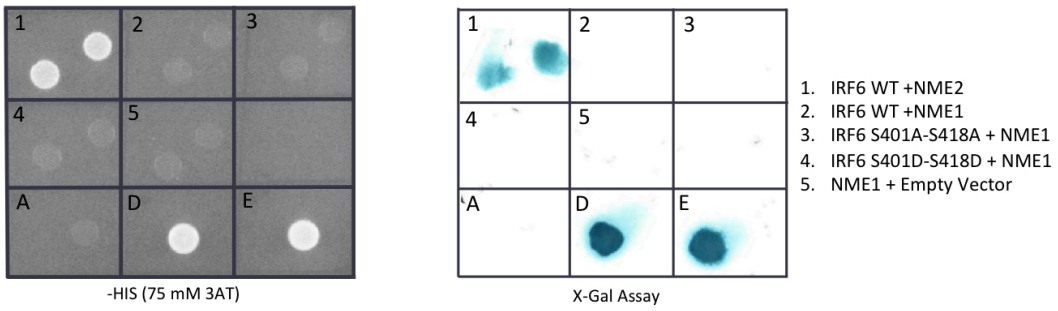

Figure 4.9. NME1, the closest related protein to NME2, does not bind to IRF6. A. Chick NME1 displays 88% identity with the chick NME2 amino acid sequence. Gray boxes highlight identical amino acids in both proteins**. B.** Yeast two-hybrid assays showing no growth of co-transformed wild type IRF6 and alanine and aspartic acid double mutants, with NME1 on SD-Leu-Trp-His media containing 75mM 3AT and no precipitate with the X-gal assay. Co-transformed IRF6:NME2 was included as a positive control. Positive and negative interacting controls (Labeled as A, D, E) were also included on each plate.

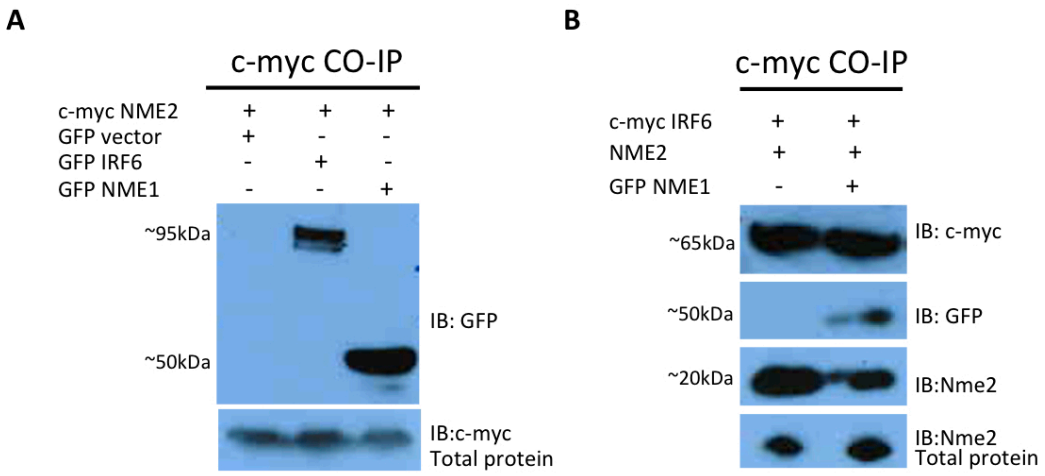

Figure 4.10. NME1 is part of the IRF6:NME2 complex via heteromultimerization with NME2. A. HEK293T cells were transfected with c-myc-NME2, GFP-NME1, GFP vector and GFP-IRF6 separately. Combinations of samples were immunoprecipitated with anti-c-myc antibody agarose beads, separated on 8-12% SDS polyacrylamide gel, transferred to a PDVF membrane and blotted with anti-GFP antibody to detect the co-precipitated GFP-NME1 protein (~50kDa). GFP-IRF6 (~95kDa) was included as a positive control, and GFP vector was included as a negative control. **B**. Similarly, HEK293T cell extracts containing ectopically expressed c-myc IRF6, untagged NME2 and GFP-NME1 were subject to co-immunoprecipitated using an anti-c-myc antibody. Western blot analysis using the following antibodies: anti-c-myc, anti-GFP, and anti-NME2 demonstrated the presence of c-myc-IRF6 (~65kDa), GFP-NME1 (~50kDa) and NME2 (~20kDa) in the sample complex.

Discussion

The major aim of the research comprising this dissertation was to begin to dissect the molecular pathway in which IRF6 functions during the development of the lip and primary palate. IRF6 belongs to a family of nine transcription factors, the interferon regulatory factors (IRFs) that have been mostly studied for their roles as transcriptional mediators of the immune response to viral or bacterial infections (Tanigushi et al, 2001). They have also been studied for their roles in hematopoietic development, cell growth regulation, apoptosis and oncogenesis (Mamane et al, 1999; Paun and Pitha, 2007;

Takaoka et al, 2008; Tamura et al., 2008). IRF6, described as the morphogenic IRF (Takaoka et al, 2008), extended the involment of the IRF family to events seemingly unrelated to the immune response since recent studies have shown a role for IRF6 in the embryonic craniofacial epithelium that mediates secondary palate fusion (Ingraham et al, 2006; Richardson et al, 2009; Thomason et al, 2010). Despite six years of investigation into the role of IRF6 during craniofacial development by numerous research groups, few inroads have been made into understanding the molecular pathways in which it is involved. For this reason, an unbiased yeast two-hybrid screen was undertaken in an attempt to identify new IRF6-interacting proteins that might provide insight into its function in epithelia. This approach has identified NME2, a known regulator of epithelial adhesion, as a *bona fide* IRF6 partner protein.

All IRF members, except IRF1 and IRF2, possess a C-terminal IAD that is responsible for homo- and heteromeric interactions among the IRFs as well as interaction with transcriptional co-modulators (Qin et al, 2003). Structural analyses of the C-terminal transactivation domain (which contains the IAD domain and the flanking autoinhibitory sequences) of IRF3 and IRF5 suggest a mechanism for their activation that may be more widely applicable to other IRF family members (Takahashi et al, 2003; Qin et al, 2003). In IRF3 and IRF5, the N- and C- terminal autoinhibitory regions flanking the IAD interact with each other as well as with the IAD to form a compact hydrophobic structure in the inactive state, thereby occluding specific regions of the IAD domain required for protein interaction (Eroshkin and Mushegian, 1999; Takahasi et al., 2003). Phosphorylation of serine residues located in the C-terminal autoinhibitory portion introduces negative charges that open the structure for binding by other proteins (Qin et

al, 2003; Chen et al, 2008). Based on the studies presented in this chapter, a similar scenario can be pictured for IRF6.

Through the use of different truncated and mutant constructs, the new data described here indicate that IRF6 and NME2 interact through the IAD domain, but require the phosphorylation of two specific serines located in a serine rich region, equivalent to that seen in IRF3 and IRF5, for strong interaction. The kinase responsible for phosphorylation of S401 and S418 is currently not known. The findings therefore support the proposed model in which the auto-inhibition state is alleviated by conformational changes involving the C-terminus of the protein (Lin et al, 1999, Qin et al, 2003). However, the role of such a conformational change and the enhanced binding of NME2/NME1 are unknown and require further investigation.

The experiments outlined in this chapter using ectopically expressed c-myc-IRF6 are consistent with previous reports describing expression of GFP-IRF6 fusions as well as endogenous protein that IRF6 is located predominantly in the cytoplasm of the various cell types examined (Little et al. 2009; Bailey et al., 2009). This situation is analogous to that seen for IRF3, IRF5, and IRF7, which are maintained in the cytosol in latent forms, where upon viral infection, they undergo phosphorylation, dimerization and translocation to the nucleus (Honda et al, 2006; Tamura et al, 2008; Chen et al, 2010; Chang Foreman et al, 2012). To provide insight into the role of IRF6 C-terminal serine phosphorylation (residues 401 and 418), co-transfection and immunostaining studies were performed in the MDCK epithelial cell line as a model for orofacial epithelia. Unexpectedly, both inactivation (S>A) and activation (S>D) mutants of the

phosphoserine residues appeared to have little effect on the intracellular localization of IRF6. One explanation may be that NME2, or perhaps one of the as yet unidentified phosphorylated proteins that co-precipitates with IRF6 and NME2, is required for the nuclear translocation of IRF6. In such a case, the high level of expression from the introduced vectors could significantly alter the stoichiometry in a way that such a putative factor would be limiting. Alternatively, NME2, in binding to the phosphorylated form of IRF6, may prevent its possible dimerization and translocation to the nucleus. In line with this co-expression of NME2 with the double aspartic substitution mutant did not have any effect on IRF6 translocation to the nucleus. Notably, similar chaperone-mediated regulation of the subcellular localization of other IRF members has been reported. For example, STAT2 (a signal transducer and activator of transcription protein) prevents nuclear translocation of IRF9 (also termed p48/ISGFY) (Lau et al, 2000). Similarly, IRF4 interacts with FKBP52, (a peptidyl-prolyl isomerase), which can inhibit IRF4 DNA-binding activity (Mamame et al, 2000). As suggested by Lau et al (2000), it is likely that regulation of the nuclear transport of IRF proteins may be a mechanism shared by IRF members, and could be determined by association with other proteins. In further support of this hypothesis, NME2 has been reported to function as a transcription factor by having the ability to both stimulate and repress transcription through interactions with, and modification of, positive and negative transcriptional elements (Postel et al, 1993; Postel at al, 2000; Marino et al, 2011). Such a function would be consistent with the degree of nuclear localization observed in MDCK cells in this study. Taking together these observations, NME2 seems to be the appropriate candidate to regulate the transcriptional activity of IRF6 not only by controlling its

translocation to the nucleus but also by regulating IRF6 binding to DNA. Consistent with this notion, the data presented in this chapter show that IRF6 and NME2 interact through the IAD protein interaction domain. This domain is the site of many of the IRF6 mutations that underlie cleft lip in patients with van der Woude Syndrome (VWS) (Kondo et al, 2002). In fact, Little et al (2009) reported that these mutations that reside in the IAD disrupt the transcriptional activation function of IRF6 in a luciferase reporter assay. It is therefore possible that many VWS mutations create an IRF6 protein that is unable to bind NME2, which in turn would impact any chaperone transcriptional function that NME2 may exert over IRF6, leading to a CLP phenotype. The next steps in this project would be to test this hypothesis.

The work presented in this chapter has also demonstrated that IRF6 binds directly to NME2, but not to the closely related NME1. There are other examples of distinct interactions that are specific to NME2 or NME1, such as Lbc/Tiam1 (Iwashita et al, 2004; Otsuki et al, 2001). This difference in binding specificity, according to Pinon et al (1999), could be explained by the fact that despite the 88% identity between NME1 and NME2, the amino acids that differ between the two proteins are located at the surface of the hexamers, which provide the interface for protein interactions. In this regard, it is relevant to mention that NME1, as a result of its binding to NME2, is still part of the complex with IRF6 as shown by co-immunoprecipitation experiments.

Interestingly, a lineup of NME1 and NME2 proteins from both chick and humans has revealed other similarities between these related members. In fact, many of the amino acid differences between NME1 and NME2 from one species are not necessarily

differences in the other species. It is therefore unlikely that these specific amino acid differences are functionally relevant. Exclusion of these residues remarkably leaves just four amino acids that appear to be completely specific to each NME protein and therefore one or more of these four residues likely are responsible for the differences in specificity for the interactors of these two NME proteins (Figure 4.11). Future experiments will be aimed at investigating this possibility.

The NME2 protein is an attractive candidate as a potential regulator of the development of primary palate due to its demonstrated expression in the orofacial epithelia, and in particular the pre-fusion epithelia, as well as its many fundamental roles in epithelial cells (Fournier et al, 2003; Bosnar et al, 2009; Marino et al, 2011; Hsu, 2011). NME1 and NME2 are the most abundant and closely related of the NME proteins (of which there are ten) as well as the most studied members of this family. Both interact with, and regulate the expression and activity of, numerous factors already known to be involved in development (Bilitou et al, 2009). Most notable is the fact that NME1/2 have been reported to function at the apical junction complex to regulate epithelial cell adhesion (Fournier et al, 2003; Marino et al, 2011; Hsu, 2011). NME2 has been reported as interacting directly with gamma-catenin and is tethered to E-cadherin in an alpha-catenin-dependent manner (Aktary et al, 2010). Such a link provides a potential mechanism for the coordination of primary palatal fusion. Indeed, studies in mice have suggested a role for IRF6 in maintaining epithelial apical junctions (Richardson et al, 2009). Consistent with this, NME2 could function by having dual roles in primary palatal epithelia; firstly as a component and regulator of the adherens junctions and broader apical junctional complex in epithelia. It is an attractive possibility that this role is linked

to IRF6 binding, and then has a second role within the nucleus as an IRF6 transcriptional co-factor. Such a balance in location between the junctional complex and nucleus would enable tight control between maintaining epithelial tissue integrity and permitting timely proliferation and tissue morphogenesis. There are several precedents for such a dual function, the classic being beta-catenin which associated with E-cadherin in epithelia but upon stimulation with Wnt or Tgf-beta ligands undergoes translocation into the nucleus to turn on gene expression (Jamieson et al, 2012; Zhou et al, 2012). Other adherens junctional proteins that also translocate to the nucleus and/or have a known transcriptional function include ZO1, p120 catenin and Afadin (Bauer et al, 2010; Polette et al, 2007; Pieters et al, 2012; Buchert et al, 2007).

Several important unresolved issues regarding the signal that triggers IRF6 phosphorylation, as well as the physiological role of the proposed chaperone function for NME2 and the details of the mechanism by which IRF6 is actually translocated to the nucleus remain unknown and require further investigation. Nonetheless, the characterization of the IRF6:NME2 interaction and our predicted regulatory and functional mechanisms highlight that the interaction of IRF6 with NME2 may be critical for their function in maintaining the proper cellular phenotype and promises to provide significant new insight into the pathogenesis of CLP.

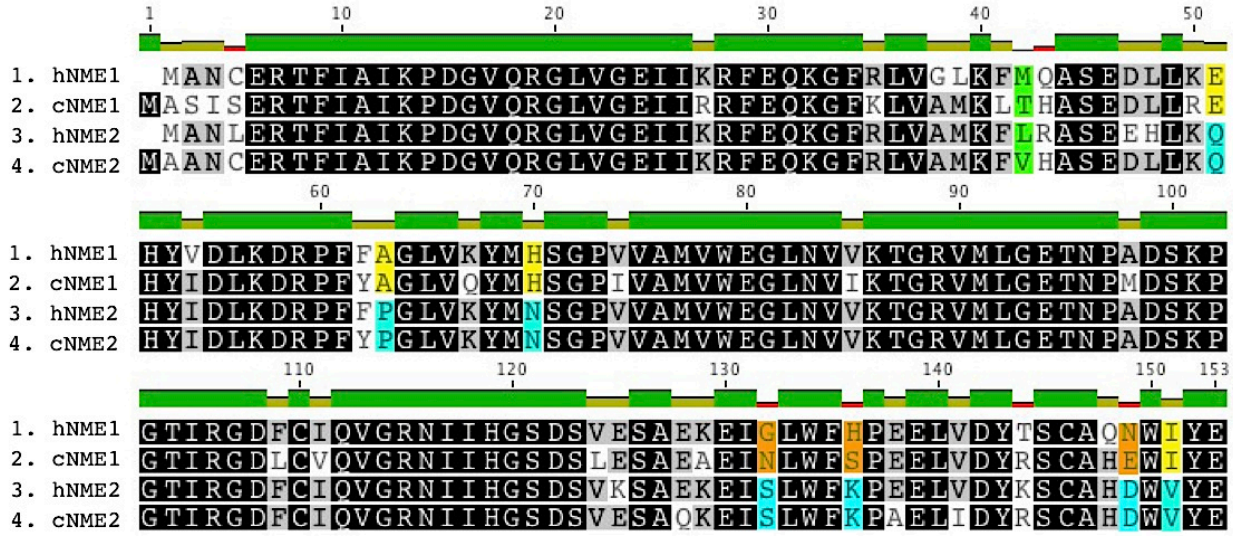

Figure 4.11. Chick and human NME1 and NME2 amino acid differences. Amino acid differences are labeled in color only where the differences were specific to the respective NME proteins. Light blue shading highlight amino acids conserved between chick and human NME2 that are not the same in either NME1 protein. Those in yellow are similarly found in NME1 proteins but not NME2. Those few residues highlighted in orange in NME1 sequences are not fully conserved in NME1 proteins but are different to NME2. There are other residues different between NME1 and NME2 but all others are not specific to either isoform. The only other possible residue is at position 42 (highlighted in green). This differs in all four NME protein sequences shown.

CHAPTER V. *IN OVO* FACIAL ELECTROPORATION, A NOVEL MODEL FOR DNA TRANSFER INTO CHICK PRIMARY PALATAL EPITHELIA

Introduction

Traditionally, transgenic and knockout mice have served as ideal models with which to study developmental gene function. However, issues of genetic redundancy of knocked out genes and potential toxicity of some ectopically expressed transgenes can sometimes be confounding factors. This is especially true when investigating genes with early or lethal phenotypes or those that form part of a small gene family. Notwithstanding these issues, the high costs associated with genetic manipulation of the mouse, the time and potential problems involved in their creation can be significant issues on their own.

The lack of a phenotype in a knockout model also severely limits the investigation of the mechanism of a disease process. Unfortunately for cleft lip and palate research, the mouse has not proven to be the best animal model as few strains or knockout animals present with classical CLP. Indeed, this has been encountered with the IRF6 knockout mice, which display craniofacial anomalies with no evidence of primary palatal clefting. This may be due to the elongated snout in the mouse and the associated increased time necessary for the facial processes to make contact (Cox, 2004). In contrast to mice, chick embryos have a relatively flat midface at the time of primary palatal fusion, which resembles that seen in developing humans (Cox, 2004). In addition, the chick face is more accessible for manipulation during most stages of craniofacial morphogenesis at a low cost (Young et al., 2000).

Molecular studies in the chick have significantly contributed to the understanding of normal lip and palate development (Jiang et al., 2006). Furthermore, the chick is gaining momentum as a predominant species for studies into vertebrate development since *in ovo* gene transfer by electroporation was introduced to the field of developmental biology (Muramatsu et al., 1997). The principle behind this technique is the use of electric pulses to create transient pores in the plasma membrane of target cells through which the negatively charged DNA enters the cell as it moves toward the anode in the electrical field. Surprisingly, although *in ovo* electroporation is widely used to transfect a variety of different of chick embryonic tissues at early embryonic development (Table 4.1), this technology has not been applied to the study of primary palatogenesis. To this end, a reproducible technique, by which DNA can be precisely introduced in a temporally and spatially controlled manner into the pre-fusion facial epithelia and expression sustained for up to 8 days post-electroporation, was developed and is described in this chapter. Electroporation of advanced stage chick embryos used to target the pre-fusion of the facial epithelia had not been reported previously. Successful implementation of this method at this advanced stage required optimization of the appropriate conditions including electroporation settings, electrode design and placement, inter-electrode distance and amount of plasmid DNA required to ensure high transfection efficiency and survival rate with no artifacts or damage of the embryo. This technique represents an efficient and inexpensive method to introduce plasmid DNA and study the function of specific genes in primary palatal epithelial cells in the chick embryo by *in ovo* electroporation. Although the technique described in this chapter was used to investigate the role of IRF6, the protocol was designed specifically for

manipulation of any candidate gene in the primary palatal epithelia by *in ovo* electroporation.

Experimental Procedures

Equipment and Materials for Electroporation

Intracel TSS20 Ovodyne Electroporator

Leica EZ4HD dissecting microscope

Leica MZ8 fluorescent stereomicroscope

Micropipette puller (Stoelting Microforge)

SMI borosilicate capillary tubes B (Cat. No. P5070-909)

Mouth pipetter (custom designed)

Sonicator Aqua Wave 9374. Barnstead/Lab-Line

Dry Sterilizer (Germinator 500).

Stationary Forced Air egg incubator (Marsh automatic incubator)

Profi Setter egg incubator

Mini plastic spoons

0.35-mm plastic petri dishes with lids

Fresh Stabilizer Disinfectant (Grapeseed oil extract)

Dumont tweezers #5

Adson forceps

Small straight pointed mini dissecting scissors

Large pointed straight dissection scissors

Tungsten wire 0.020” diameter (Cat. #73800, Electron Microscopy Sciences)

Watchmaker Pliers

Kimwipes

Scotch tape

Egg holder

Hyclone DPBS (Thermo Scientific)

White Leg-horn Cross fertilized chicken eggs (Featherland farms, Coburg Oregon)

Chicken physiological saline (137 mM NaCl, 5 mM KCl, 2 mM $CaCl_2$, 1 mM $MgCl_2$, 1 mM Na-phosphate, 5 mM HEPES, 11 mM glucose, pH 7.4)

MQ H_2O (Autoclaved)

Fast green solution (0.1%)

0.22 μm Millex GP filter (Millipore Co., Bedford, USA).

Electroporation System

The Intracel TSS20 Ovodyne Electroporator is a square wave pulse generator specifically designed for in ovo electroporation. This system combines several features including low cost, simplicity of operation with adjustable voltage from 0.1V to 60V and space between pulses (Intracel) that allows both high transfection efficiency and survival. Furthermore, as shown on Table 5.1 this system has been used successfully to electroporate a wide range of embryonic age chick embryos from Hamburger & Hamilton stages HH9 to HH19. Electroporation conditions used in these studies served as reference to optimize the technique for primary palatal epithelia. Therefore, the

combination all of these features made this system the choice for the work presented in this chapter.

Plasmid DNA Preparation

Plasmid DNA was purified using the Qiagen maxiprep kit to ensure the obtention of concentrated high-quality DNA. DNA pellets were dissolved in TE buffer to a concentration of 4-8 µg/ul, and 4 µg of DNA was used for each electroporation. A small volume (no more than a microliter) of highly concentrated DNA was necessary to obtain sufficient expression in the electroporated pre-fusion epithelial cells. Two plasmid constructs were used in this study; control plasmids pEGFP-N2 (4.7 kb) and pENTR-D/TOPO-CMV-mCherry-SV40 (4.1 kb), which contain the coding sequence for enhanced green fluorescent protein EGFP and mCherry proteins respectively, driven by the CMV promoter.

Fast Green Preparation

A 0.1 % (w/v) solution of Fast Green dye was prepared by dissolving in chicken physiological saline or MQ H_2O. The Fast Green solution was then filtered the through a 0.22 µm Millex GP filter.

Preparation of Needles

To fabricate needles for delivery of DNA constructs, capillary tubes were pulled by a vertical puller. The needles were stored in plastic containers with the pulled tip protected from contact with the edges of the container. Before electroporation, the tip was gently broken using forceps and examined under a dissecting microscope to ensure that the

opening was not too large. In general, the optimal tip size was grossly determined by feeling how easy or hard is to pull liquid into the needle. If there was extreme resistance, the tip was too small and the tip was broken again a little higher up. If there was little or no resistance, the opening was too large and a new needle should be used (Blank, M. et al, 2007) (Figure 5.1 A, B). Unless a needle broke during use, a prepared glass needle was used repeatedly and cleaned by rinsing with PBS.

Electrodes

Homemade tungsten electrodes were produced for all experiments. Electrodes were insulated with nail polish leaving only a few millimeters of metal exposed facing the target tissue in order to avoid current leakage and subsequent damage to the blood vessels and non targeted tissue. It was important to make sure the anode tip was as smooth as possible to avoid poking the heart during its placement (Figure 5.1C). Electrodes were gently washed in PBS between or during long experiments that involved electroporating more than 36 eggs at a time, so that coagulated yolk or albumen does not gradually insulate them affecting the passage of the current. In addition, the use of wet sand paper to remove these deposits or forceps to scrape them damaged the coating of the wire affecting their conductivity (Huang 2011, personal communication).

Fertilized Egg Storage

Fertilized eggs were stored in a humidified refrigerator at 16°C for a maximum of one week without significant loss of viability. Storage at 16°C was used as needed to prevent development prior to readiness for incubation. It is worthwhile to mention that

extreme changes in temperature during winter and summer seasons become an undesirable variable affecting the viability of the embryos. For this reason, under these climate conditions, the number of ordered eggs was increased to ensure the collection of the sample size desirable for each manipulation. Before incubation, eggs were warmed to room temperature for at least 30 minutes to avoid the formation of sweating/condensation on the shell due to rapid changes of temperature, that could lead to infection during incubation at a higher temperature.

Egg Incubation

The eggs were cleaned with kimwipes saturated with grapeseed disinfectant solution to avoid contamination during incubation. Eggs were set with their pointy ends down and incubated at a temperature of 100.4°F and humidity of 65% with turning at least three time a day (if using a manual turning incubator) or every 15 minutes (if using an automatic turning incubator) for three and half days, which according to our incubation condition corresponds to HH 21-23, After incubation, eggs were removed from the incubator and kept in an upright position for 30 minutes so that the embryo moved to the center of the egg, facilitating access and promoting proper embryo positioning for electroporation.

Egg Windowing

One or two pieces of scotch tape were placed across the top (blunt side) of the egg so that the shell could be cut without it shattering. When windowing the egg, the point of a sharp-straight pair of large dissection scissors was used to stab or twist a small hole in the center of the taped area. The hole was then used to start cutting the window. The

taped shell was cut slowly in a circle keeping the scissors angled horizontally to prevent damage of the underlying membrane or embryo until a small round window was made through which to view the embryo. If necessary the hole was enlarged to have better access to the embryo. The inner shell membrane was left intact at this stage to prevent dehydration and the window was closed with scotch tape until the embryo was ready for electroporation. The eggs were replaced in a static incubator if not needed for some time.

Taking Care of the Membranes

Eggs to be manipulated were placed on an egg holder to support the egg and avoid any movement during the procedure. Working under the microscope and using Adson forceps, the shell and inner shell membrane over the head of the embryo was carefully pulled back to an area away from vessels to reveal the embryo (Figure 5.2 A, B). The egg was discarded if not fertilized and the developmental stage of the embryo was estimated by using evidence of eye pigment, dorsal contour from hindbrain to tail, size and shape of limb buds, and size of the maxillary and mandibular processes as landmarks to estimate Hamburger & Hamilton developmental stage 21- 23 for this study. Outliers were discarded.

Both the vitelline membrane and sub-adjacent amnion just above the heart were pulled up using fine #5 tweezers and cut leaving a small hole for insertion of DNA solution and anode.

Injecting DNA

Addition of fast green to the DNA solution enabled visualization and monitoring of the injection (Figure 5.2 C). 1µl of plasmid DNA (4µg/µl) and 0.1µl of fast green (0.1%) was mixed on a small piece of parafilm. The needle was filled with the DNA solution by applying gentle suction through a mouth pipetter. The glass needle was then slowly inserted into the hole and DNA solution was expelled gently over the primary palatal surface ectoderm, avoiding formation of any bubbles. If the DNA solution was not placed correctly, it dispersed instantly over the embryo. Although the DNA solution was expelled under both membranes on the outer surface of the face, it was not confined within an enclosed space. As a consequence, this required the speedy performance of the following steps.

Placing Electrodes

The electrodes were held with the right hand in a fixed distance of 4.5mm making sure the end of the electrodes were properly aligned, and pushed down so that they were immersed in the albumin to allow passage of the current with the developing face situated between them (Figure 5.2 c, d). While the cathode was positioned near the top of the head on the vitelline membrane, the anode was quickly inserted through the hole and positioned ventralaterally to the frontonasal prominence, in the space between the maxillary/nasal primordia and the heart with no direct contact between the head. This was performed gently to avoid pushing the DNA solution away and depressing the embryo into the albumin.

Electroporation

After electrode placement, five 30V pulses, each lasting 50ms with 1s in between were applied using a foot pedal. Electroporation under these parameters generated an electric field through the head in which the negatively charged plasmid DNA was pulled to the cells adjacent to the anode side, leading to transfection of the pre-fusion facial epithelia. Electroporation was performed on the right side and the non-transfected side was used as a negative control so that assessment of the effects of manipulation could be made in the same embryo.

Egg Incubation after Electroporation

Following electroporation, the electrodes were carefully removed and one drop of PBS was added, if needed, to hydrate the embryo and facilitate the repositioning of the inner membrane on the top of the embryo. Following this manipulation, the window on the operated egg was tightly sealed with scotch tape to avoid desiccation of the embryo with further incubation. The eggs were labeled accordingly, and returned to the humidified incubator without turning to allow embryonic development to continue until they reached the desired stage. Of note, evidence of death was monitored daily and removed as soon as detected to reduce contamination sources that could affect proper development of the embryos.

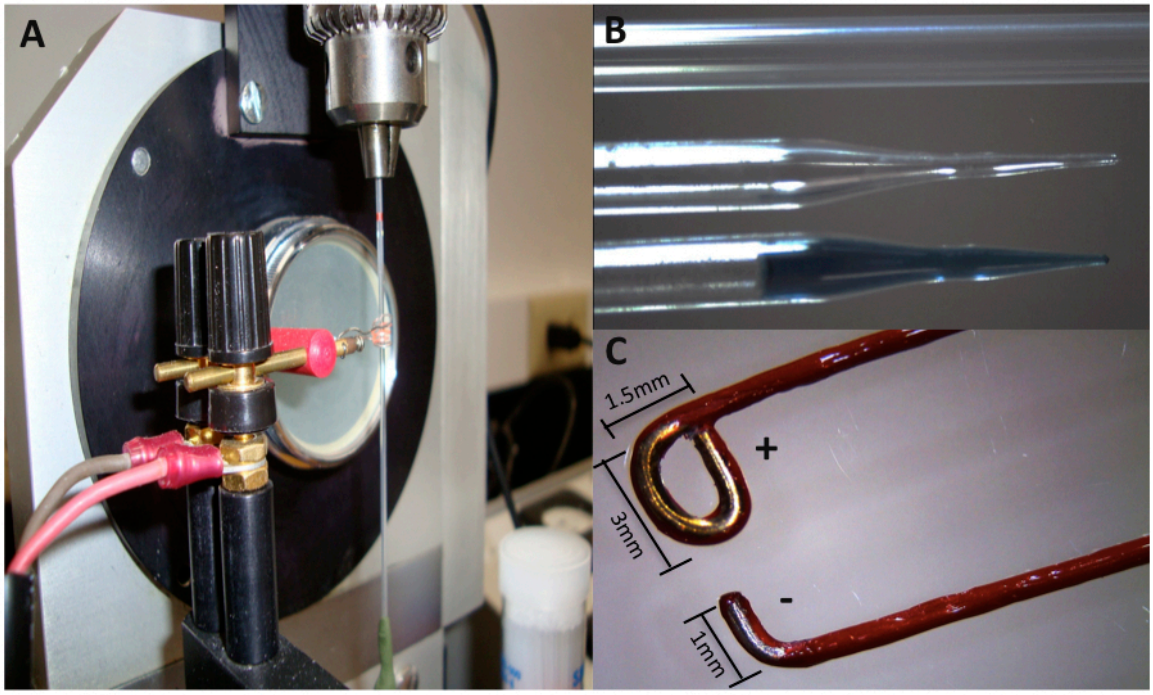

Figure 5.1. Features of the needles and electrodes. A. Glass capillary tubes were pulled vertically to make the needles for DNA injection. Correct alignment of the glass tube and low heating during its rotation were required for even and slow elongation of the tip so that it could hold one microliter of DNA and green fast dye solution, as shown on **B**. Homemade tungsten electrodes were insulated with nail polish exposing 1 mm and 3mm of metal (wide) on the anode (-) and cathode (+) respectively on the side facing the tissue **C.** This particular design facilitated electroporation of a larger population of orofacial epithelia.

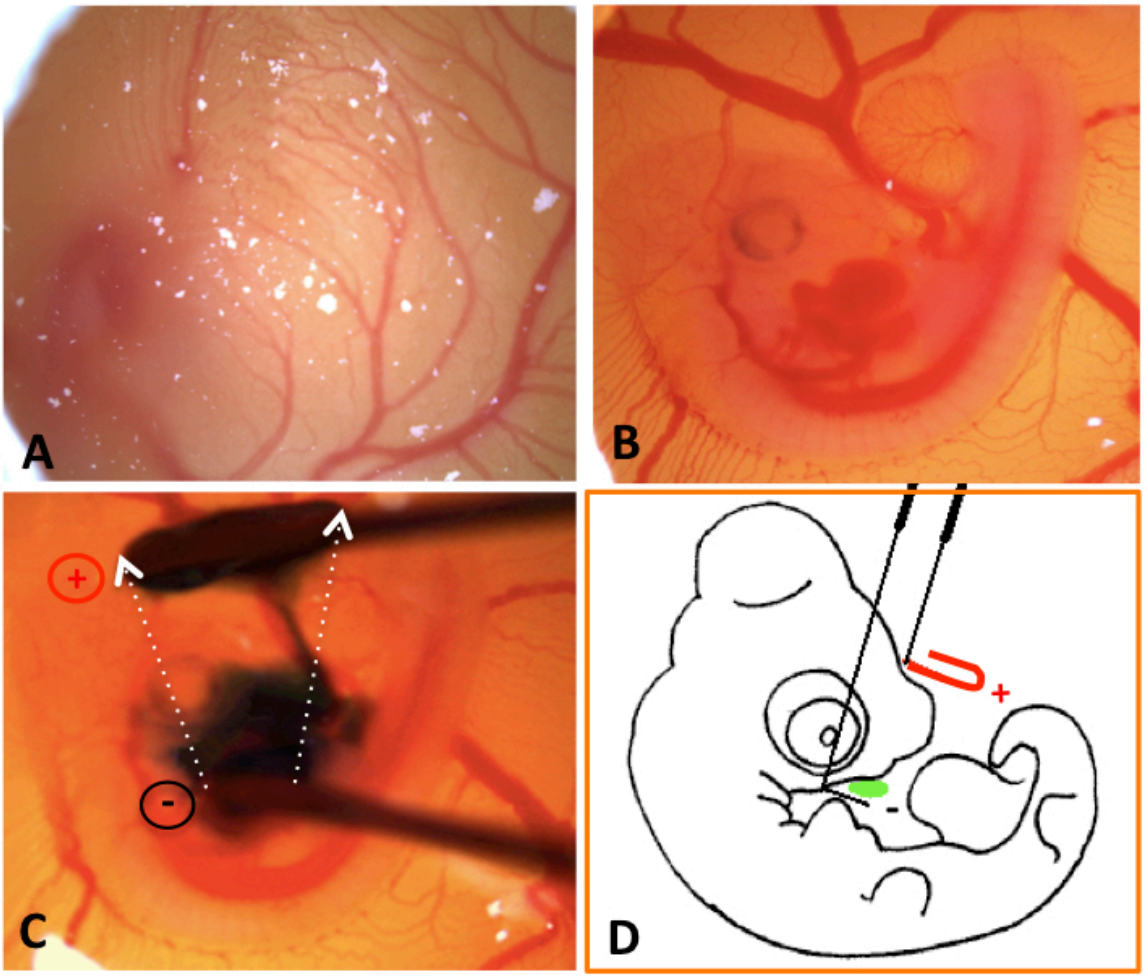

Figure 5.2 Unilateral electroporation of plasmid DNA into the pre-fusion epithelia. The shell above the air pocket (**A**) and the inner membrane (**B**) are removed to expose the 3.5 day old embryo for *in ovo* manipulation under a stereomicroscope. Fast Green is added to DNA to facilitate visualization of DNA solution injection over the developing chick face. Electrodes: anode (-), cathode (+) held with the right hand are placed immediately after to direct gene transfer into the primary palatal epithelia (**C**). Schematic illustration of the *in ovo* electroporation method. The green circle represents the location of the DNA. The anode in black and the cathode in red are positioned with the right hand so that the face is located between them (**D**).

.

Analysis of Control/Treated Embryos

Chick embryos were harvested at different time points after electroporation. The head of the embryos were dissected directly in cold PBS removing the attached extra-embryonic membranes under a dissecting microscope. EGFP or mCherry expression in electroporated embryos was visualized under a fluorescent stereomicroscope and images collected. Chick heads were then fixed in 4% paraformaldehyde/4%sucrose in PBS for 2.5 h at 4°C on a rocking platform for wholemount immunohistochemistry, OPT analysis or using Methacarn (methanol:chloroform:acetic acid; 6:3:1) for paraffin embedding.

GFP Chick Whole Mount Immunohistochemistry for OPT

After fixation, chick heads were washed three times with PBST 15 minutes at room temperature, and incubated in blocking solution normal goat serum in PBST overnight at 4°C. The heads were then incubated with rabbit polyclonal anti GFP antibody (1:500; ab290, Abcam) diluted in blocking solution overnight at 4°C, followed by frequent and gentle washes with PBST during the day. After these washes, heads were incubated with Alexa Fluor 568-conjugated goat anti rabbit (1:300; A-11011, Invitrogen) diluted in blocking solution overnight at 4°C, and washed in PBST during the following day before OPT processing.

Immunohistochemistry on Frozen Sections

Following fixation, the heads were washed 4 consecutive times for 15 minutes each in ice-cold 4%Sucrose in PBS and cryoprotected with 30%sucrose in PBS overnight (until the tissue sank). Specimens were then embedded in optimum cutting temperature

compound (Tissue-Tek O.C.T.), frozen in dry ice and stored at -80°C freezer for up to several months. Cryostat sections (10µm) were collected using a Leica cryostat microtome (model CM3050S) and transferred onto Superfrost® Plus microscope slides. Sectioned tissue was allowed to air dry 2 h at room temperature, washed with PBS 3 times for 5 minutes each at room temperature to remove O.C.T. Then, a hydrophobic pen (Aqua-Hold,Scientific Device Laboratories) was used to create a barrier around the tissue section for the following incubation steps. Sections were incubated in PBS containing 0.25%Triton-X-100 for 10 minutes, followed by 3 washes in PBS for 5 minutes each. The sections were then incubated in blocking solution (10% (v/v) goat serum in PBST) for 40minutes, followed by incubation overnight in a moist chamber at 4°C with mouse monoclonal anti E-Cadherin antibody (1:1000; 610181, BD Biosciences) diluted in blocking solution. The next day, followed by four 5 min washes in PBS and 1h incubation at room temperature in the dark with the Alexa Fluor 488-conjugated goat ant mouse antibody (1:300; A-11001, Invitrogen), the slides were washed 4 times with PBS and then mounted onto coverglass (Corning) with mounting media with Dapi (Vector Laboratories). Images were captured using the Leica confocal microscope SP5.

OPT Sample Preparation, Scanning and 3D Reconstruction

OPT was carried out as described in Sharpe et al. (2002). Anti-GFP stained chick heads were embedded in a 1.0% low melting point agarose in H_2O and attached to a metal stub. After trimming the agarose around the specimen, the mounted embryos were magnetically attached to the metal lid of glass containers and kept protected from the light. Embedded embryos were dehydrated with 100% MeOH 24 hrs with 3 changes

prior to clearing by immersion in BABB solution (1 part benzyl alcohol: 2 parts benzyl benzoate) for 24hrs. Fresh BABB was used in the final step before scanning to ensure removal of all MeOH. The specimen was then loaded into the Bioptonics OPT Scanner 3001M installed in the Seattle Craniofacial Center's SANTA facility, University of Washington, USA. Images were acquired using UV light at different wavelengths to capture embryo morphology/anatomy (via autofluorescence) and the antibody staining (via the attached fluorophore). The resulting images were reconstructed using Skyscan proprietary software, automatically thresholded and merged to a single 3D image output using Drishti V2.0 Volume Exploration Software. GFP expression patterns around the primary palatal region were analyzed by 3D reconstruction data externally and in detail by viewing section planes through the embryo head.

Histological Staining

After fixation, heads were dehydrated using 95%EtOH (30min) and 100EtOH (30min; 2 times), and cleared with Histoclear (National Diagnostics; 30min, 2 times) at room temperature on a rocking platform. Then heads were transferred into hot paraffin baths (30min, 2 times), and embedded in paraffin blocks. Heads were oriented for transversal sections. To do this, the top the head stood in the mold so that the longitudinal axis was in upright position. Once paraffin was solidified, the wax mold was kept at room temperature for an hour, and then placed in a plastic bag at 4°C. The mold was detached and the wax block was trimmed to produce a trapezoid shape to aid orientation when sectioning. Sections (8μm) were cut using a microtome (Reichert-Juang model 2030), and transferred to a 39°C water bath. Super frost plus slides were used to pick up the sections onto the surface of the slide, which were placed in an

upright position to let them dry, before placing them in a 37°C oven overnight. At this point the sections were ready for Hematoxylin and Eosin (H&E) staining. The slides were placed in a slide holder and were taken through the following steps: *deparaffinization and rehydration of the sections*, Histoclear (3min, 2min and 1 min), 100%EtOH (1min; 3 times), 80%EtOH (1min), and MQ H_2O (1min). *Hematoxylin staining*, Hematoxylin 560 (SurgiPath, 2min), rinse with MQ H_2O; tap H_2O (3min), acidic rinse (250 ml H_2O and 6 drops of glacial acetic acid, 30sec), rinse twice with H_2O (1 min, 2 times), and rinse with MQ H_2O (1min). *Eosin staining and dehydration,* Eosin 515 (SurgiPath; 1min), 95%EtOH rinse, 100%EtOH (1 min, 2 times); Histoclear (1min, 3 times). Slides were then mounted using Permount taking care to leave no bubbles. To do this, the coverslip was angled and let fall gently onto the slide and the Permount was allowed to spread beneath the coverslip. The sections were dried in the hood overnight. Images were captured using a light microscope (DM 4000B, Leica).

Representative Results

Assessment of Chick Primary Palate Development Following Electroporation

The *in ovo* electroporation technique was adapted and optimized for the study of the primary palate development. This process begins with the formation of the frontonasal primordia and the paired maxillary process at embryonic day E3 (HH18; Hamburger and Hamilton, 1951). Then, the formation of the nasal grooves within the frontonasal process generates the lateral and medial nasal processes, the tips of which subsequently join with the maxillary process to form the nasal openings, the upper beak, jaw and primary palate (Cox, 2004). Remarkably, while this is completed by 5.5

weeks of gestation in humans, contact of the facial processes takes place in the chick by 5.5 days (HH26) and the fusion is completed by day 6 (HH28) (Figure 5.3). Primary palatal fusion is characterized by the breakdown of the contacting epithelia, and formation of a mesenchymal bridge that joins the maxillary, lateral and medial nasal processes. These mesenchymal cells continue to proliferate, but now drive the outgrowth of the upper beak (Sun et al, 2000) in later stages of development. Embryos at around E3.5 (HH 21-23 according to our incubation conditions) were chosen for *in ovo* electroporations since at this age the growth of the frontonasal prominence and the paired maxillary processes are most pronounced yet still readily accessible right before contact of the facial processes. Of note, anatomically, the *in ovo* access to the face can be achieved only up to E4 since the embryonic face starts to sink down and is extensively covered by the allantois and surrounded by bigger vitelline vessels, making it difficult to access at later stages.

Several experiments were performed to elucidate whether the current, electroporation parameters and incubation conditions used in facilitating gene transfer into the chick faces were adequate to ensure that the dynamic morphological changes occurring during primary palate development were not disturbed by this procedure. To determine this, three different control groups were included for this study. 1) *Control vector group* (n:22): embryos that were electroporated with either the GFP or mCherry plasmid DNA. This group controlled for unspecific effects created by the expression of non-functional proteins in the epithelia. 2) *Electroporation control group* (n:20): embryos in this group were subjected to electroporation without expelling DNA. This group was included to assess the presence of artifacts by the application of the current. And 3) *Incubation*

control group (n:21): comprised by embryos that did not receive any pulses or DNA, but were windowed. This group assessed the conditions used for incubation post-electroporation.

After these treatments, embryos were dissected at two time points, E5.5 and E10.5. We compared the gross morphology of the face of embryos under 10x and 20x magnifications. At E5.5 embryos from all the groups did not show any delay in the contact of the facial process. Similarly, at E10.5 the morphology of the upper beak formation was normal. These observations demonstrated that exposure of embryos to the selected electric pulses, manipulation and subsequent incubation of opened eggs during this stage of embryonic development, and over-expression of the non-functional proteins GFP/mCherry do not interfere with the normal development of the manipulated side of the face. Furthermore, histological studies of four mCherry transfected embryos at E5.5-6 (HH 26, 27, 28) showed no visible changes on the morphology of the primary palatal epithelial cells compared to the non-transfected side (Figure 5.4).

Figure 5.3. The rapid development of the chick face. Frontal view of chick faces show the progressive and dramatic changes that takes place in only three days to form the primary palate. The development of the face starts with the formation of the FNP process that appears as a single entity (HH18-19). The nasal pits appear as small depressions at the lateral margins of the FNP (HH21), and the nasal and lateral nasal prominences are still undistinguishable at this point (HH22). As development proceeds, with the elongation of the nasal pits, all the facial prominences become identified and the face takes a square shape (HH23, HH24). Contact of the facial prominences is evident by HH26 and leads to the fusion and formation of the primary palate. And, the shape of the face changes as it starts assuming the shape of a beak (HH27, HH28). FNP (Frontonasal process); MN (medial nasal process); LN (lateral nasal process); MX (maxillary process); MD(mandibular process).

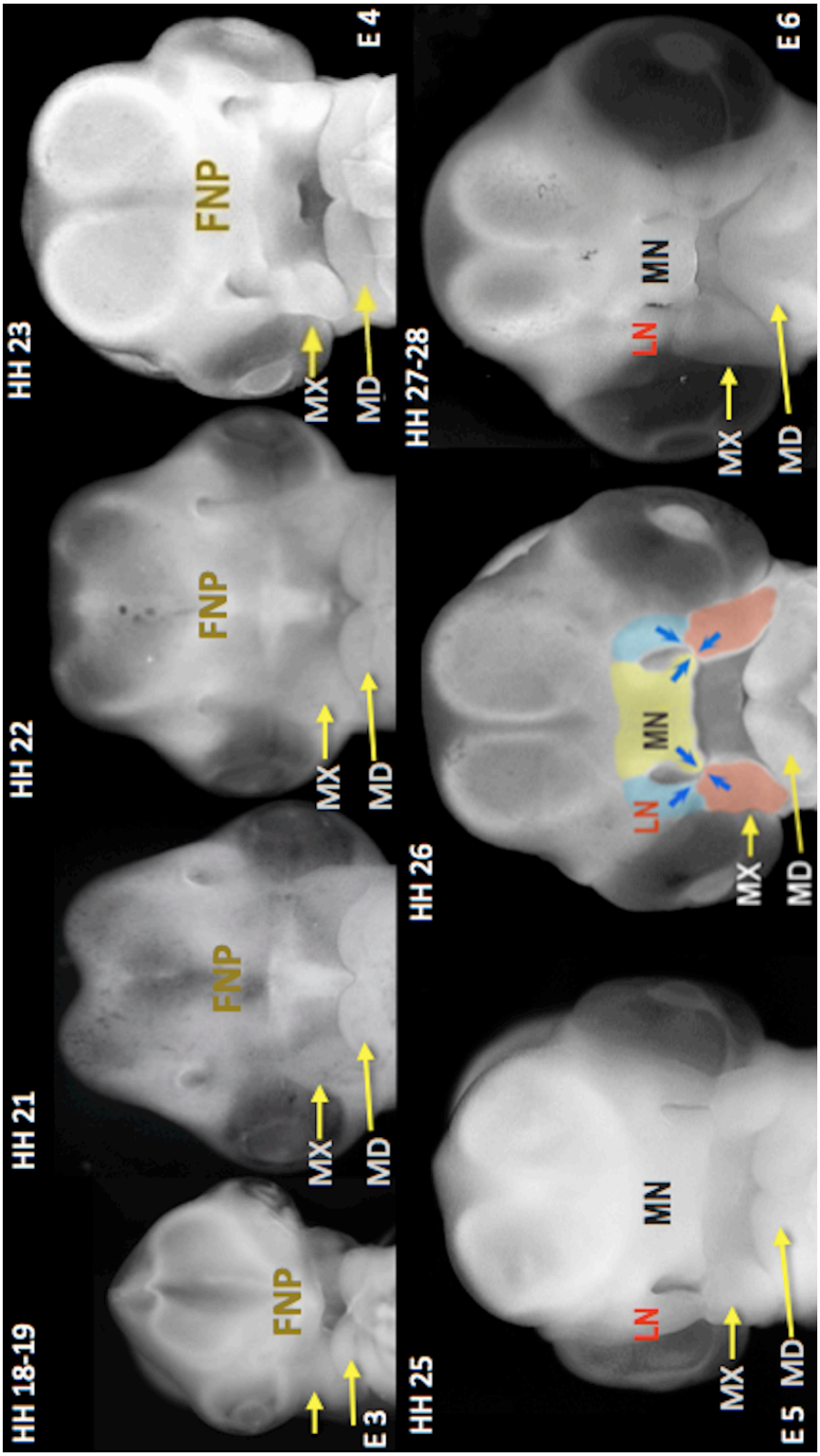
HH 18-19
HH 21
HH 22
HH 23
HH 25
HH 26
HH 27-28
FNP
MX
MD
E 3
E 4
E 5
E 6
LN
MN

Persistent Epithelial Expression of EGFP /mCherry Post - Electroporation

To monitor the success and transfection efficiency by *in ovo* electroporation performed at E3.5, the faces of manipulated embryos were evaluated for the expression of the green fluorescent protein (GFP) and mCherry protein under a dissection fluorescent microscope. Persistent expression of the fluorescent proteins on the manipulated side of the face involving the medial, nasal and maxillary processes remained detectable up to 8 days after electroporation (Figure 5.5), although a gradual decrease of GFP/mCherry expression was observed after 72 hours. This is likely to be the result of degradation and/or dilution of the plasmid DNA during cell proliferation, as plasmid DNA is not incorporated into the host chromosomal DNA (Mamose et al., 1999). Using Optical Projection Tomography (OPT) reconstruction analysis of GFP, it was demonstrated that this expression was restricted to the facial epithelia (Figure 5.6. A, B, C). Furthermore, this epithelial restricted expression was confirmed by immunohistochemistry analysis of E-cadherin on frozen sections of embryos transfected with mCherry (Figure 5.6. D, E).

Efficiency of Pre-Fusion Epithelia Electroporation

Although every attempt was made to consistently target exactly the same electroporation area in order to minimize variation from embryo to embryo, there are inevitable variations among each electroporation, due to individual differences in embryo size, replication of exact electrode position and amount of DNA that actually gets into the cells. However, it is worthwhile to acknowledge that these variations as well as the error that could be introduced by the operator in specific steps such as

cutting the membranes, introducing the needle and placing the electrodes, decreased substantially with the practice and expertise of the operator. Considering these observations, the survival rate of successfully manipulated embryos 2 days after electroporation (E5.5) is high, around 70-80%, and decreases to 60-50% as the embryos are incubated longer (up to 10 days after). Importantly, the transfection efficiency in those that survive is 100%. Furthermore, a large number of embryos with similar transfection efficiency were collected for further analysis to compensate for variability.

Figure 5.4. mCherry control embryos display normal epithelial morphology. mCherry electroporated embryos were collected two days after electroporation (E5.5). Left images show contact and fusion of the facial processes on both side of the face. Right images show histological sections from the same embryos showing, how the primary palatal epithelia is formed by a layer of basal cells covered by a flatted periderm cell layer that initiate contact between the opposing processes at HH26, on both sides of the face (electroporated and non-electroporated). Then, the epithelia on both sides undergo transition to mesenchyme with breakdown of the basal lamina at HH27. Finally, fusion of the primary palatal epithelial is completed on both sides with the formation of a mesenchymal bridge at HH28. MN (medial nasal process); MX (Maxillary process.

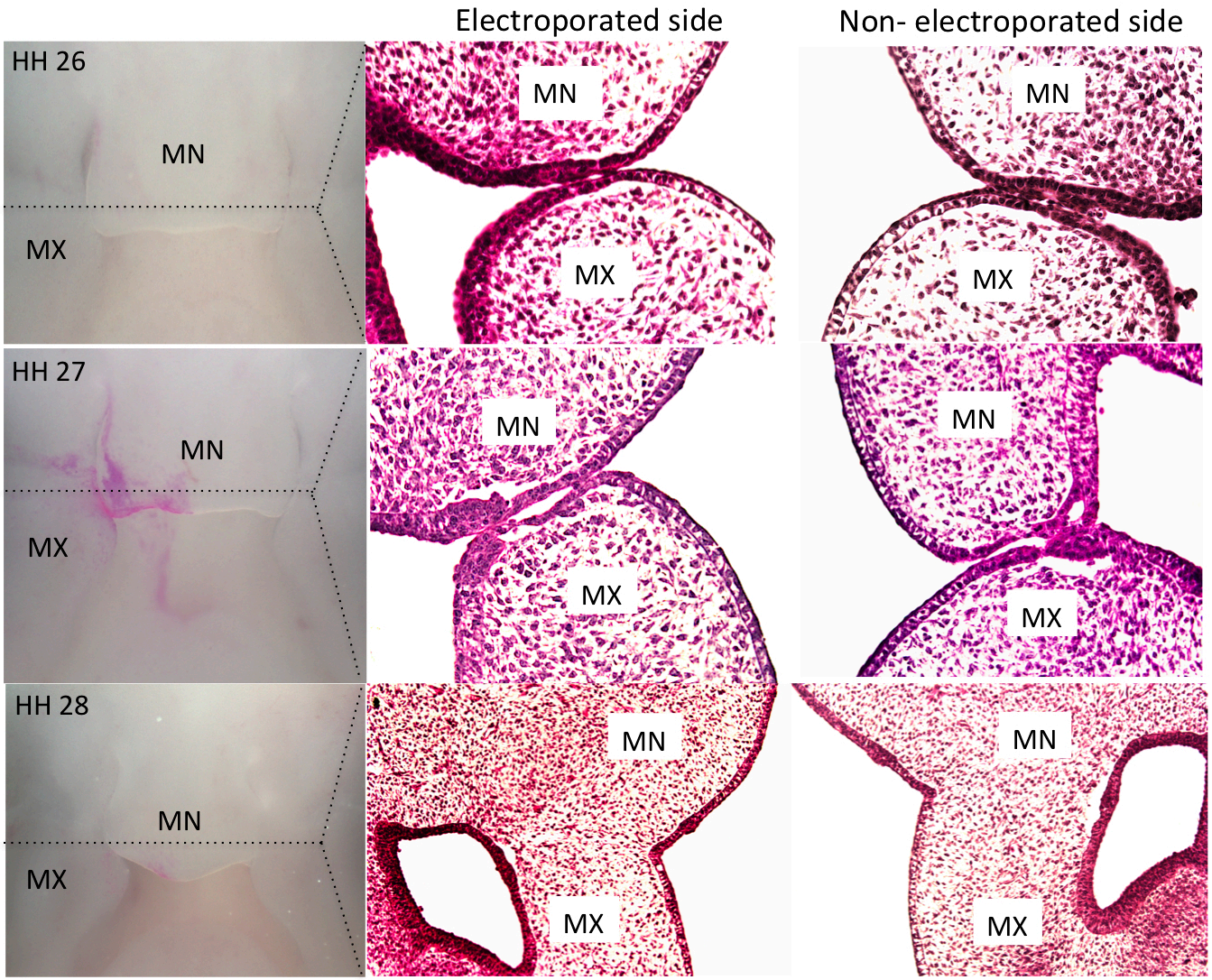
Electroporated side
Non- electroporated side
HH 26
MN
MX
HH 27
MN
MX
HH 28
MN
MX
MN
MX
MN
MX
MN
MX
MN
MX
MN
MX

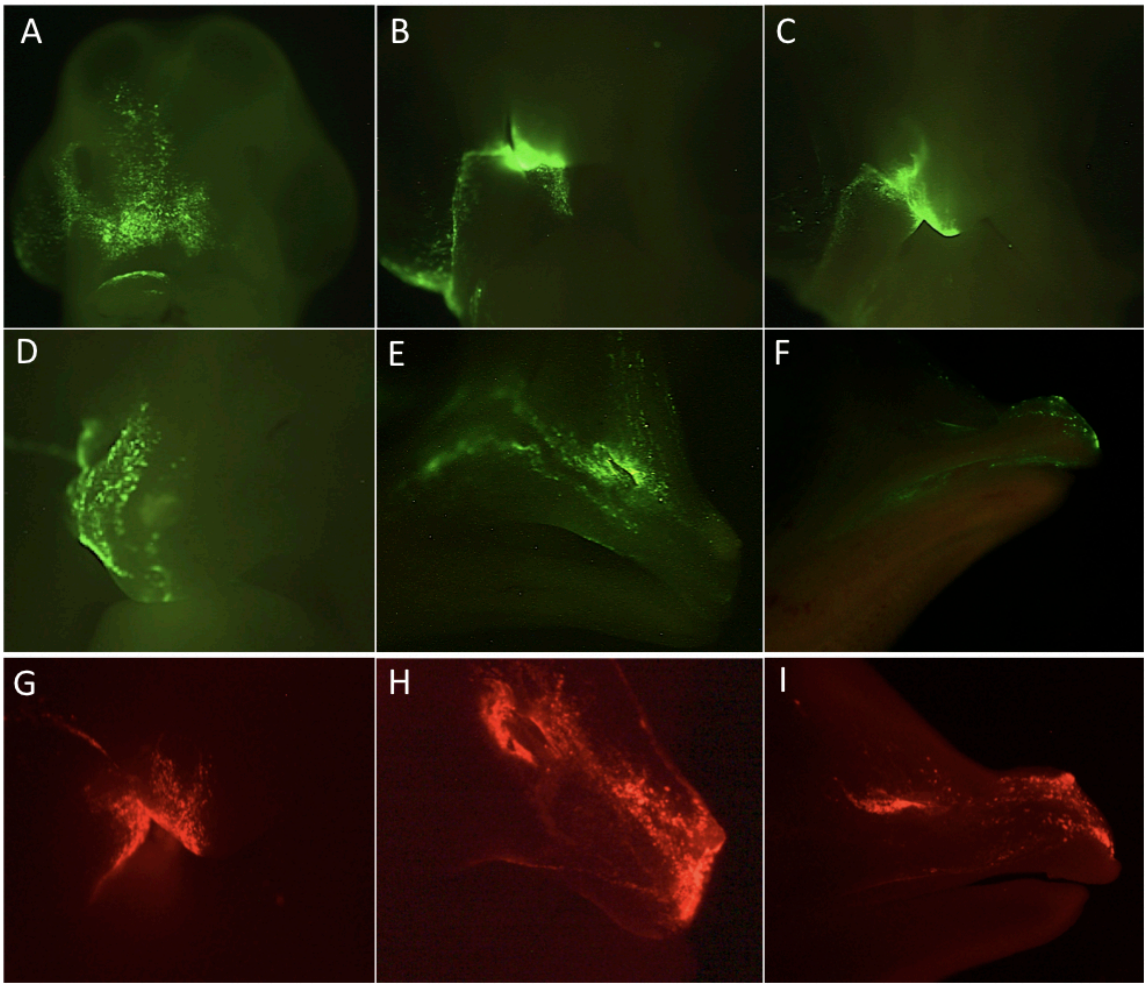

Figure 5.5. Expression of independently GFP or mCherry transfected constructs post-electroporation. Transfection efficiency was observed by detection of GFP or mCherry fluorescent proteins in the facial processes using a dissecting fluorescent microscope. Frontal view images of control electroporated embryos show GFP expression 1(**A**), 2(**B**), 3(**C**) and 5 (**D**) days after electroporation. Similarly, lateral view images show GFP and mCherry expression on the right side of the electroporated beaks 6 (**E, H**) and 8 (**F, I**) days after electroporation respectively. The expression observed for GFP (**C**) and mCherry (**G**) 3 days after, starts to decrease at this point with the outgrowth of the beak. This persistent expression shows that DNA can be electroporated not only in a temporally but also spatially controlled manner as it targets the region that involves the three facial prominences on the right side of the face.

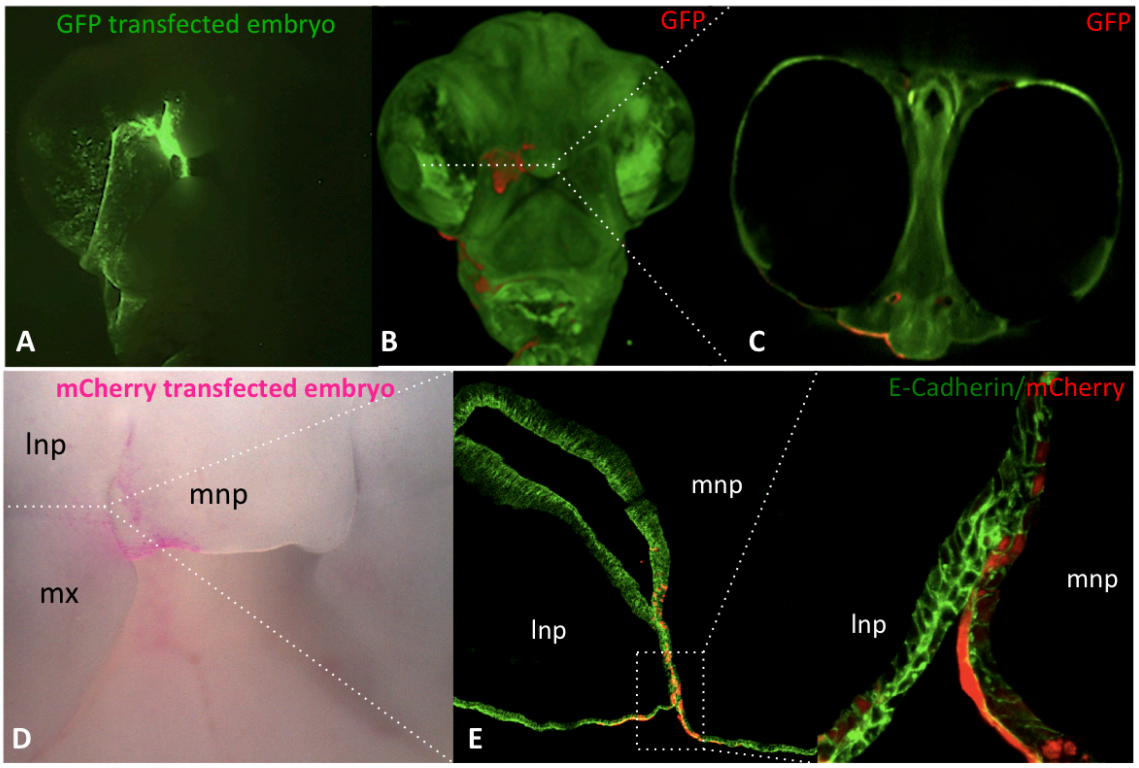

Figure 5.6. *In ovo* electroporation targets only primary palatal epithelia. A. Transfection efficiency was observed by detection of GFP using a fluorescence dissecting microscope**. B.** Optical Projection Tomography (OPT) was used to recreate a rendered three-dimensional image of an anti-EGFP antibody stained embryo, 3 days post-electroporation. In the OPT images, the anti-EGFP signal is colored red, while autofluorescence (green) is used to reveal anatomical detail. **C.** Virtual transverse section of the embryo in **B** showing the epithelial restricted expression (red). Similarly, a transverse section of a mCherry-transfected embryo collected 2 days after electroporation (**D**), stained with E-cadherin antibody (green on **E**) shows that mCherry positive cells (red in **E**) are restricted to the epithelia where E-cadherin is only expressed. mnp (medial lateral process); lnp (lateral nasal process); mx (maxillary process).

Discussion

Optimizing Conditions for Electroporation of the Pre-Fusion Epithelia

Although *in ovo* electroporation is a technique widely used for the study of chick embryonic development, this technique has been mostly applied in the embryonic eye and neural tissues at much younger stages of development (Table 5.1). *In ovo* electroporation of pre-fusion primary palatal epithelia at E3.5 is a novel application of this technology for the investigation of primary palate development. The appropriate parameters for the successful electroporation of the specific target tissue were determined and the most reproducible results with high levels of expression in terms of area electroporated and duration of expression with no damage of the embryo were obtained when using the experimental set-up described in this chapter. The age of the embryo, position and electrode design, inter-electrode distance, and DNA concentration were all critical for the success of this technique.

Design and Position of the Electrodes

Initial experiments were conducted using insulated “L” shaped homemade tungsten electrodes (anode, 1 mm; cathode 3mm wide). These electrodes created a linear electrical field across the head resulting in limited cell numbers being transfected as evidenced by the linear pattern of GFP positive cells in Figure 5.7.B. A “P” shaped cathode with the same dimensions was then used to produce a radial electric field. The new combination of electrodes led to greater area of epithelia being targeted (Figure 5.7.D). In addition to the design, the position of the electrodes was also a critical factor to reach the required electrical charge across the target area. Experiments with both

electrodes positioned on top of the membranes led to very low transfection efficiency. The presence of the membranes along the electrical field interfered with the flow of the current across the head. Therefore, taking into account that the cathode is the electrode that initiates this flow, and it is the closest to the face, it was reasoned that placing the cathode directly in front of the developing face (by removing the interfering membranes at this side) was sufficient to ensure the transmission of the electrical pulses that were required to transfect the primary palatal cells. In line with this, we observed that the "internal" position of the cathode diminished the possibility of disturbing the position of the embryo by creating a tensile force when depressing the membranes, and as a consequence, interfering with the steady position of the electrodes during the electroporation procedure.

Inter-Electrode Distance

Although the cathode did not touch directly the face during manipulation, burned embryos were occasionally observed when using an inter-electrode distance of less than 4mm. In order to overcome this issue, it was taken into consideration the fact that electrical field (E) is dependent upon the voltage (V) and distance between electrodes (d) (E=V/d) (Croteau and Kania, 2011), and it was decided to manipulate only the distance between the electrodes by increasing it to 4.5 mm. This approach diminished the damage to the target tissue as it was decreased the current applied to the target tissue (Krull, 2004).

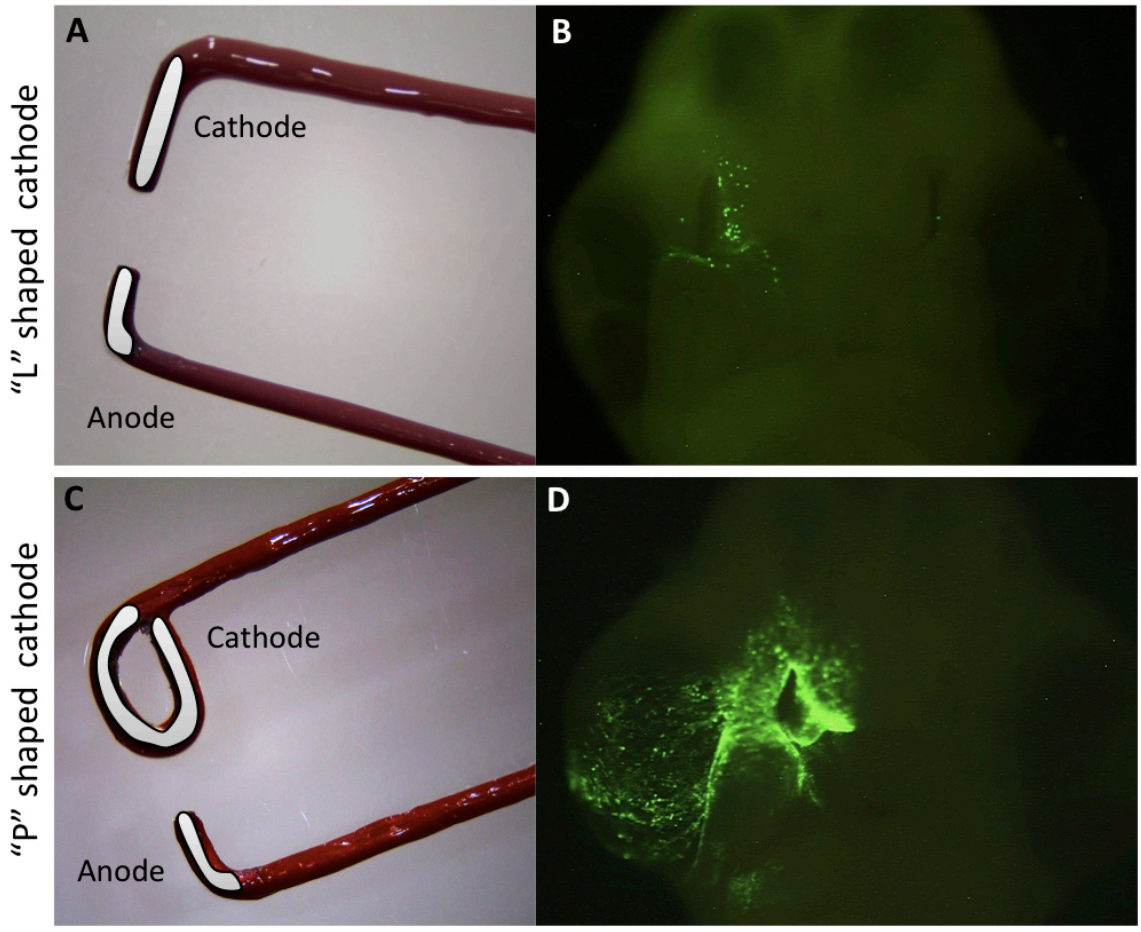

Figure 5.7. Electrode design defines the area to be transfected. Changing the design of the cathode from a "L" shape (A) to a "P" shape (B), but keeping the same design for the anode was crucial to remarkably increase the area of transfection involving the three facial prominences, as shown on B and D.

Optimal Plasmid DNA Concentration

In ovo electroporation has been employed successfully in the neural tube, which is the ideal place for injection of DNA since the lumen serves as a reservoir, limiting DNA diffusion and localizing DNA to the tissue to be transfected (Krull, 2004). However, in this specific case, in order to target the pre-fusion facial epithelia by electroporation, the DNA solution needed to be placed on the outer surface of the face, which meant the use of a small volume of highly concentrated DNA. This approach was in line with the fact that efficiency of DNA transfer by *in vivo* electroporation is dependent on plasmid concentration (Momose et al., 1999). It was observed that a maximum of one microliter of plasmid DNA with a concentration of 4 µg/ul allowed high transfection efficiency and in so doing it was noticed that the high viscosity of the more highly concentrated plasmid DNA prevented its rapid diffusion. Therefore, the presence of additives was not required to thicken the DNA solution and keep it in place. Conversely, it was observed that when a larger volume of a less concentrated DNA was used in order to expel the same amount of DNA (4µg), it diffused away from the face rapidly.

The chick embryo as an animal model is usually used to study the development of the face using more invasive approaches than the *in ovo* electroporation. The replication competent chicken retrovirus (RCAS) was used as an alternative effective gene transfer method to study craniofacial morphogenesis by over-expressing genes such as Sprouty2 (Goodnough et al, 2007), Wnt2b and Wnt3b (Brugmann, et al., 2010), Tbx22 (Higashihori, et al, 2010), Dlx 2 and Dlx5 (Gordon, et al, 2010); however, it requires injecting viral particles or infected cells directly into the tissue so that a broad expression is extended into the mesenchyme. *In ovo* electroporation offers three advantages over

this approach. First of all, the fact that production of plasmid DNA is much simpler than the preparation of high titer virus solutions, which minimizes production time and safety issues (Momose et al, 1999, Yasugi and Nakamura, 2000). Second, expelling a DNA solution over the target region abolishes the likehood of injuring tissue by poking the tissue with a needle. And, furthermore and more importantly, in contrast to the RCAS method, the facial in *ovo* electroporation allows a localized and restricted epithelial expression around the fusion area of the primary palate without involving the mesenchyme.

The development of the facial *in ovo* electroporation technique presented here arose as a necessity of using an alternative animal model to mouse models to the study the unrevealed role of IRF6 during primary palatal epithelial. Three Irf6 mouse mutants have been reported, Irf6gt1, a gene trap VWS-like allele (Ingraham et al., 2006), Irf6R84C, a knock-in PPS-like allele (Richardson et al., 2006), and the IRF6clft1, a knock-in VWS-like allele (Stottmann et al, 2009). All of them present cleft palate, skin and skeletal defects, but they do not reproduce the CLP phenotype seen in humans. Although *in ovo* electroporation has been widely used to study the specific role of genes, mostly associated with neural and optical tissues, by transfecting them with dominant negative DNA constructs or vector-based shRNAs (Table 5.1) at relatively early stages of development. The application of this method to the facial epithelia at later developmental stages had not been undertaken until now. Therefore, the work presented in this thesis extends the utility of this technique to later developmental stages, making gene transfer by *in ovo* electroporation a feasible tool for the study of primary palate development. Furthermore, since primary palate development

progresses rapidly, gene regulation occurs in a very narrow time window. This approach extends the use of the chick model system as rapid means to investigate the function of genes, such as IRF6, that have been implicated in the presentation of CL/P in humans by opening avenues to manipulate its gene expression using loss of gene function studies at desired time points as discussed and demonstrated in Chapter VI.

In conclusion, the present study shows that *in ovo* electroporation provides an easy and efficient method for introducing plasmid DNA into primary facial epithelial cells in the chick embryo at E3.5, and proves to be a strong alternative approach to analyze gene function in chick primary palate development.

Table 5.1. Electroporation parameters in chick tissues other than facial epithelia

STAGE (HH)/ TISSUE	VOLTAGE	PULSES	LENGTH (ms)	INTERVAL	ELECTRODES LENGTH/ DIAMETER (mm)	DISTANCE	ELECTROPORATOR	PLASMID DNA	REFERENCE
9/ Neural Tube	15	5	50		4/0.4-0.5				(Itasaki et al, 1999)
9-11/ Neural Tube	25	5	50	30ms	Platinum 5/0.5		TSS20 Ovodyne (Intracel)	shRNA constructs 3-5ug/ul	(Hernandez and Bueno, 2006)
10/ Neural Tube	10-24	5	50	1s	Platinum 5/0.25	1 mm	BTX T820	DNA diluted in TE or PBS. 2-5ug/ul (3ul use)	(Blank et al., 2007)
10-15/ Neural Tube	20-25	5	50		4/0.4-0.5	4 mm	T820,OPTIMIZER 500, BTX	DNA diluted in TE buffer.	(Itasaki et al., 1999) (Funashi 1999)
11/Anterior neural tube	25	5	25	1s		3-4 mm	Intracel TSS10	RNAi vectors 0.5ul (1ug/ul)	(Mende et al., 2008)
10-12/ Neural tube	27	6	10-50			4 mm	TSS20 Ovodyne (Intracel)	RNAi vectors 0.2-1ul (1ug/ul)	(Das et al, 2006)
13-14/ Neutal tube	25	3	50				BTX	pSilencer 1.0 U6. shRNA vector (0.5-1.8ug/ul)	(Chesnutt et al., 2004)
11-12/ Somites	10-25	5	50 50-90		12/	8 mm		DNA in TE buffer	(Muramatsu et al., 1997)
15/ Somites	55	5	20	200ms			Intracel	2ug/ul in PBS	(Wang et al, 2011)
18-20/ Somites	40	5	50	500ms	(+) Platinum (-) Tungsten		TSS20 Ovodyne (Intracel)	3 ug/ul in Water	(Smith et al, 2005)
18-19/ Spinal Cord	30	5	50	1s	Platinum/ Iridium		TSS20 Ovodyne (Intracel)	Dominant negative, mutant constructs. 5-10ug/ul in TE buffer	(Kao et al., 2009)
7-12/Foregut Visceral mesoderm	5-9 (HH 7-10) 9-14 (HH1012)	1-2	50-90		(+) Platinum (-) Tungsten/ Platinum /0.5 both		CUY 21	8-15ug/ul in TE buffer	Sakiyama et al.,2003)
13-14/ Limb buds	8	3	60	50ms	Platinum		CUY 21	2 ug/ul in PBS	(Suzuki et al., 2008)
10-11/ Lens Placode-Eye	10	3	50		Platinum/ Tungsten		BTX T-820		Momose et al., 1999
9-10/Lens-Eye	25	5	50						(Ogino et al.,1998)
11-12/ Optic vesicles. Retinal pigment Epithelium	2x7		30				CUY21	2 ug/ul in PBS injected into the optical vesicle	(Tsukiji et al., 2009)
15/ Corneal Epithelial cells. Lens fiber cells.	18 20	3 5	50 50		Platinum /0.01 inch		BTX ECM839	2 ug/ul in PBS. DNA injected into the vitreous cavity	(Chen et al., 2004)

HH is Hamburger and Hamilton stage. Spaces in blank indicate that this parameter was not specified in the relevant reference. Gray rows highlight studies using the Intracel electroporator.

CHAPTHER VI. IRF6 MANTAINS THE BALANCE BETWEEN ADHESION AND PROLIFERATION IN PRIMARY PALATAL FUSION. A PROPOSED ROLE FOR NME1/2

Introduction

Lip and primary palate fusion is a dynamic and tightly orchestrated process that starts with a well organized, polarized pre-fusion epithelium that covers the mesenchyme of the merging lateral nasal, medial nasal, and maxillary processes. As these processes start approaching each other, the epithelia undergo a series of remarkable cellular changes, that ultimately allow the formation of an epithelial seam, and its subsequent dissolution through either epithelial to mesenchymal transformation (EMT), collective epithelial migration, or apoptosis. This reproducible developmental program requires the temporal and spatial regulation of the expression of many gene products involved in processes such as proliferation, polarized cell movement, cell adhesion, cytoskeletal reorganization, and programmed cell death (Cox, 2004). Notably, the function of the newly identified IRF6 interactor, NME1/2, although characterized primarily in other epithelial contexts, has been linked to many similar cellular processes (Braun et al, 2007; Boissan et al, 2010; Aktary at el, 2010).

Mutations and common polymorphisms in the *IRF6* gene have been found to be the major genetic contributor to CLP susceptibility in most populations, yet the failure of IRF6 deficient mouse lines to reproduce the cleft lip phenotype seen in patients has hampered progress on understanding the molecular mechanisms controlling primary palatal development (Ingraham et al, 2006; Richardson et al, 2006; Stottmann et al,

2010). To this end, IRF6 DNA inhibitory molecules were designed and delivered into the chick pre-fusion facial epithelia by *in ovo* facial electroporation. The effects of altered *IRF6* gene expression/function were assessed and characterized later in embryonic development. Manipulation of IRF6 function caused failure of primary palatal fusion due to decreased adhesive properties and increased proliferation of primary palatal epithelial cells. In line with these findings, this chapter provides evidence of the possible role of NME1/2 in the presentation of the IRF6 CLP phenotype in the chick system. Furthermore, IRF6 seems to be the principal player orchestrating NME protein locations and their interaction with other proteins to exert their critical functions in maintaining the normal epithelial phenotype.

In summary, a new CLP model for IRF6 that reproduces the phenotype seen in humans is described for the first time in this chapter, and has validated the utilization of *in ovo* electroporation in the chick as an alternative system to investigate the role of IRF6 and its protein partners NME1/2 in primary palatogenesis. More importantly, it has opened new avenues to enhance the understanding of the pathogenesis of CLP.

Materials and Methods

Plasmid Preparation

For Beta Galactosidase assays

Full-length chick IRF6 (cIRF6) cDNA was cloned into the pSCREEN-iT/lacZ Gateway destination vector by an LR recombination reaction. This reaction placed the IRF6 cDNA in frame with the 3' end of the *lacZ* reporter gene such that a lacZ-IRF6 fusion

protein is produced upon introduction into cells.

Double-stranded oligonucleotides (ds oligos) encoding shRNA sequences targeting cIRF6 were designed using the Block-IT RNA Designer online tool (http://rnaidesigner.invitrogen.com/rnaiexpress/). This program automatically performs a BLAST analysis against the UniGene nonredundant chicken (*Gallus gallus*) database to identify unique regions for targeting, thereby preventing undesired RNA interference for other genes. Ten ds oligos containing 21-nucleotide sequences that target *cIRF6* were designed and ranked by the program using a "Star Scoring System" used to indicate knockdown probability. Only the duplexes with the highest probability of success are provided by the program, which means that out of a possible five stars, no duplex has less than a three-star ranking. The three top ranked designs, each of five stars, were selected for cIRF6 targets.

As shown in Table 6.1, the target sequences initiate with a guanine (G) because according to manufacturer (Invitrogen), the transcription of native U6 snRNA from the Polymerase III-type promoter initiates at this nucleotide, thus allowing more efficient processing by the Dicer enzyme in the endogenous cellular RNAi system. In order for the double-stranded shRNA molecule to take the form of an intramolecular stem loop hairpin structure following transcription, the shRNA strands were designed with a sense-loop-antisense orientation. The target sequence and its complement were designed to anneal with one another to form the stem, with a four-nucleotide spacer – CGAA – acting as a flexible loop structure. To complete the double-stranded shRNA design, appropriate linker sequences were incorporated to facilitate cloning into the pENTR/U6

entry vector (in purple color). A 5'-CACC sequence was added to each top strand oligomer, as it was necessary for directional cloning via the 5' -GGTG- 3' overhang in the pENTR/U6 vector. The sequence – AAAA – was added to the 5' end of each bottom strand oligomer, as it constituted the first four bases of the Polymerase III terminator and was complementary to a TTTT overhang in the pENTR/U6 vector (Invitrogen).

Table 6.1. Sequences of cIRF6 shRNA oligomer designs

cIRF6 shRNAs start position	Oligo type	Oligo sequence (linker, Sense sequence, loop, antisense sequence)
shRNA 243	Top	5'- CACCGCAGCTCCGATGTGCTCTTAACGAATTAAGAGCACATCGGAGCTGC -3'
	Bottom	3'- CGTCGAGGCTACACGAGAATTGCTTAATTCTCGTGTAGCCTCGACGAAAA -5'
shRNA 269	Top	5'- CACCGCCGGGAGTTTAATCTGATGTCGAAACATCAGATTAAACTCCCGGC -3'
	Bottom	3'- CGGCCCTCAAATTAGACTACAGCTTTGTAGTCTAATTTGAGGGCCGAAAA -5'
shRNA 1155	Top	5'- CACCGGTTCAGGTCATCCCTGTTGTCGAAACAACAGGGATGACCTGAACC -3'
	Bottom	3'- CCAAGTCCAGTAGGGACAACAGCTTTGTTGTCCCTACTGGACTTGGAAAA -5

The selected top and bottom strand oligos were annealed and directionally ligated into the BLOCK-iT™ entry vector, pENTR™/U6 (Invitrogen). The generated constructs contain the full U6 RNAi cassette, comprising the eukaryotic U6 promoter, the ligated shRNA-encoding oligonucleotide and the Polymerase III terminator.

Production of final shRNA vectors for in ovo electroporation.

The MultiSite Gateway technology was used to generate a single construct that contained a shRNA together with the fluorescent reporter, mCherry. Two independent U6-shRNA vectors (shRNA 269 and 1155) together with a CMV promoter-driven

mCherry entry vector were cloned into a Gateway pcDNA 3.2/V5 destination vector in which the CMV promoter had been deleted (pcDNA3.2/V5 del. CMV vector).

Full length and dominant negative IRF6 constructs

IRF6 cDNA sequence corresponding to only the DNA binding domain (DBD, amino acids 1-128) was used for construction of IRF6-DBD, the dominant negative form of IRF6. IRF6-DBD and IRF6-FL (full-length) were amplified using the following combination of primers: forward 5'-CAGATCTCGAGCATGGCGTTACACCCGCGC-3' and reverse primers 5'-CCGCGGTACCTCAGGACCCTGGATTAATG-3' and 5'-CATCGGTACCTCACTGCGCAGGCAGTGGC'3' respectively. The amplified cDNAs were digested with KpnI and XhoI and independently ligated into the KpnI and XhoI sites of the expression vector pEGFP-C2 (Clontech), placing the reading frames downstream of and in-frame with the GFP reporter gene. All constructs were sequence verified and purified by large-scale plasmid DNA preparation.

Transient Transfections for Beta Galactosidase Assay

HEK293T cells were incubated at 37°C in 5% CO_2 and seeded at 90% confluency in 24-well tissue culture plates (Falcon) with complete DMEM media devoid of antibiotics. The pSCREEN-iT/lacZ screening construct containing the chick IRF6 cDNA, and the individual selected pENTR/U6-shRNA vectors, were co-transfected into the cells using Lipofectamine LTX (Invitrogen) at concentrations recommended by the manufacturer. Complexes were formed in OPTI-MEM media for 30min and then added to the cells. For consistency and accurate interpretation of results, the same positive and negative controls were employed in parallel with each screening experiment; these are listed as

follows: Mock transfection, screening vector construct only, screening vector construct + positive control RNAi molecule (Positive lacZ Stealth RNAi Control, Invitrogen) and screening vector construct + negative control RNAi molecule (Scrambled Negative Stealth RNAi control, Invitrogen).

Beta Galactosidase Assays

In order to assess the degree of chick IRF6 knockdown, measurement of enzymatic β-galactosidase reporter activity was performed 24 hours after transfection. Procedures were performed according to the BLOCK-iT RNAi Screening Manual guidelines (Invitrogen). Transfected HEK293T cells were lysed by freezing them at -80°C in cell lysis buffer. Then, each sample was assayed in a 96-well black solid bottom microtitre plate (Cat No. 3915; Costar) using the FluoReporter LacZ/Galactosidase Quantification Kit (Cat No. F-2905; Molecular Probes/Invitrogen). To begin the assay, 10μL of thawed cell lysate was pipetted into individual microplate wells (three wells per different transfection sample), followed by the addition of 100μL of the 1.1mM CUG Substrate Reagent. The samples were then incubated at room temperature for 30min, after which 50μL of 200mM Na_2CO_3 was added to raise the pH of each sample to terminate the reaction. The fluorescence in each well was then measured using the Tecan Safire II microplate reader equipped with an excitation filter centered at 390nm and an emission filter centered at 460nm. In order to increase accuracy and reduce assay variability, both transfections and assays were performed in triplicate for each sample condition. In each case, the β-galactosidase activity determined for each lysate was normalized to the activity obtained from the reporter screening vector alone, which was designated as 100%. Results were presented as the mean ± standard deviation of percentage β-

galactosidase activity and data analysis performed using a Students t-Test (two sample assuming equal variances), with two-tailed p-values less than 0.05 considered statistically significant.

Immunohistochemistry on Frozen Sections

Immunohistochemistry was performed as described previously in Chapter V, except that antigen retrieval treatment was performed before immunostaining for NME2. For this treatment, tissue slides were placed into a coplin jar filled with 10mM sodium citrate buffer, pH6.0 at 95°C for 10 minutes. Slides were cooled for approximately 20 minutes before blocking. Cells transfected with IRF6-DBD or IRF6-FL were detected by anti-GFP immunostaining as the antigen retrieval treatment quenched the autofluorescence of EGFP. This was not the case for mCherry-shRNA transfected cells. These transfected cells were detected without antibody staining even after antigen retrieval.

The following dilutions for primary and secondary antibodies were used: mouse monoclonal anti-NME2 (1:200; Abcam), rabbit polyclonal anti-GFP (1:1000, Abcam), and mouse monoclonal E-cadherin (1:1000; BD Biosciences). For the Alexa Fluor 488-conjugated goat anti-mouse and Alexa Fluor 568-conjugated goat anti-rabbit secondary antibodies, a 1:300 dilution was used.

Immunofluorescent Studies

Immunofluorescence staining was performed as described previously in Chapter IV, except that the following primary antibodies were used: mouse monoclonal anti-NME2 (1:200; Abcam) and rabbit polyclonal anti-beta catenin (1:000; ab6302, Abcam). For

goat polyclonal anti-beta tubulin (1:250; ab21057, Abcam), 3% BSA/PBS-T was used for blocking instead of 10% normal goat serum. In addition to secondary antibodies mentioned in Chapter IV, a Texas Red rabbit anti-mouse secondary (1:300; ab6726, Abcam) was also used.

For Rhodamine Phalloidin staining of actin filaments, a 100nM working solution was prepared by using 0.7µl of the 14µM stock solution (Cat. No. PHDR1, Cytoskeleton, Inc.) in 100µl PBS. The solution was kept at room temperature in the dark, and was incubated in a humidified chamber for 30min and washed three times with PBS at the end of the procedure before mounting.

Alcian Blue Staining

Chick heads were dehydrated in 95% EtOH for 3 days and stained for cartilage with Alcian stain solution (15 mg of Alcian Blue 8GX A 3157, Sigma; 80ml of 95% EtOH; 20ml of glacial acetic acid) for 24 hrs. Heads were rinsed twice in 95% EtOH, kept in 95% EtOH for 24hrs and then replaced with fresh 95% EtOH and kept in 95% EtOH for another 24hrs. Heads were then cleared by placing them in 1% KOH at 4°C for 12hrs, and stored in 50% glycerol/50% EtOH.

Confocal Microscopy

Immunofluorescence images were acquired using a TCS SP5 Leica confocal microscope.

Results

Characterizing Chick IRF6 shRNAs in Epithelial Cells

The ability of the selected shRNAs to decrease chick IRF6 (cIRF6) protein expression was first verified in tissue culture experiments. HEK293T cells were co-transfected with the cIRF6-LacZ screening construct and individual shRNAs. 24 hours later, a β-galactosidase assay was carried out to measure the level of mRNA knockdown achieved with each shRNA. For the purpose of these screening experiments, shRNAs were transfected using 400ng and 500ng, as per the manufacturer's recommendations (Invitrogen). High baseline β-galactosidase expression values were observed (indicating high cell viability), and positive and negative controls were as predicted: 66.68% knockdown using the positive control (percent residual activity: 33.32 ± 5.95, $p < 0.0001$), no knockdown effect when using the negative control (98.80 ± 6.60, $p=0.2278$). Two chick IRF6 shRNAs, 269 and 1155, consistently demonstrated moderate to high inhibition of β-galactosidase activity at the concentration of 400ng: 76.37% knockdown with shRNA 269 (23.63 ± 5.18, $p < 0.0001$), 78.64% with shRNA 1155 (21.36 ± 6.86, $p < 0.0001$) Furthermore, when using 500ng of DNA, the RNAi activity of shRNAs, 269 and 1155, showed a dose-dependent increase in knockdown: shRNA 269 increased to 91% knockdown (9 ± 5.93, $p < 0.0001$) and shRNA 1155 increased to 95.2% knockdown (4.81 ± 5.11, $p < 0.0001$) respectively (Figure 6.1). In contrast, several tests of the shRNA 243 did not show a consistent knockdown efficiency. It was assumed that this unusually variable response was due to technical error such as the presence of impurities in the DNA preparation that interfered with the DNA-lipid complex formation. In summary, transient RNAi screening analysis revealed that two of the IRF6-derived

shRNAs, 269 and 1155, had a consistent ability to induce a moderate to high RNAi response on ectopically expressed targets. Therefore, both shRNAs were chosen for in *in ovo* electroporations.

Disruption of IRF6 Function Results in CLP in the Chick Model

In addition to knocking down IRF6 mRNA expression by RNAi technology, a dominant negative form of IRF6 that contains the DNA binding domain only (dnIRF6) was also included. It was expected that dnIRF6 would act as a competitive inhibitor of the endogenous wild-type IRF6 through occupancy of target *cis*-regulatory elements (Figure 6.2). The same approach was previously used in zebrafish embryos by Sabel et al (2005). Here, ectopic expression of a dnIRF6 form led to the presentation of severe gastrulation defects and late defects in pectoral fin and skin, with elements of the craniofacial cartilaginous skeleton present, but smaller and disorganized (Sabel et al, 2005).

In order to test the hypothesis that alteration of IRF6 activity in the pre-fusion epithelia was sufficient to cause CLP, chick embryos were electroporated at E3.5 as described previously in Chapter V. Embryos were collected 6, 7, 10 and 12 days after electroporation to assess the effects on the formation of the beak. Independent electroporation of the pre-fusion facial epithelia with dnIRF6, shRNA1155 and shRNA269 constructs results in chick embryos (16.67%, 7.84%, and 3.03% respectively) with clefts on the transfected side of the beak. In contrast, independent *in ovo* electroporations using control vectors did not produce any embryos (Table 6.2).

Gross anatomical analysis of embryos collected 10 and 12 days after electroporation revealed two types of cleft: a mild but visible cleft or indentation that caused a slight deviation of the beak to the non-transfected side, and a more severe cleft that extended along the right side of the beak causing severe deviation of the beak and allowing external visualization of the oral cavity. Often, the external appearance of the soft tissue around the beak was irregular (see the oral surface outline in each embryo; Figure 6.3). This observation raised the possibility of underlying skeletal deficiencies or irregularities. To investigate this further, both alcian blue staining for cartilage and microCT analysis for assessment of the bony cranioskeleton were performed. Of note, mildly clefted IRF6 targeted beaks (observed 6 days after electroporation) showed discontinuation of the cartilage in the region were normally the pre-maxilla and maxilla would join (Figure 6.4A', A''), consistent with the surface appearance on the soft tissue analysis obtained using optical projection tomography (Figure 6.4A). Of greater interest, were the findings from the skeletal analysis of embryos with the more severe phenotype (collected 12 days after electroporation). These embryos showed marked bony deficiencies that included significant reduction of the palatine bone, and shortening of the maxilla and premaxilla on the transfected side. Because of the failure to anchor the premaxilla on the cleft side, the beak deviated markedly in the direction of the non-transfected side. These findings demonstrated that disrupted IRF6 function by itself is a contributing factor in the susceptibility to CLP in the chick model. Furthermore, disruption of IRF6 in the orofacial epithelia is sufficient to interfere with subsequent osteogenesis of the underlying neural crest derived tissue in the maxillae, premaxilla, and most notably in the palatal shelves. This latter observation suggests a disruption of epithelial-

mesenchymal interactions that normally are required to maintain neural crest proliferation and differentiation.

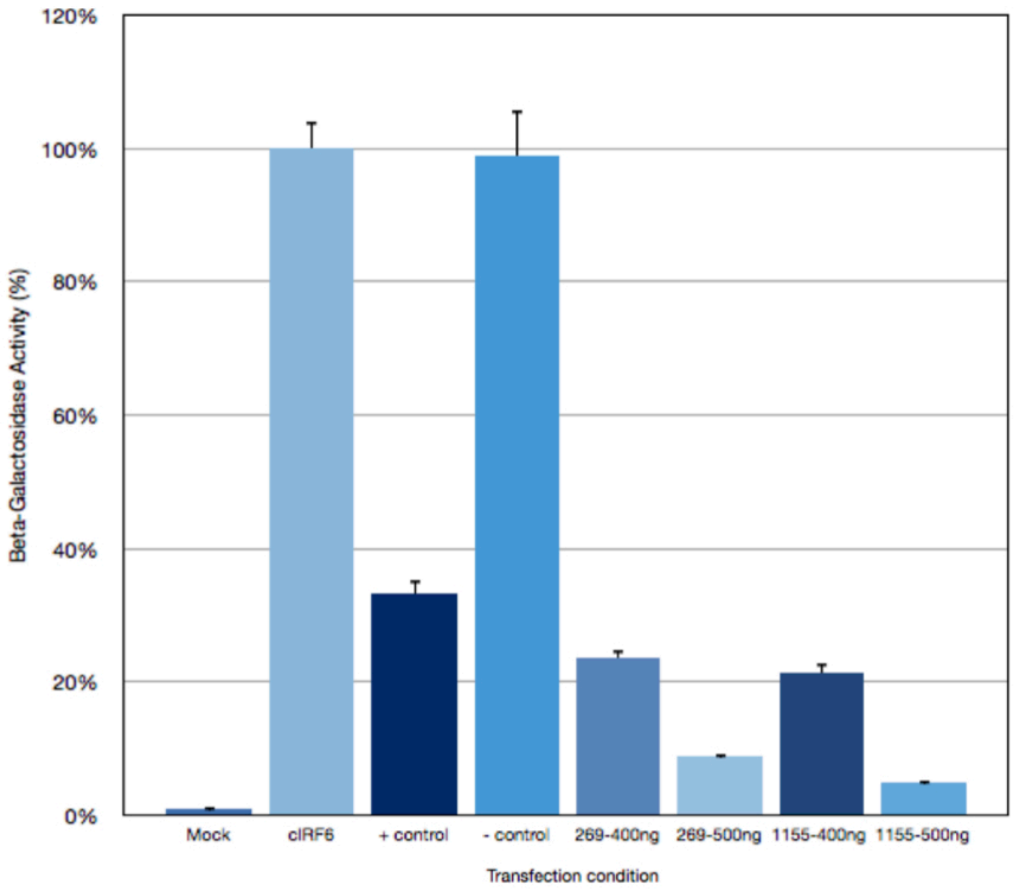

Figure 6.1. Beta-galactosidase activity of shRNA constructs against chick IRF6. Both cIRF6 shRNA269 and shRNA1155 proved effective at targeting cIRF6 expression, as measured by the percentage of knockdown of the LacZ reporter activity at both concentrations (400ng and 500ng). The "cIRF6" column corresponds to the lacZ expressing screening vector construct only; "+control" corresponds to the screening vector construct + LacZ Stealth RNAi positive control (Invitrogen); "-control" corresponds to the screening vector construct + scrambled negative stealth RNAi control (Invitrogen).

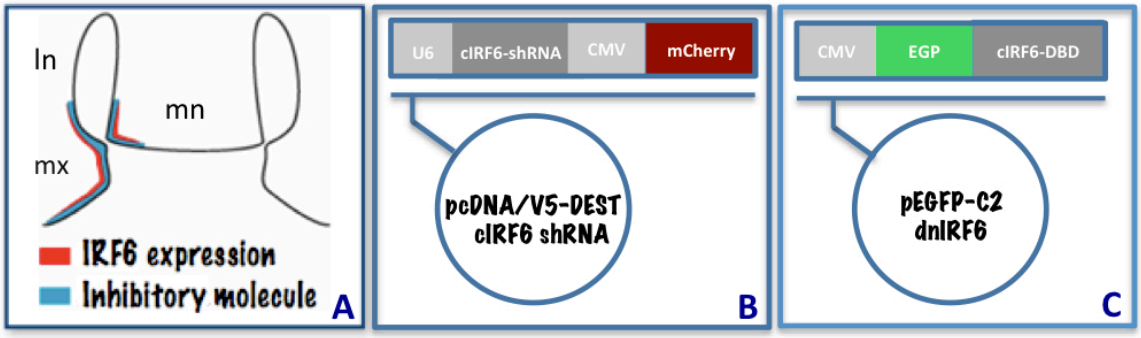

Figure 6.2. IRF6 inhibitory molecules for *in ovo* electroporation. Unilateral and independent electroporation of specific inhibitory factors into the facial processes employed to disrupt IRF6 expression / function (A) included shRNA-mCherry constructs (B), and a construct to express a dominant negative form of IRF6 (dnIRF6) that contains the intact DNA binding domain only. An outline of the pre-fusion upper orofacial processes is shown in (A) to highlight the specific targeting achieved by the in ovo electroporation procedure. mn (medial nasal process); ln (lateral nasal process); mx (maxillary process).

Table 6.2. Effects of inhibitory molecules on primary palatal formation

	shRNA 1155	shRNA 269	mCherry vector	EGFP vector	pEGFP-dnIRF6
Normal development	47 (92.16%)	32 (96.97%)	19 (100%)	46 (100%)	35 (83.33%)
Cleft	4 (7.84%)	1 (3.03%)	0 (0.00%)	0 (0.00%)	7 (16.67%)
n*	**51**	**33**	**19**	**46**	**42**

*Embryos were collected 6, 7, 10 and 12 days after electroporation

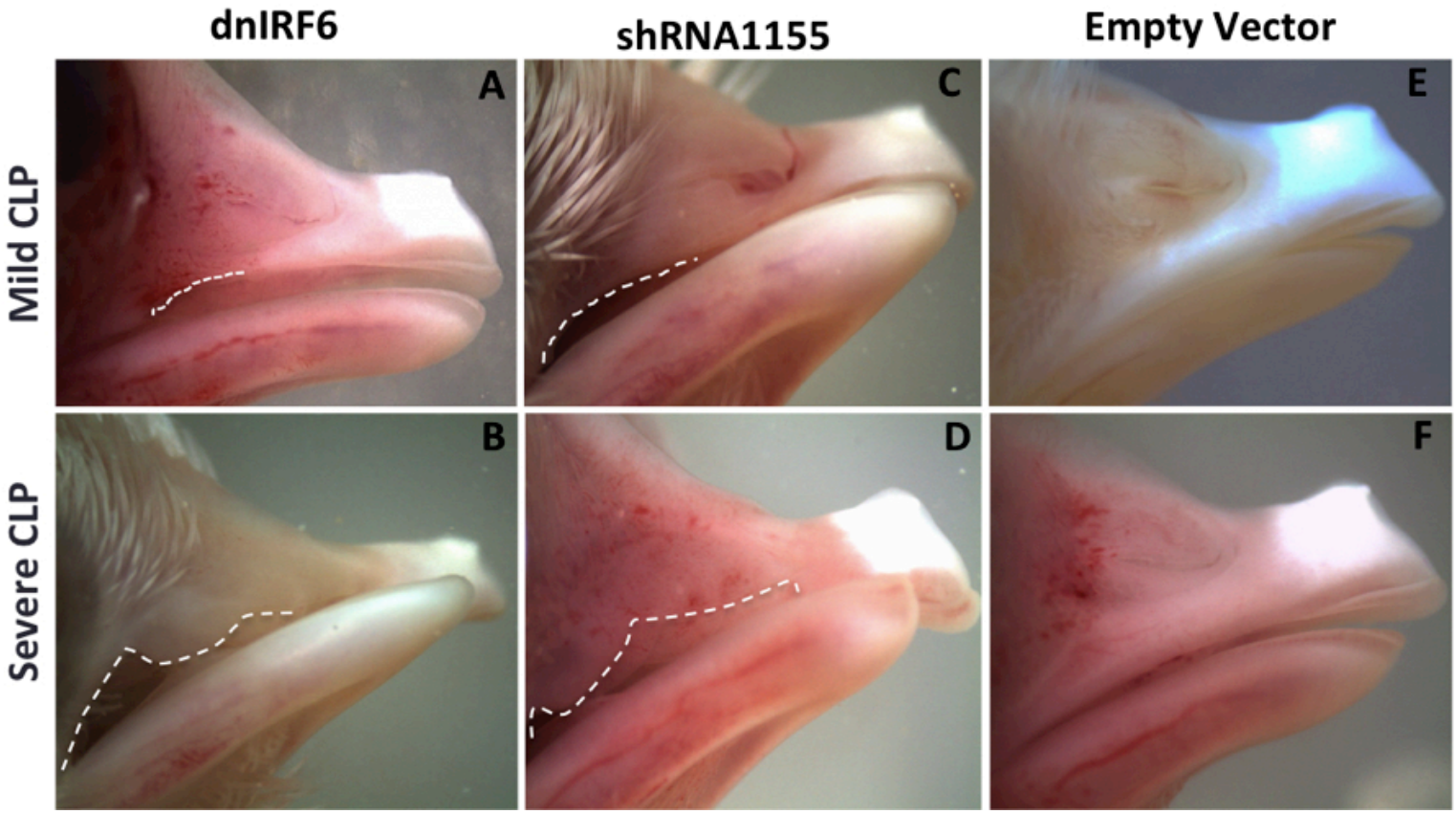

Figure 6.3. Disruption of IRF6 expression/function leads to CLP in the chick. Normal beak development was observed in GFP control embryos collected 12 days after electroporation (**E**, **F**). In contrast, embryos electroporated with dnIRF6 and shRNA1155 showed either a small cleft on the electroporated side (delineated with white dashed white lines on (**A**) and (**C**)) or occasionally a more severe cleft phenotype (demarcated by the white dashed lines in (B) and (D)). This severe presentation caused severe deviation of the beak to the non-electroporated side (see **B**, **D**).

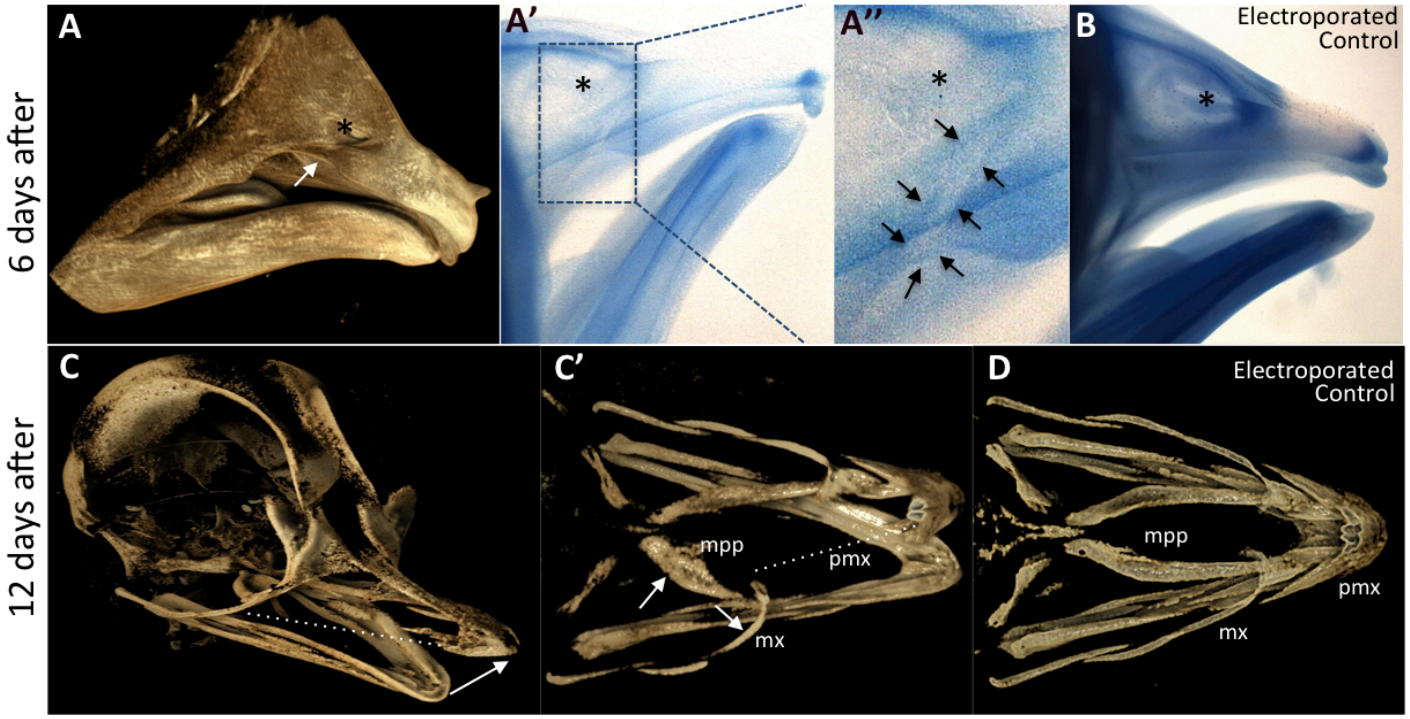

Figure 6.4. Effect of IRF6 inhibitory molecules on cartilage and bone formation. Lateral view of 3D rendered OPT image of an embryo electroporated with dnIRF6 (**A**). The white arrow highlights the full extension of the cleft to the nostril (*). Alcian blue staining was performed on the same embryo as in (**A**). This staining showed a deficiency of cartilage formation (**A'**) in the corresponding position, which is indicated by black arrows on A''. MicroCT scans of later stage embryos electroporated with IRF6 inhibitory constructs showed cranioskeletal deficiencies (**C**). A lateral view shows the deviation of the beak to the non-electroporated side as well as the defect in osteogenesis (white dashed lines). A top view shows in better detail this defect. The white dashed line highlights the bony deficiency. Although some of this region corresponds to the cleft itself, there are additional reductions of the premaxillary bone (pmx) and the maxilla (mx), as well as significant loss of the palatine (mpp) bone on the electroporated side. Control electroporated embryos were included for the respective analyses, and are shown in (**B**) and (**D**).

IRF6 Mutant Epithelia Show a Delay of the Fusion of the Tips of the Facial Processes

In order to analyze the cellular basis of these facial clefts, experimental and controls transfected embryos were collected 2 days after electroporation at a time when the maxillary and lateral/medial nasal prominences would normally have contacted and undergone fusion. Embryos independently transfected with dnIRF6, shRNA1155 and shRNA269 at E3.5 (HH22 and HH23) displayed a delay in the fusion of the facial processes (21.43%, 19.05% and 8.16% respectively; Table 6.3). In line with the phenotype observed in the older embryos shown in Figures 6.3 and 6.4, mutant IRF6 embryos showed variability in presentation around the site of fusion of the facial prominences. In some embryos, none of the converging facial processes made contact, suggesting a delay in mesenchymal growth or incompetency of the epithelia to adhere strongly with the facial processes being subsequently pulled apart by the torsional stresses due to continuous growth of the processes (Figure 6.5 C, F). In others, there appeared to be incomplete fusion or delayed contact between medial nasal and maxillary processes, with the slightly younger embryos frequently showing a small gap or notch between the lateral nasal and maxillary processes (Figure 6.5 A, D). These latter presentations most likely would result in a less severe cleft phenotype as the embryos developed (Figure 6.5 B, E). The variability in phenotype may be due to the number or position of the epithelia that were successfully electroporated. Nevertheless, these findings demonstrated that epithelial IRF6 expression is required for normal outgrowth and fusion of the facial prominences.

Abnormal Fusion of the Facial Processes is Associated with Alterations in Adhesion and Proliferation

To further analyze the cellular basis underlying the IRF6 cleft phenotype, tissue sections through the defective medial/lateral nasal and maxillary processes were processed for immunohistochemical assessment of E-cadherin, a marker for epithelial integrity and adhesion. Analysis of the tissue sections revealed that E-cadherin expression was reduced, consistent with the hypothesis that IRF6 mutant epithelia display abnormal adhesive properties. In addition, the cells appeared disorganized and had formed a multilayer epithelium, an indication of a loss of epithelial polarity and concomitant increased cell division (Figure 6.6).

Table 6.3. Effect of IRF6 inhibitory molecules on fusion of the primary palate

	shRNA 1155	shRNA 269	mCherry vector	EGFP vector	pEGFP-dnIRF6
Normal development	17 (80.95%)	45 (91.84%)	16 (100%)	23 (100%)	11 (78.57%)
Delay in fusion	4 (19.05%)	4 (8.16%)	0 (0.00%)	0 (0.00%)	3 (21.43%)
n*	**21**	**49**	**15**	**23**	**14**

*Embryos were collected 2 days after electroporation

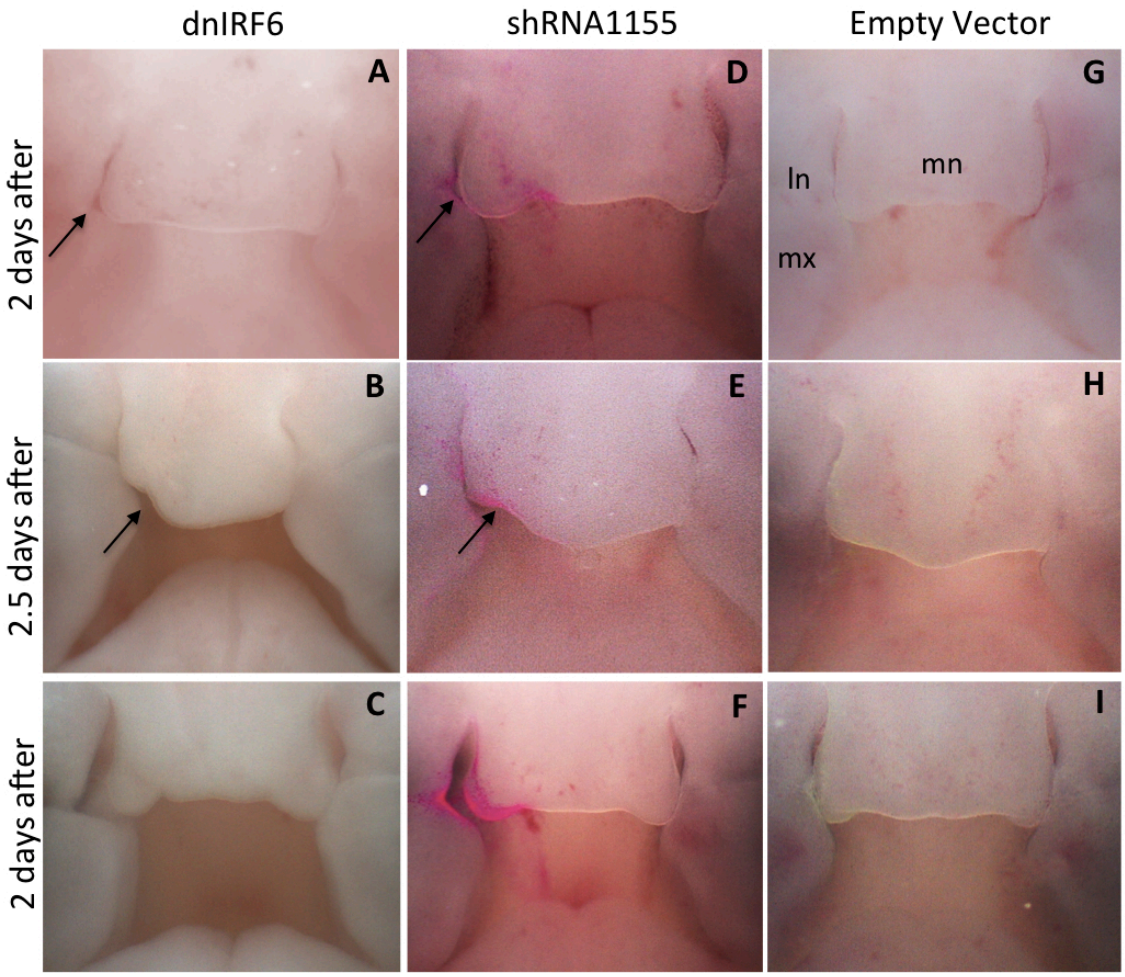

Figure 6.5. Epithelial IRF6 expression is required to promote directed outgrowth and primary palate fusion. Normal development was observed in GFP control embryos collected 2 (**G**, **I**) and 2.5 (**I**) days after electroporation. In contrast, embryos electroporated with dnIRF6 and shRNA1555 showed abnormal contact on the electroporated side. Black arrow on (**A**) and (**D**) are indicating a gap between the lateral nasal and maxillary processes, which could result in an uncompleted fusion as shown on (**B**, **E**). A more severe defect was also observed, where the three processes failed to fuse. Red color on (**D**, **E**, **F**) corresponds to the ectopically expressed mCherry protein, which could also be detected under white light. This marker is therefore also an indicator of the number and position of electroporated epithelial cells, which could have an impact on the severity and variability in presentation. mn (medial nasal process); ln (lateral nasal process); mx (maxillary process).

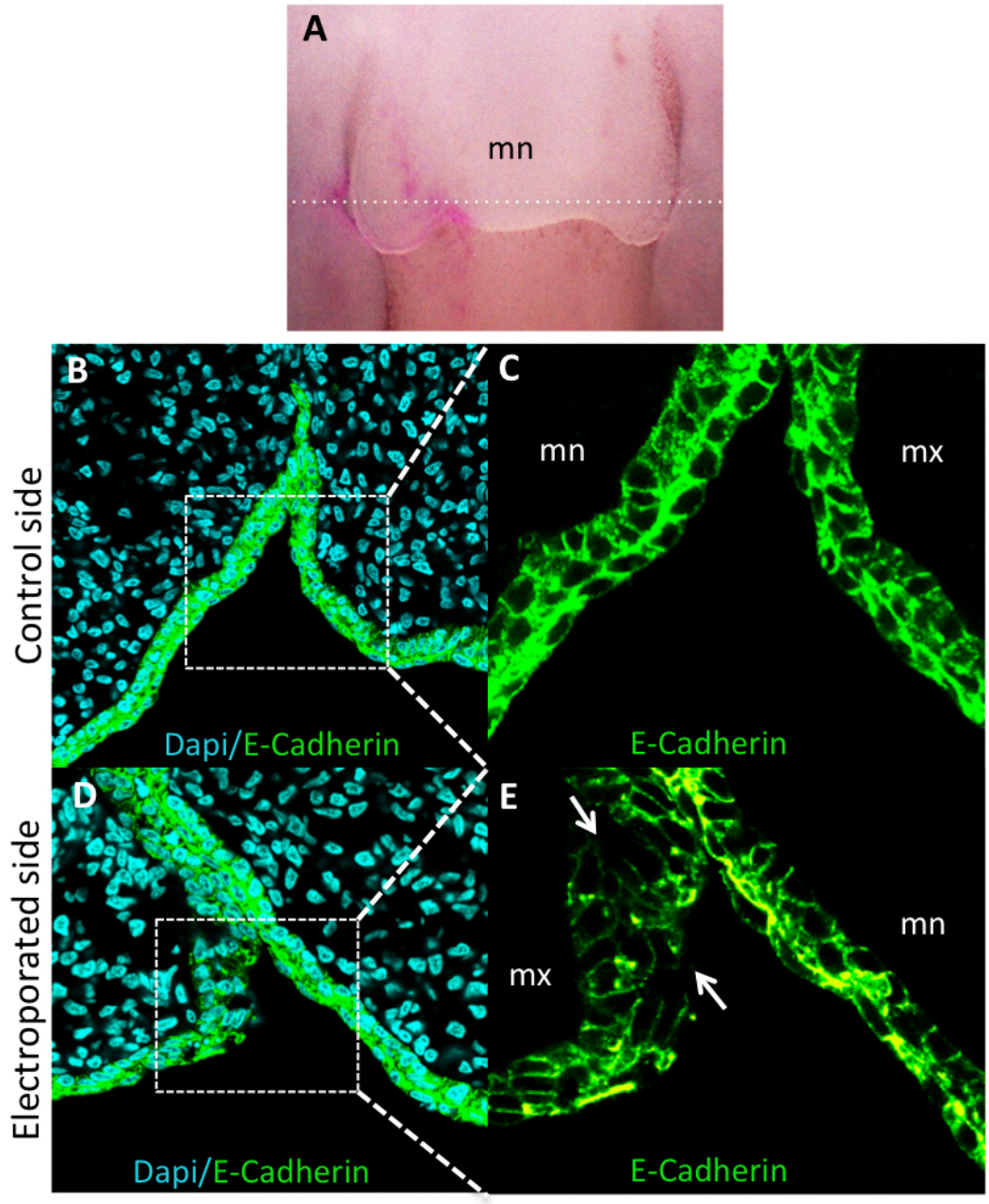

Figure 6.6. Altered adhesive and proliferative properties of IRF6 mutant epithelia. A mCherry-shRNA1155 electroporated chick face showing abnormal fusion of the facial prominences two days after electroporation was processed for confocal microscopy. Ectopically expressed mCherry protein (red color) could be detected under white light (**A**)**.** Transverse (10μm) frozen section (indicated by dashed lines on (**A**) was stained with a E-cadherin antibody (**C**, **E**). White arrows indicate decreased E-cadherin expression on the electroporated side, which shows thicker and disorganized epithelia. Nuclei were counterstained with DAPI (blue on **C**, **F**). mn (medial nasal process); mx (maxillary process).

Understanding the Physiological Role of NME2 in the IRF6 CLP Phenotype

In order to gain further insights into the cellular etiology of the IRF6 CLP phenotype, NME2 protein was investigated in more detail in primary palatal epithelia. Endogenous NME2 protein was highly localized in the cytoplasm of primary epithelial cells, where it co-localized with transfected GFP-IRF6 in electroporated embryonic epithelia (Figure 6.7). Furthermore, NME2 expression, although weaker, could also be detected in the underlying facial mesenchyme. The epithelial expression remained consistent at all stages of primary palatal development including the pre-fusion epithelia, the contacting epithelia of the merging facial processes, and in the epithelia that disperse as the fusion of the primary palate is completed (Figure 6.8). Significantly, on the non-electroporated side, NME2 also localized to the filamentous-like structures in the weakening periderm layer as contact is being initiated between the maxillary and medial nasal epithelia (Figure 6.8 A, A'). On the electroporated side of embryos, NME2 signal in epithelia expressing either dnIRF6 or shRNA1155 was evident in all the layers of the disorganized and thicker mutant epithelium (Figure 6.9). No filamentous cellular projections were observed associated with this thicker epithelium.

NME2 Co-localizes with Microtubules in MDCK Epithelial Cells

To investigate the intracellular localization of NME2 more closely, immunohistochemical detection of endogenous NME2 was performed in cultured MDCK epithelial cells. Confocal microscopy analysis demonstrated that endogenous NME2 localized in a fibrous pattern within the epithelia. Co-localization studies were then performed to identify the cytoskeletal structure matching that of NME2 staining. Co-staining with rhodamine phalloidin did not show co-localization of signals indicating that NME2 does

not associate with actin fibers. However, the NME2 signal did partially co-localize with beta tubulin staining (Figure 6.10), indicating that endogenous NME2 is associated with the microtubule cytoskeleton in MDCK epithelia. Ectopic expression of GFP-NME2 fusion protein also showed a somewhat filamentous appearance although much of the fluorescence showed a general cytoplasmic distribution. In contrast, preliminary data on ectopically expressed kinase-dead NME2 (as a GFP-NME2H118F fusion protein) showed no evidence of filamentous structures (Figure 6.11). Further studies are needed to verify that the kinase activity of NME2 is required for microtubule association.

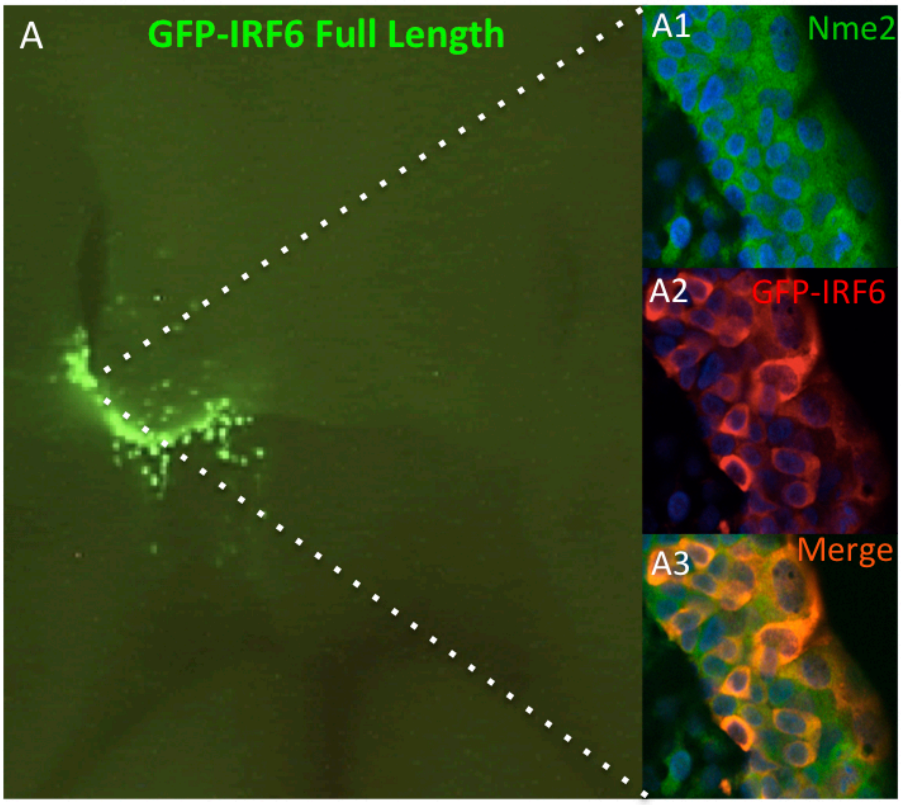

Figure 6.7. IRF6 and NME2 in primary palatal epithelia. Embryonic facial epithelia expressing full-length IRF6 (as a GFP fusion protein) two days after electroporation of the construct (A). Transverse (20μm) frozen section stained with NME2 (A1) and anti-GFP (A2) antibodies showed they predominantly co-localize in the cytoplasm of primary palatal cells (A3).

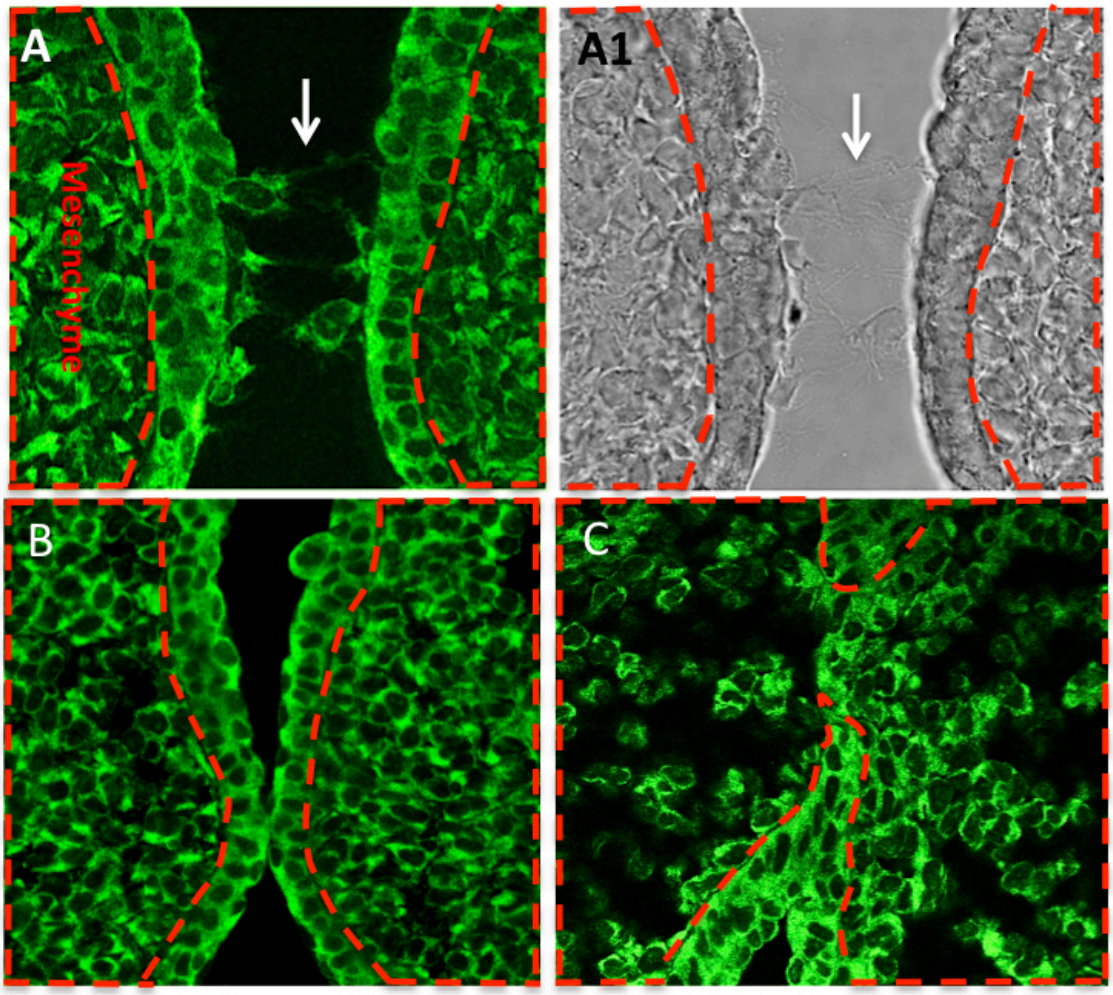

Figure 6.8. NME2 expression during normal primary palatal development. Transverse sections showing the non-electroporated side of an embryo electroporated with dnIRF6 showed that NME2 is expressed in the facial epithelia, and also at a lower level in the mesenchyme (delimited by the red dashed line) before (A), during (B) contact and fusion (C) of the maxillary and medial nasal processes. NME2 exhibited filamentous like structures right before fusion that are indicated by the white arrow on (A), and on the bright field image on A1.

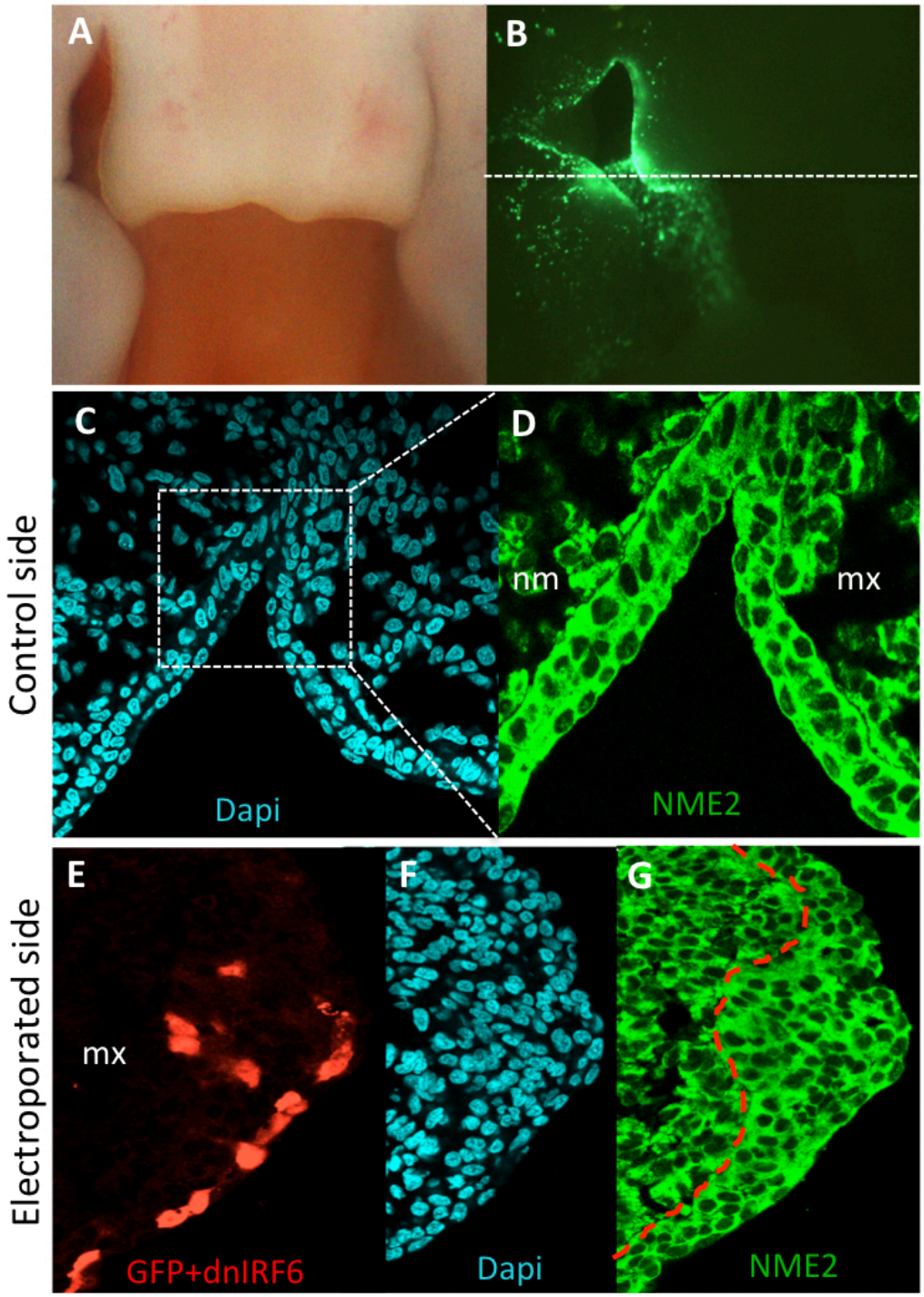

Figure 6.9. NME2 expression in IRF6 mutant epithelia. A GFP-dnIRF6 electroporated chick face showing no fusion of the facial prominences two days after electroporation (**A**) was processed for detection of GFP signal under a dissecting fluorescent microscope before immunostaining (**B).** Transverse (10μm) frozen section (indicated by dashed lines on **B**) was stained with NME2 (D, G), and GFP (**E**) antibodies. Red dashed lines on **G** indicate the boundary of the thicker epithelia on the electroporated side. Nuclei were counterstained with DAPI (blue on **C**, **F**). mn (medial nasal process); mx (maxillary process).

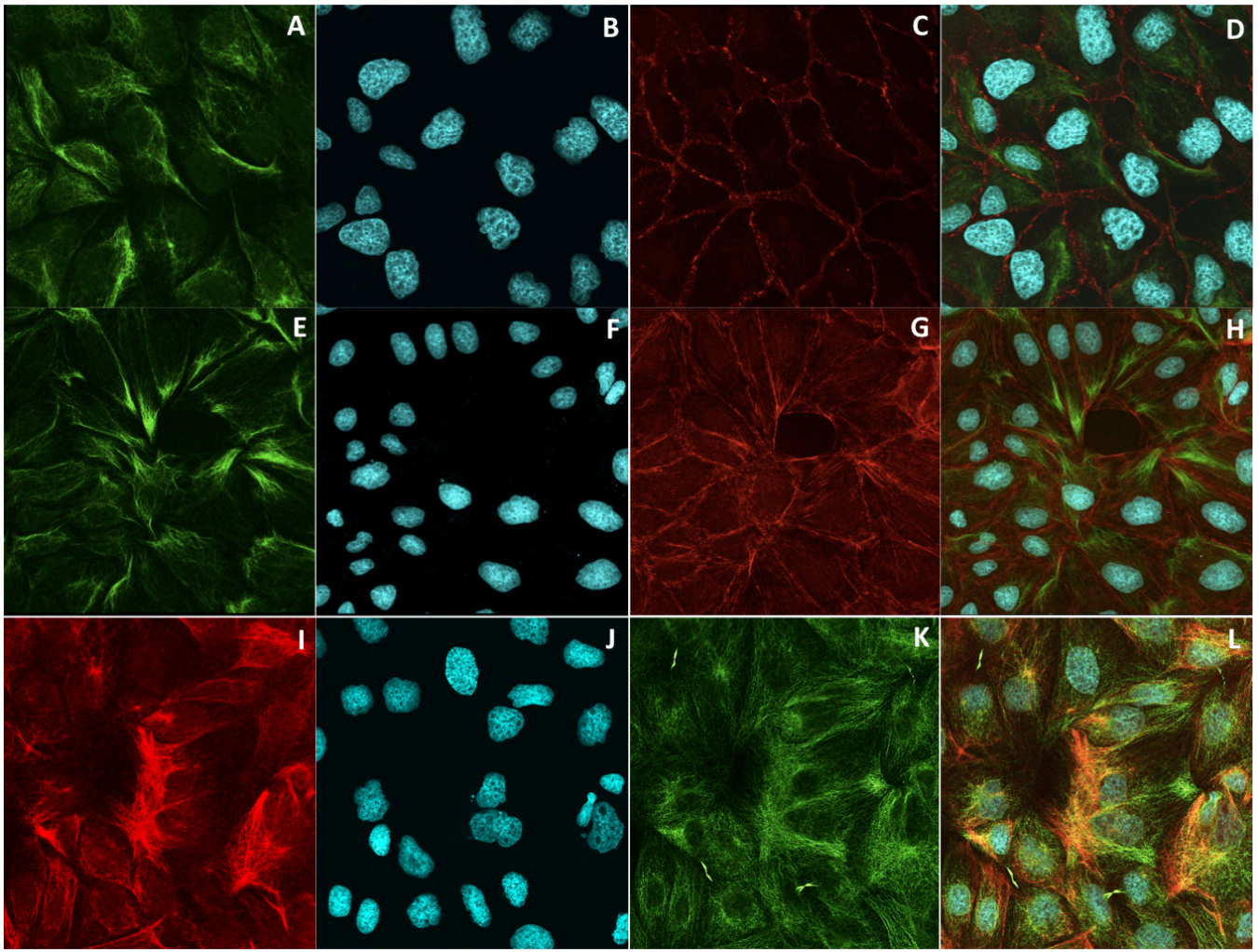

Figure 6.10. NME2 co-localizes with microtubules in MDCK epithelia. Fixed MDCK cells were processed for confocal microscopy using a NME2 antibody shown in green **(A, E)** and in red **(I);** a beta-Catenin antibody **(C);** phalloidin-actin staining (G) and a beta-Tubulin antibody **(K).** Nuclei were counterstained with DAPI **(B, F, J).** Overlay images are shown on the right **(D, H, L).**

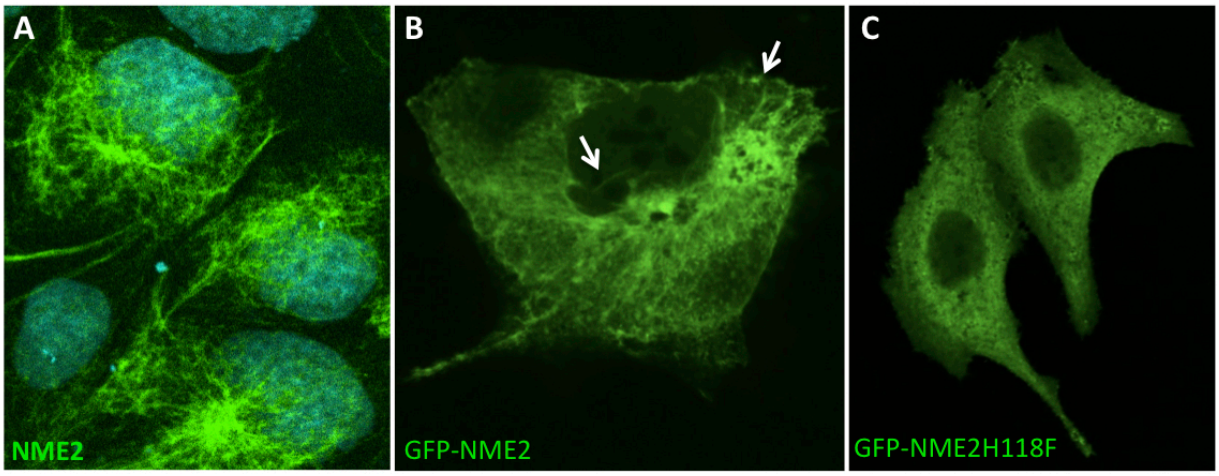

Figure 6.11. Intracellular localization of ectopically expressed NME2 fusion proteins. Fixed MDCK cells were processed for confocal microscopy using a NME2 antibody (**A).** Nuclei were counterstained with DAPI (blue on **A**). Over-expressed GFP-NME2 (**B**) and GFP-NME2H118F (**C**) were detected using a GFP antibody. White arrows indicated the presence of filamentous-like structures, not as numerous as observed on **A.**

Discussion

IRF6 Mutant Faces Exhibit Abnormal Morphogenesis on the Manipulated Side

Results presented in this chapter demonstrate that manipulating IRF6 gene expression by *in ovo* electroporation is a powerful approach to study its function during primary palate development. Indeed, disruption of IRF6 activity in the pre-fusion epithelia led to the presentation of CLP in the chick. Two types of phenotypes were variably observed, a mild and severe CLP. The mild cleft was a result of an incomplete fusion of the maxillary and medial nasal process, while the severe CLP, in which the cleft extends into the nostril, is clearly indicative of failure of the contact of the three processes: the medial nasal with both maxillary and lateral nasal processes. This failure may be due in part to secondary effects of an altered epithelium, in that the evident change in epithelial

polarity may disrupt the basal secretion of growth-stimulatory factors that promote mesenchymal outgrowth.

In the described experiments, it should be noted that a higher percentage of embryos presented with a subtle delay in fusion compared to those with obvious clefting at later stages. This suggests that not every delay in fusion may result in an overt cleft. This phenotypic variation can be explained by the inherent variability in the electroporation procedure. In particular, although the transfection efficiency of the facial electroporation is very high and reproducible, the position and number of the cells transfected at the right time of development can vary. As a consequence, these variables likely impact on whether a cleft will result or not as well as the severity of the phenotype (mild or severe) when a cleft does present.

In addition, more embryos transfected with shRNA1155 displayed CLP compared to the ones transfected with shRNA269. These findings were roughly in line with the results from the tissue culture–based beta galactosidase assays in that shRNA1155 showed slightly higher knockdown efficiency than shRNA269. Although low efficiency shRNAs were not tested in ovo, these data are consistent with the guidelines for shRNA design and selection and reinforce the usefulness of performing this type of *in vitro* experiment before proceeding to *in vivo* manipulation. Despite the variation in phenotype, the chick system – the first to reproduce the presentation of CLP as seen in humans - offers the possibility of understanding the contribution of IRF6 to primary palatal development and the role of mutations in contributing to the incidence of CLP in patients.

A Proposed Role for NME2 Prior to Fusion

Primary palatal fusion is a tightly coordinated multistep process in which the epithelia undergo extensive cellular changes in response to extracellular signals. This requires the precise regulation of the cell's cytoskeletal and adhesive properties as well as cell-matrix interactions (Cox, 2004). In order to determine the possible role for the identified NME1/2-IRF6 interaction in orofacial epithelia and primary palatal fusion, several processes involved in epithelial morphogenesis must be considered. CLP is caused by a defect in fusion or joining of three separate epithelial-covered tissue masses: the maxillary and lateral nasal processes with the medial nasal process. This fusion normally involves coordinated mesenchymal growth below the epithelial layer, ultimate adhesion of the converging epithelial covered processes, and subsequent removal of the intervening epithelial seam. Notably, it was demonstrated that IRF6 activity is required to maintain epithelial integrity by controlling two critical events during fusion: adhesion and proliferation.

Apical-basal polarity in epithelial cells is established and maintained through the formation of specialized intercellular junctions, the adherens junctions and the tight junctions (Schock and Perrimon, 2002; Gumbiner, 2005). Prior to the formation of adherens junctions, nectins and cadherins localize in actin-rich lamellipodial or filopodial protrusions, which probe the environment for neighbouring cells (Vasioukhin and Fichs, 2001; Etienne-Manneville, 2011). Several studies in the chick have found that the primary palatal epithelia undergo distinct morphological changes prior to contact including the appearance of filamentous structures on the surface. These filamentous structures project toward the apposing surface and, as the gap between the two

processes narrows, the number of filamentous structures increases (Yee and Abbott, 1978; Sun et al, 2000; Cox, 2004). These structures have been proposed to facilitate the correct alignment and guidance of cell sheets that are going to fuse (Schock and Perrimon, 2002). Interestingly, NME1/2 has been associated with cilia and flagella, which are microtubule-based structures. Indeed, NME1 and NME2, localize to flagella of spermatozoa (Munier et al., 2003) and primary cilia in A6 epithelial cells (Mitchell et al, 2004). More importantly, NME1 silencing in epithelial cancer cell lines that normally would express high levels of NME1, was found to lead to the formation of filopodial-like structures on the free surface of the cells (Boissan at al, 2010). Although further validation is required, immunofluorescence studies presented in this chapter suggested that NME2 localized within similar filamentous structures on normal chick pre-fusion primary epithelia but the structures were not evident when IRF6 was knocked down. Thus, the IRF6:NME2:NME1 protein complex may regulate epithelial polarity and therefore integrity of the orofacial epithelium. As the facial processes converge, epithelial adhesion is weakened slightly to enable cellular extensions to appear on the apical surface to direct adhesion of the processes. However, if the IRF6-NME2:NME1 complex is significantly disrupted, polarity may be completely lost (as evidenced by down-regulation or redistribution of adherens junctions localized E-cadherin) resulting in increased proliferation and thickening of the epithelium and altered communication with the underlying mesenchyme.

Nme2 as a Microtubule-Associated Protein Could Regulate Epithelial Adhesive Properties During Fusion

The correct assembly, positioning and maintenance of the microtubule pattern is crucial for their specialized function in polarity and cell motility (Wittmann and Waterman-Storer; 2001, Bellet et al, 2009). Cell-cell contact and polarization involve a dramatic reorientation of the microtubule cytoskeleton. The majority of the microtubules in polarized epithelia are non-centrosomal. In such polarized epithelia, the centrioles migrate to the apical surface (where they may direct formation of primary cilia), and the microtubules are reorganized from a radial array to an apical-basal array with the minus-ends anchored at apical non-centrosomal sites, including the adherens junctions, and the plus-ends at the cell base (Bre et al, 1987; Buendia et al, 1990; Mongensen M, 1999; Bartolini and Gundersen, 2006; Bellet et al, 2009). In line with this model, specific microtubule interactions with adherens junction proteins are required for both the formation and regulated disassembly of these junctional complexes. For example, the microtubule plus-end binding protein (EB1), the cytoplasmic linker protein 170 (CLIP170), and dynein all have been shown to co-localize with β-catenin (Mimori-Kiyosue et al, 2003; Bellet et al, 2009). An additional example is a recently identified protein complex containing the novel microtubule minus-end binding protein Netza and the pleckstrin homology domain protein PLEKHA7, which also co-localizes to the adherens junctions via p120 catenin (Meng et al, 2008).

Although argued by others (Melky et al, 1992), several studies have reported the association of NME1/2 proteins with the microtubule network. Nickerson and Wells first reported the NME interaction with microtubules in 1984. The “Abnormal wing discs”

(Awd) protein in Drosophila, which is the homolog of NME1/2, was found to be associated with microtubules with a suggested role in spindle microtubule polymerization (Biggs et al, 1990). More recently, loss and gain of function experiments with Drosophila Awd have shown that it regulates epithelial integrity in this species through regulated endocytosis of adherens junction components (Woolworth et al, 2009) as well as FGF receptor levels (Dammai et al, 2003). NME1 has been found as a component of the centrosome and it co-immunoprecipitates with γ-tubulin (Roymans et al., 2001). Others have shown that NME1/2 proteins bind to microtubules in interphasic cells (Pinon et al., 1999), are associated with membranes that co-pellet with taxol-stabilized microtubules, and co-localize with β-tubulin around cytoplasmic vesicles in fibroblasts (Gallagher et al., 2003). This latter observation is consistent with its role in endocytosis (Woolworth et al, 2009).

Immunofluorescent studies presented in this chapter also support co-localization, at least in part, with the microtubule cytoskeleton. Endogenous NME2 in MDCK epithelial cells is seen as filamentous structures that co-localize partially with β-tubulin. In contrast, preliminary data on GFP-NME2H118F (a kinase-dead NME2) showed no evidence of filamentous structures. This observation supports the hypothesis that the kinase activity of NME2 could be required to provide a high concentration of nucleotides for both microtubule polymerization and vesicular dependent movement along the microtubules driven by the motor proteins kinesin and dynein (Marino et al, 2011;Bosnar et al, 2009; Biggs et al, 1990; Lombardi et al, 1995).

In addition to the association to microtubules, it has been reported that NME1 and predominantly NME2 interact with and co-localize with E-cadherin, α catenin and γ catenin, which also supports a role for NME1/2 in the stabilization of junctional complexes (Aktary at el, 2010). Consistent with this, NME1 silencing by RNA interference induces a marked reduction of E-cadherin/catenin expression at cell-cell contacts in non invasive cancer cells that would normally express E-cadherin/catenins at cell-cell contacts (Boissan et al, 2010). Taken together, the association of NME2 with microtubules and the decreased E-cadherin expression in mutant IRF6 epithelia shown in this study, and the association of NME2 with components of adherens junctions and its implication in the endocytic regulation of these junctional components in Drosophila, point to a role for the IRF6:NME complex in regulating epithelial integrity and hence the ability of the orofacial epithelia to facilitate the fusion of the primary palate.

Role for NME2 and IRF6 in Proliferation

IRF6 mutant epithelia appear thicker (an indication of increased cell division) with NME2 highly expressed in the multilayer epithelia. These findings are consistent with two reports in which Irf6 mutant mice display a hyperproliferative epidermis (Ingraham et al, 2006; Richardson et al, 2006). This is also consistent with the suggested role of IRF6 in cell cycle arrest in mammary epithelial cells (Bailey et al, 2008). Interestingly, it has been reported that NME1/2 expression was increased in the hyperproliferative and poorly differentiated epidermis of wounded skin, which has high levels of KGF and also epidermal growth factors (Grotendorst et al, 1989; Werner et al, 1992). In support of this, it was also demonstrated that NME1/2 overexpression in keratinocytes resulted in marked thickening of the epidermis in an organotypic culture system (Braun et al, 2007).

IRF6 and NME2 interact in the cytoplasm. By disrupting IRF6:NME2 interaction, free IRF6 in the cytoplasm of the cell would be available to translocate into the nucleus to activate transcription of genes involved in proliferation by the proposed mechanisms mentioned in chapter IV.

Role for Nme1 in Adhesion

The establishment of cell polarity requires the interplay between signaling by polarity proteins and the coordinated regulation of the actin and microtubule cytoskeleton. This balance leads to the expansion of the cell-cell contact area, while locally inhibiting membrane ruffling and filopodia formation (Mertens et al, 2006; Etienne-Manneville, 2011). E-cadherin and nectin engagement increase Rho-GTPase Rac1 activity. Once Rac1 is activated at the right time and place, it interacts with its effectors to promote polymerization of the actin network in the plane of the cell membrane and increases cell-cell contact area (Etienne-Manneville, 2011).

Nme1 was found to interact with Tiam1, a GEF (guanine nucleotide exchange factor) that specifically activates Rac1 (Otsuki et al, 2001; Rossman et al, 2005). Tiam1 and Rac1 are required for the establishment of cadherin-mediated cell adhesion (Sander et al, 1998; Sander et al, 1999; Watanabe et al, 2009). In support of this function, both proteins localize to adherens junctions (Sander et al, 1998, Mertens et al, 2005; Tahiski et al, 2007).

NME1 associates with Tiam1 in the cytoplasm of HEK293T cells, and down-regulates Tiam-Rac1 signaling (Otsuki et al, 2001). Consistent with this, NME1 silencing in

HepG2 cells increased levels of active (GTP bound) Rac1 compared to control cells (Boissan, 2010). These findings support the notion that interaction of NME1 with Tiam1 in the cytoplasm prevents localization of Tiam1 to the membrane, which consequently diminishes its function as a Rac1 activator. The result of such an interaction would be impairment of cell adhesion and lamellopodia formation (Bosnar et al, 2009). Taken together, it is predicted that IRF6, NME1, Tiam1 and Rac1 are in the same E-cadherin mediated adhesion regulatory pathway. Furthermore, disrupted IRF6 function/expression in primary epithelia could enhance NME1 association with Tiam1, which results in loss of lateral-basal polarity via inhibited Tiam-Rac1 adhesion signaling, affecting in turn the regulation of Adherens Junctions through E-Cadherin endocytosis, which would occur otherwise under a normal physiological response, as during fusion of the facial prominences.

IRF6 Mutant Epithelia Secondarily Impacts the Underlying Mesenchyme

Epithelial and mesenchymal interactions are required for proper growth of the facial primordia (Richman and Tickle, 1989). Although rapid proliferation of the neural crest derived mesenchyme in chick embryos between stages HH20 to HH28 is the driving force for the outgrowth of the facial prominences (McGonnell et al., 1998; Wu et al., 2004; Szabo-Rogers et al., 2008), fate mapping and tissue recombination experiments in chick showed that proliferation and directed expansion of the facial mesenchyme depend on signals from the facial epithelia (Wedden, 1987; Richman and Tickle, 1989; McGonnell et al., 1998 Jiang et al., 1999, Young et al, 2000). In this chapter, it was found that disruption of epithelial IRF6 function prior to fusion of the facial processes results in disorganization of the orofacial epithelia as well as reduced outgrowth of the

facial processes. Somewhat surprisingly, osteogenesis of the maxilla, palatine bones and pre-maxilla on the manipulated side was impeded. It is therefore proposed that disruption of epithelial IRF6 function affects the integrity/polarity of the orofacial epithelia, with secondary effects on underlying neural crest-derived mesenchyme, which does not express IRF6. Disruption of epithelial integrity/polarity may reduce basolateral epithelial-derived growth factor secretion otherwise required to drive the proliferative growth and differentiation of the underlying facial mesenchyme.

GTPases are some of the most ubiquitous regulators of intracellular signaling not only for modulating cell-cell adhesion and cytoskeletal reorganization but also for cell-extracellular matrix (ECM) adhesion (Schock and Perrimon, 2002). Recent studies show evidence that Tiam1-mediated Rac1 activation is also required for integrin signaling and necessary for the proper production and secretion of basement membrane protein, laminin 5 (Hamelers et al, 2005; Mertens et al, 2006). Therefore, it is possible that the effects on Rac1 also impact the basement membrane composition, which could also affect the communication between the epithelia and underlying mesenchyme.

In conclusion, although the exact role of IRF6 in primary palatal fusion is still to be elucidated, the results presented in this study imply a role for IRF6 in maintaining the balance between the adhesiveness and proliferation potential of primary palatal epithelia. More importantly, these findings indicate that NME localization and interactions with other cellular proteins may provide clues as to the cellular pathways in which IRF6 is involved, and therefore an explanation of the cellular etiology of the IRF6 CLP. Furthermore, this study has opened new directions not only for future studies on

IRF6 itself, but in particular on the possible role of NME proteins in governing the behavior of the facial epithelia during fusion of the primary palate and hence susceptibility to CLP.

CHAPTER VII. GENERAL CONCLUSIONS AND FUTURE DIRECTIONS

Clefting of the lip and primary palate (CLP) is the most common congenital deformity of the face, occurring globally with an incidence of approximately 1 out of every 600 to 700 live births (Murray, 2000; Murray, 2002; Nixon et al., 2011). CLP is a complex disease because both genetic and environmental risk factors contribute to its etiology (Murray, 2000; Murray, 2002). A better understanding of the molecular pathways in which these genetic factors function will ultimately provide insight into how genetic susceptibilities may be influenced by maternal nutritional factors to determine whether a child is born with CLP.

Polymorphisms in the *IRF6* gene represent the greatest genetic contribution to isolated CLP, while more deleterious changes are associated with syndromic CLP. Unlike some cleft syndromes, mutations in IRF6 can present with primary and/or secondary palatal clefts. In line with this, recent findings indeed suggest that the *IRF6* gene polymorphisms may influence risk of CLP through interaction between the gene variants and both multivitamin supplementation and smoking, at least in the Chinese population (Wu et al., 2010).

CLP is the result of an aberration in the fusion of embryonic structures during facial development (Cox, 2004; Sun et al., 2000). Development of the primary palate is a highly evolutionarily conserved morphogenetic process that is dependent on proper temporally regulated fusion of the maxillary process with the medial and lateral nasal processes, the latter which are derived from the frontonasal prominence (Cox, 2004).

This fusion occurs during the sixth week of human development, whereas in the chick it occurs around embryonic day 5.5. IRF6 is expressed in the epithelium that mediates the outgrowth and contact of the embryonic tissue masses that fuse to form the upper lip and primary palate as well as in the epithelium that mediates fusion of the palate shelves to form the secondary palate later in development. It is not expressed in the facial mesenchyme. Despite the significance of IRF6's contribution to CLP in humans, mice in which the *Irf6* gene has been deleted or mutated only display secondary palatal clefts and abnormal intraoral adhesions, but do not show classic primary palatal clefts.

The overarching objective of this research was to understand the role of IRF6 in primary palatal development. There was specific interest in discovering the mechanisms by which alteration of IRF6 function could lead to primary palatal clefting and for this reason the development of tools for genetic manipulation in the developing chick system were pursued. The work presented in this thesis has both technical and biological significance. Technically, the facial *in ovo* electroporation method described in Chapter V, constitutes a reproducible method to deliver DNA locally into the pre-fusion epithelia to perform gain and loss of function studies. Biologically, the findings reported in this thesis provide the most detailed insights, to date, into the role of IRF6 in primary palatal epithelia: that is, its association with the NME proteins, NME1 and NME2, which are well known regulators of epithelial integrity that function via control of adherens junction assembly and disassembly.

The application of dominant negative forms and small interfering RNA molecules to mediate disruption of function and silencing of IRF6 during development, in combination

with the application of the electroporation technique to transfer these inhibitory molecules *in ovo,* have greatly extended the utility of the chick embryo as a powerful alternative animal system for clefting research. The work presented in this thesis also extends the utility of *in ovo* electroporation to much later developmental stages than previously reported and has revealed that the expression from electroporated constructs can persist in the orofacial epithelia for up to eight days after electroporation. This extended expression period may open up further avenues of research using the chick, for example, for studies of epithelial stratification or specialization as seen with feather production. With respect to the orofacial region, this approach offers a rapid means by which to investigate the function of not only IRF6, but also other genes that have been implicated in the presentation of CLP in humans by opening avenues to manipulate their expression / function.

These findings, described in detail in Chapter VI, have revealed several important facts about the role of IRF6 in primary palate development. First, it was demonstrated that normal IRF6 expression in epithelial cells is required to promote outgrowth and fusion of the facial prominences. Second, IRF6 is an essential regulator of epithelial cell proliferation and adhesion. And third, it was shown that changes in IRF6 activity lead to clefting with secondary effects on growth and differentiation of the underlying mesenchyme.

Protein-protein interactions are required for the regulation of essentially all biological processes in a living cell. Upon interaction, proteins can be subjected to several events such as protein modification, transport, folding or signaling in order to regulate their

interaction with other proteins and ensure their proper control of processes within the cell. Therefore, in order to further assist the dissection of IRF6 function in primary palatal epithelia, carefully controlled yeast two-hybrid screens were performed, as described in Chapter IV, which led to the identification of NME2 as a direct IRF6 protein interactor. Expression analysis in chick heads demonstrated that NME2 is present in the epithelium and to a slightly lesser degree in the underlying neural crest derived mesenchyme of the medial nasal, lateral nasal and the maxillary process during facial development and colocalizes with IRF6 in the cytoplasm of primary palatal epithelial cells. Further studies showed that this interaction was enhanced by IRF6 phosphorylation. Furthermore, it was demonstrated that NME1, the member of the NME family most closely related to NME2, forms part of the same complex as a result of the heteromultimerization between the NME proteins even though IRF6 does not appear to directly interact with NME1.

Based on the described findings and evidence in the literature from studies regarding other IRF members, as well as on the function of the NME proteins in other epithelial systems, it is proposed that the IRF6:NME complex functions to maintain primary palatal epithelial integrity and perhaps control its unique behavior that is observed during primary palatal fusion. In this model, it is proposed that IRF6 in primary epithelia is largely phosphorylated, perhaps in response to continual stimulation by EGF or other regulators of ‘epithelial’ integrity. This phosphorylation of IRF6 ensures a conformational change that allows exposure of the IAD promoting its interaction with NME2/1 (NME). This interaction in the cytoplasm could regulate NME association with microtubules to exert their function in the assembly and disassembly of E-cadherin. In turn, the NME

interaction would sequester IRF6 preventing its translocation into the nucleus. When IRF6 is mutated (as in patients) or knocked down, there is non-functional or less IRF6 to interact with NME proteins. As a consequence, there would be excess free NME1/2. It is proposed that the available NME1/2 would bind to Tiam1, localizing Tiam1 to the early endocytic vesicle membrane. This interaction would have two effects. First, deregulation of E-cadherin endocytosis, and second, inactivation of Rac1. This would result in decreased apicolateral E-cadherin and ultimately loss of apical-basal polarity, in turn probably affecting basal secretion of factors supporting growth and differentiation of the underlying facial mesenchyme. Finally, remaining IRF6 no longer bound to NME proteins would undergo dimerization and translocation into the nucleus for activation of genes involved in proliferation (Figure 7.1).

Although this model is merely speculative, it suggests novel and interesting molecular pathways to explain the etiology of IRF6 clefting. Furthermore, it provides support to IRF6 functions in both a cell-autonomous manner to regulate epithelial proliferation and integrity of adherens junctions, specifically E-cadherin, and in a non-cell autonomous manner regulating mesenchymal outgrowth.

Experimental results presented in this thesis do not provide data about several important issues regarding the signal that triggers IRF6 phosphorylation or the details of the mechanism by which IRF6 is actually translocated to the nucleus. Hence, deciphering the function and regulation of the IRF6:NME2 protein interaction will likely provide important details to validate this model, which would be the main goal of future research. Next steps in this approach could include the examination of activated Rac1

as well as endocytosis of E-cadherin following IRF6 manipulation. Furthermore, the interaction of NME proteins with microtubules and adherens junctions in primary palatal epithelial should be confirmed. Confirmation of the identity of the unknown phosphorylated proteins that were immunoprecipitated with IRF6 (Chapter IV) may also provide more direction in these future studies.

Information generated from this study and subsequent investigations will slowly elucidate the complex function of IRF6, the major cleft gene, and position it within one or more molecular pathway(s) that have not been previously investigated for the role in primary palatal development or, more specifically, susceptibility of CLP.

In conclusion, the work presented in this thesis has provided some novel insights into IRF6 function in maintaining the balance between adhesion and proliferation during primary palatal development, most likely through its interaction with NME proteins.

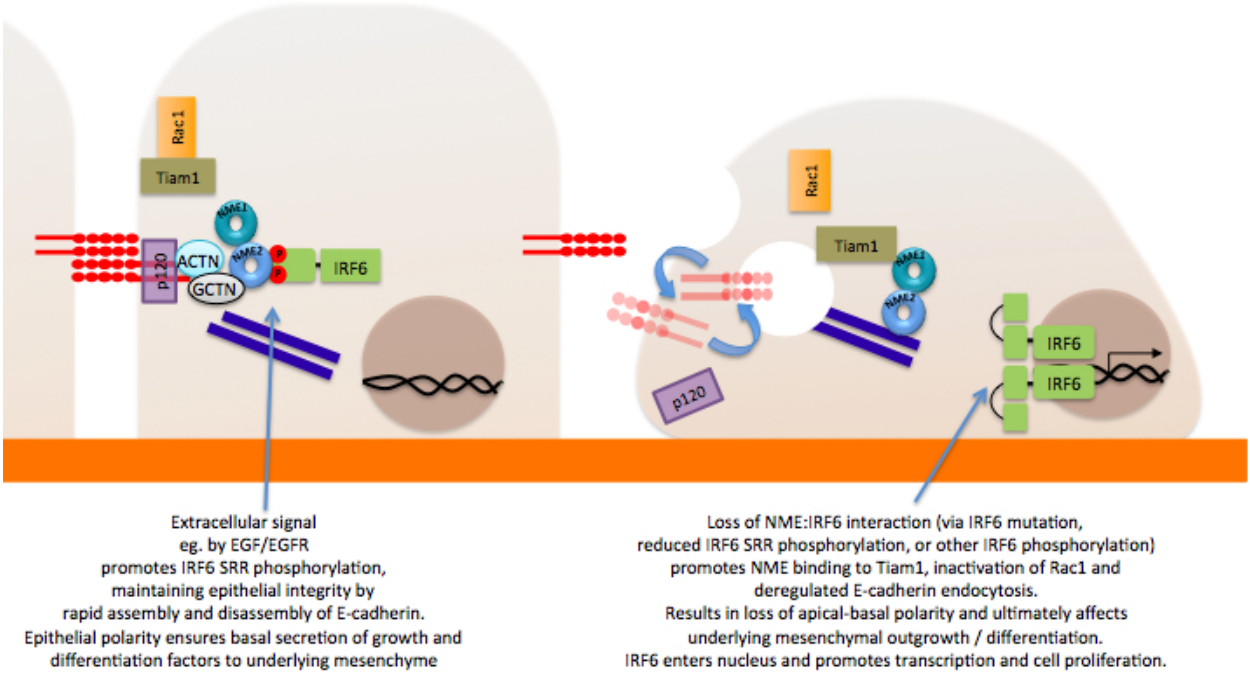

Figure 7.1. Hypothetical model of IRF6 function in orofacial epithelia. In normal epithelia (on the left), localization of Tiam1-Rac1 and p120 catenin at the membrane functions to maintain epithelial polarity and promote assembly of E-cadherin complexes. Phosphorylation of IRF6 under these conditions occurs by unknown kinases, which favors its association with NME2/1. This interaction regulates NME binding between microtubules (thick purple lines) and adherent junctions components (gamma-catenin (GCTN), E-cadherin (in red) and alpha-catenin (ACTN). Decreased phosphorylation of IRF6 (or reduced expression or binding to NME2/1 through mutation) promotes the interaction of NME1/2 with Tiam1, localizing Tiam1 to the early endocytic vesicle membrane, which in turn causes inactivation of Rac1 and increased E-cadherin endocytosis, that is associated with dissociation of p120. The consequence of excessive endocytosis (right side) is decreased apicolateral E-cadherin localization, disassembly of the larger adherens junction complexes, and ultimately loss of apical-basal polarity. This loss of polarity probably affects the basal secretion of factors supporting growth and differentiation of the underlying facial mesenchyme. Free IRF6 undergoes dimerization and translocation into the nucleus for activation of genes involved in proliferation.

BIBLIOGRAPHY

Aktary, Z., Chapman, K., Lam, L., Lo, A., Ji, C., Graham, K., Cook, L., Li, L., Mackey, J.R., Pasdar, M. (2010). Plakoglobin interacts with and increases the protein levels of metastasis suppressor Nm23-H2 and regulates the expression of Nm23-H1. *Oncogene.* 29, 2118-29.

Bailey, C.M., Khalkhali-Ellis, Z., Kondo, S., Margaryan, N.V., Seftor, R.E., Wheaton, W.W., Amir, S., Pins, M.R., Schutte, B.C., Hendrix, M.J. (2005). Mammary serine protease inhibitor (Maspin) binds directly to interferon regulatory factor 6: identification of a novel serpin partnership. *J. Biol. Chem*. 280, 34210-7.

Bailey, C.M., Khalkhali-Ellis, Z., Seftor, E.A., Hendrix, M.J. (2006b). Biological functions of maspin. *J. Cell. Physiol.* 209, 617-24.

Bailey, C.M., Abbott, D.E., Margaryan, N.V., Khalkhali-Ellis, Z., Hendrix, M.J. (2008). Interferon regulatory factor 6 promotes cell cycle arrest and is regulated by the proteasome in a cell cycle dependent manner. *Mol. Cell. Biol.* 28, 2235-43.

Bailey, C.M., Margaryan, N.V., Abbott, D.E., Schutte, B.C., Yang, B., Khalkhali-Ellis, Z., Hendrix, M. J. (2009). Temporal and spatial expression patterns for the tumor suppressor Maspin and its binding partner interferon regulatory factor 6 during breast development. *Dev. Growth. Differ*. 51, 473-81.

Barnes, B.J., Kellum, M.J., Field, A.E., Pitha, P.M. (2002). Multiple regulatory domains of IRF-5 control activation, cellular localization, and induction of chemokines that mediate recruitment of T lymphocytes. *Mol. Cell. Biol.* 22,5721-40.

Basch, M.L., Bronner-Fraser, M., García-Castro, M.I. (2006). Specification of the neural crest occurs during gastrulation and requires Pax7. *Nature*. 11, 218-22.

Barembaum, M., Bronner-Fraser, M. (2007). Spalt4 mediates invagination and otic placode gene expression in cranial ectoderm. *Development*. 134, 3805-14.

Bartolini, F., Gundersen, G.G. (2006). Generation of noncentrosomal microtubule arrays. *J. Cell. Sci.* 119, 4155-63.

Bauer, H., Zweimueller-Mayer, J., Steinbacher, P., Lametschwandtner, A., Bauer, HC. (2010). The dual role of zonula occludens (ZO) proteins. *J. Biomed. Biotechnol.* 2010, 402593.

Boissan, M., De Wever, O., Lizarraga, F., Wendum, D., Poincloux, R., Chignard, N., Desbois-Mouthon, C., Dufour, S., Nawrocki-Raby, B., Birembaut, P., Bracke, M., Chavrier, P., Gespach, C., Lacombe, M.L. (2010). Implication of metastasis suppressor NM23-H1 in maintaining adherens junctions and limiting the invasive potential of human cancer cells. *Cancer. Res.* 70, 7710-22.

Bellett, G., Carter, J.M., Keynton, J., Goldspink, D., James, C., Moss, D.K., Mogensen, M.M. (2009). Microtubule plus-end and minus-end capture at adherens junctions is

involved in the assembly of apico-basal arrays in polarised epithelial cells. *Cell .Motil. Cytoskeleton.* 66, 893-908.

Bech-Otschir, D., Seeger, M., Dubiel, W. (2002). The COP9 signalosome: at the interface between signal transduction and ubiquitin-dependent proteolysis*. J. Cell. Sci.* 115, 467-73.

Bilitou, A., Watson, J., Gartner, A., Ohnuma, S. (2009).The NM23 family in development. *Mol. Cell. Biochem.* 329, 17-33.

Borello, U., Berarducci, B., Murphy, P., Bajard, L., Buffa, V., Piccolo, S., Buckingham, M., Cossu, G. (2006). The Wnt/beta-catenin pathway regulates Gli-mediated Myf5 expression during somitogenesis. *Development.* 133, 3723–32.

Bosnar, M.H., Bago, R., Cetković, H. (2009). Subcellular localization of Nm23/NDPK A and B isoforms: a reflection of their biological function? *Mol. Cell. Biochem*. 329, 63-71.

Boulet, A.M., Capecchi, M.R. (2004). Multiple roles of Hoxa11 and Hoxd11 in the formation of the mammalian forelimb zeugopod. *Development.* 131, 299-309.

Boulyjenkov, V., Mastroiacovo, P., Mossey P., Munjer, R., Murray, J., Shaw W. (2004). In WHO Meeting Report: Addressing the global challenges of craniofacial anomalies. Geneva, Switzerland.

Bowie, M.L., Troch, M.M., Delrow, J., Dietze, E.C., Bean, G.R., Ibarra, C., Pandiyan, G., Seewaldt, V.L. (2007). Interferon regulatory factor-1 regulates reconstituted extracellular matrix (rECM)-mediated apoptosis in human mammary epithelial cells. *Oncogene.* 26, 2017-26.

Bré, M.H., Kreis, T.E., Karsenti, E. (1987). Control of microtubule nucleation and stability in Madin-Darby canine kidney cells: the occurrence of noncentrosomal, stable detyrosinated microtubules. *J. Cell. Biol.* 105,1283-96

Bridge A.J., Pebernard, S., Ducraux, A., Nicoulaz, A.L., Iggo, R. (2003). Induction of an interferon response by RNAi vectors in mammalian cells. *Nat. Genet.* 34, 263-4.

Braun, S., Mauch, C., Boukamp, P., Werner, S. (2007). Novel roles of NM23 proteins in skin homeostasis, repair and disease. *Oncogene*. 26, 532-42.

Brugmann, S.A., Powder, K.E., Young, N.M., Goodnough, L.H., Hahn, S.M., James, A.W., Helms, J.A., Lovett, M. (2010). Comparative gene expression analysis of avian embryonic facial structures reveals new candidates for human craniofacial disorders. *Hum. Mol. Genet.* 19, 920-30.

Buchert, M., Poon, C., King, J.A,, Baechi, T., D'Abaco, G., Hollande, F., Hovens, C.M. (2007). AF6/s-afadin is a dual residency protein and localizes to a novel subnuclear compartment. *J. Cell. Physiol.* 210, 212-23.

Byrom, M., Pallotta, V., Brown, D. & Ford, L. (2002). Visualizing siRNA in mammalian cells: Fluorescence analysis of the RNAi effect. Ambion Technotes Newsletter. 9, 6–8.

Buendia, B., Bré, M. H., Griffiths, G., Karsenti, E. (1990) Cytoskeletal control of centrioles movement during the establishment of polarity in Madin-Darby canine kidney cells. *J. Cell. Biol*. 110,1123-35.

Carroll, D.K., Carroll, J.S., Leong, C.O., Cheng, F., Brown M., Mills, A.A., Brugge, J.S., Ellisen, L.W. (2006). p63 regulates an adhesion programme and cell survival in epithelial cells. *Nature*. 8, 551-61.

Celli, J., Duijf, P., Hamel, B.C., Bamshad, M., Kramer, B., Smits, A.P., Newbury-Ecob, R., Hennekam, R.C., van Buggenhout, G., van Haeringen, A., Woods, C.G., van Essen, A.J., de Waal, R., Vriend, G., Haber, D.A., Yang, A., McKeon, F., Brunner, H.G., van Bokhoven, H. (1999). Heterozygous germline mutations in the p53 homolog p63 are the cause of EEC syndrome. *Cell.* 99,143-53.

Chang Foreman, H.C., Van Scoy, S., Cheng, T.F., Reich NC. (2012). Activation of interferon regulatory factor 5 by site specific phosphorylation. *PLoS One*. 7, e33098.

Chapman, R.S., Duff, E.K., Lourenco, P.C., Tonner, E., Flint, D.J., Clarke, A.R., Watson, C. J. (2000). A novel role for IRF-1 as a suppressor of apoptosis. *Oncogene.* 19, 6386-91.

Claret, F.X., Hibi, M., Dhut, S., Toda, T., Karin, M. (1996). A new group of conserved coactivators that increase the specificity of AP-1 transcription factors. *Nature.* 383, 453-7.

Chen, Y.X., Krull, C.E., Reneker, L.W. (2004) Targeted gene expression in the chicken eye by in ovo electroporation. *Mol. Vis.* 10,874-83.

Chen, W., Lam, S.S., Srinath, H., Jiang, Z., Correia, J.J., Schiffer, C.A., Fitzgerald, K.A., Lin, K., Royer, W.E. Jr. (2008). Insights into interferon regulatory factor activation from the crystal structure of dimeric IRF5. *Nat. Struct. Mol. Biol*. 15,1213-20.

Chen, W., Royer, W.E. Jr. (2010). Structural insights into interferon regulatory factor activation. *Cell. Signal.* 22, 883-7

Chesnutt, C, Niswander, L. (2004) .Plasmid-based short-hairpin RNA interference in the chicken embryo. *Genesis*. 39,73-8.

Cox, T.C., Allen, L. R., Cox, L. L., Hopwood, B., Goodwin, B., Haan, E., and Suthers, G. K. (2000). New mutations in MID1 provide support for loss of function as the cause of X-linked Opitz syndrome. *Hum. Mol. Genet.* 9,2553-62.

Cox, T.C. (2004). Taking it to the max: the genetic and developmental mechanisms coordinating midfacial morphogenesis and dysmorphology. *Clin. Genet*. 65,163–176.

Cuervo, R., Valencia, C., Chandraratna, R. A., Covarrubias, L. (2002) Programmed cell death is required for palate shelf fusion and is regulated by retinoic acid. *Dev. Biol.* 245,145-56.

Dal Zotto, L., Quaderi, N.A., Elliott, R., Lingerferter, P.A., Carrel, L., Valssechi, V., Montini, E., Yen, C.H., Chapman, V., Kalcheva, I., Arrigo, G., Zuffardi, O., Thomas, S., Willard, H.F., Ballabio, A., Disteche, C.M. and Rugarli, E.I. (1998). The mouse Mid1 gene: implications for the pathogenesis of Opitz syndrome and the evolution of the mammalian pseudoautosomal region. *Hum. Mol. Genet.* 7, 489-99.

Dai, F., Yusuf, F., Farjah, G.H., Brand-Saberi B. (2005). RNAi-induced targeted silencing of developmental control genes during chicken embryogenesis. *Dev Biol.* 285, 80-90.

Dammai V., Adryan, B., Lavenburg, K.R., Hsu, T. (2003) Drosophila awd, the homolog of human nm23, regulates FGF receptor levels and functions synergistically with shi/dynamin during tracheal development. *Genes. Dev.* 17, 2812-24.

Darnell, J.E. Jr., Kerr, I.M., Stark, G.R. (2004). Jak-STATpathways and transcriptional activation in response to IFNs and other extracellular signaling proteins. *Science.* 264,1415–21.

Desvignes, T., Pontarotti, P., Fauvel, C., Bobe, J. (2009). Nme protein family evolutionary history, a vertebrate perspective. *BMC. Evol. Biol.* 23, 9:256.

Dixon, M.J., Marazita, M.L., Beaty, T.H., Murray, J.C. (2011). Cleft lip and palate: understanding genetic and environmental influences. *Nat. Rev. Genet.* 12,167-78.

Eroshkin, A., Mushegian, A. (1999). Conserved transactivation domain shared by interferon regulatory factors and Smad morphogens. *J. Mol. Med.* 77,403-405.

Etienne-Manneville, S. (2011). Control of polarized cell morphology and motility by adherens junctions. Semin. *Cell. Dev. Biol.* 22, 850-7.

Fisher, M.E., Clelland, A.K., Bain, A., Baldock, R.A., Murphy, P., Downie, H., Tickle, C., Davidson, D.R., Buckland, R.A. (2008). Integrating technologies for comparing 3D gene expression domains in the developing chick limb. *Dev. Biol.* 317,13-23.

Fitchett, J.E., Hay, E. D. (1989). Medial edge epithelium transforms to mesenchyme after embryonic palatal shelves fuse. *Dev. Biol.* 131,455-74

Fournier, H.N., Albigès-Rizo, C., Block, M.R. (2003). New insights into Nm23 control of cell adhesion and migration. *J. Bioenerg. Biomembr.* 35, 81-7.

Froster-Iskenius, U.G. (1990). Popliteal pterygium syndrome. *J. Med. Genet.* 27,320-6.

Fujii, Y., Shimizu, T., Kusumoto, M., Kyogoku, Y., Taniguchi, T., Hakoshima, T. (1999). Crystal structure of an IRF-DNA complex reveals novel DNA recognition and cooperative binding to a tandem repeat of core sequences. *Embo. J*. 18, 5028-5041.

Gilles, A.M., Presecan, E., Vonica, A., Lascu, I. (1991). Nucleoside diphosphate kinase from human erythrocytes. Structural characterization of the two polypeptide chains responsible for heterogeneity of the hexameric enzyme. *J. Biol. Chem.* 15, 8784-9.

Gong, S.G. & Guo, C. (2003). Bmp4 gene is expressed at the putative site of fusion in the midfacial region. *Differentiation.* 71, 228-36.

Goodnough, L.H., Brugmann, S.A., Hu, D., Helms, J.A. (2007). Stage-dependent craniofacial defects resulting from Sprouty2 overexpression. *Dev. Dyn.* 236,1918-28.

Gordon, C.T., Brinas, I.M., Rodda, F.A., Bendall, A.J., Farlie, P.G. (2010). Role of Dlx genes in craniofacial morphogenesis: Dlx2 influences skeletal patterning by inducing ectomesenchymal aggregation in ovo. *Evol. Dev.* 12,459-73.

Gumbiner, B.M. (2005). Regulation of cadherin-mediated adhesion in morphogenesis. *Nat. Rev. Mol. Cell. Biol.* 6, 622-34.

Hamelers, I.H., Olivo, C., Mertens, A.E., Pegtel, D.M., van der Kammen, R.A., Sonnenberg, A., Collard, J.G. (2005) The Rac activator Tiam1 is required for (alpha)3(beta)1-mediated laminin-5 deposition, cell spreading, and cell migration. *J. Cell. Biol.* 171, 871-81.

Hannon, G.J. (2002). RNA interference. *Nature.* 418:244-51.

Hilton, J. L., Kearney, P. C., Ames, B. N. (1965). Mode of action of the herbicide 3-amino-1,2,4-triazole (amitrole): inhibition of an enzyme of histidine biosynthesis. *Arch. Biochem. Biophys.* 112, 544-547.

Honda, K. & Taniguchi, T. (2006) IRFs: master regulators of signalling by Toll-like receptors and cytosolic pattern-recognition receptors. *Nat. Rev. Immunol*. 6, 644–658.

Honda, K., Takaoka, A., Taniguchi, T. (2006). Type I interferon [corrected] gene induction by the interferon regulatory factor family of transcription factors. *Immunity.* 25, 349-60.

Hsu, T. NME genes in epithelial morphogenesis. (2011). *Naunyn. Schmiedebergs. Arch. Pharmacol*. 384, 363-72.

Hu, D., Marcucio, R.S., J.A. Helms. (2003). A zone of frontonasal ectoderm regulates patterning and growth in the face. *Development.* 130,1749-1758.

Ingraham, C.R., Kinoshita, A., Kondo, S. et al. (2006). Abnormal skin, limb, and craniofacial morphogenesis in mice deficient for interferon regulatory factor (IRF6). *Nat. Genet.* 38, 1335-340.

Itasaki, N., Bel-Vialar, S., Krumlauf, R. (1999). 'Shocking' developments in chick embryology: electroporation and in ovo gene expression. *Nat. Cell. Biol.* 1, E203-7.

Iwashita, S., Fujii, M., Mukai, H., Ono, Y., Miyamoto M. (2004). Lbc proto-oncogene product binds to and could be negatively regulated by metastasis suppressor nm23-H2. *Biochem. Biophys. Res. Commun.* 320, 1063-8.

Jamieson, C., Sharma, M., Henderson, B.R. (2012). Wnt signaling from membrane to nucleus: β-catenin caught in a loop. *Int. J. Biochem. Cell .Biol*. 44, 847-50.

Jiang, R., Bush, J.O., Lidral, AC. (2006). Development of the upper lip: morphogenetic and molecular mechanisms. *Dev. Dyn.* 235,1152-66.

Kimura, N., Shimada, N., Fukuda, M., Ishijima, Y., Miyazaki, H., Ishii, A., Takagi, Y., Ishikawa, N. (2000). Regulation of cellular functions by nucleoside diphosphate kinases in mammals. *J. Bioenerg. Biomembr.* 32, 309-15.

Katahira, T., Nakamura, H. (2003) Gene silencing in chick embryos with a vector-based small interfering RNA system. *Develop. Growth. Differ.* 44,361–367.

Kerwin, J., Scott, M., Sharpe, J., Puelles, L., Robson, S.C., Martinez-dela-Torre, M., Ferran, J.L., Feng, G., Baldock, R., Strachan, T., Davidson, D., Lindsay, S. (2004). 3 dimensional modelling of early human brain development using optical projection tomography. *BMC. Neurosci.* 5,27.

Klopotowski, T., and Wiater, A. (1965). Synergism of aminotriazole and phosphate on the inhibition of yeast imidazole glycerol phosphate dehydratase. *Arch. Biochem. Biophys.* 112,562-566.

Knight, A.S., Schutte, B.C., Jiang, R., Dixon, M.J. (2006). Developmental expression analysis of the mouse and chick orthologues of IRF6: the gene mutated in Van der Woude syndrome. *Dev. Dyn.* 235,1441-7.

Kondo, S., Schutte, B.C., Richardson, R.J., Bjork, B.C., Knight, A.S., Watanabe, Y., Howard, E., de Lima, R.L., Daack-Hirsch, S., Sander, A., McDonald-McGinn, D.M., Zackai, E.H., Lammer, E.J., Aylsworth, A.S., Ardinger, H.H., Lidral, A.C., Pober, B.R., Moreno, L., Arcos-Burgos, M., Valencia, C., Houdayer, C., Bahuau, M., Moretti-Ferreira, D., Richieri-Costa, A., Dixon, M.J., Murray, J.C. (2002). Mutations in IRF6 cause Van der Woude and popliteal pterygium syndromes. *Nat. Genet.* 32,285-289.

Kos, R., Reedy, M.V., Johnson, R.L., Erickson C.A. (2001). The winged-helix transcription factor FoxD3 is important for establishing the neural crest lineage and repressing melanogenesis in avian embryos. *Development*. 128,1467-79.

Kraeft, S.K., Traincart, F., Mesnildrey, S., Bourdais, J., Véron, M., Chen, L.B. (1996) Nuclear localization of nucleoside diphosphate kinase type B (nm23-H2) in cultured cells. *Exp. Cell. Res.* 227, 63-9.

Lau, J.F., Parisien, J.P., Horvath, C.M. (2000). Interferon regulatory factor subcellular localization is determined by a bipartite nuclear localization signal in the DNA-binding domain and interaction with cytoplasmic retention factors. Proc. Natl. Acad. Sci. 97,7278-7283.

Leoyklang, P.S., Shotelersuk ,V. (2006). A mutation of the p63 gene in non-syndromic cleft lip*. J. Med. Genet*. 43, e28.

Lee, K., Avondo, J., Morrison, H., Blot, L., Stark, M., Sharpe, J., Bangham, A., Coen, E. (2006). Visualizing plant development and gene expression in three dimensions using optical projection tomography. Plant. Cell. 18, 2145–2156.

Li, X., Liu, J., Davey, M.G., Duce, S., Jaberi, J., Liu, G., Davidson, G., Tenent, S., Mahood, R., Brown, P., Cunningham, C., Bain, A., Beattie, K., McDonald, L., Schmidt, K., Towers, M., Tickle, C., Chudek, J.A. (2007). Micro-magnetic resonance imaging of avian embryos. *J. Anat*. 211, 798–809.

Lin, R., Mamane, Y., Hiscott, J. (1999). Structural and functional analysis of interferon regulatory factor 3: localization of the transactivation and autoinhibitory domains. *Mol. Cell. Biol.* 19, 2465-74.

Little, H. J., Rorick N. K., Su, L., Baldock, C., Malhotra, S., Jowitt, T., Gakhar L., Subramanian, R., Schutte, B. C. Dixon, M. J., Shore, P. (2009). Missense mutations that cause Van der Woude syndrome and popliteal pterygium syndrome affect the DNA-binding and transcriptional activation functions of IRF6. *Hum. Mol. Genet*. 18, 535–545.

Lombardi, D., Lacombe, M.L., Paggi, M.G. (2000). nm23: unraveling its biological function in cell differentiation. *J. Cell. Physiol*. 182, 144-9.

Ma, J. and Ptashne, M. (1987). A new class of yeast transcriptional activators. *Cell*. 51, 113–119.

MacDonald, M.E., Abbott, U.K., Richman, J.M. (2004). Upper beak truncation in chicken embryos with the cleft primary palate mutation is due to an epithelial defect in the frontonasal mass. *Dev. Dyn.* 230,335-49.

McGonnell, I.M., Clarke, J.D., Tickle, C. (1998). Fate map of the developing chick face: analysis of expansion of facial primordia and establishment of the primary palate. *Dev. Dyn.* 212,102-18.

Mamane, Y., Sharma, S., Petropoulos, L., Lin, R., Hiscott, J. (2000). Posttranslational regulation of IRF-4 activity by the immunophilin FKBP52. *Immunity.* 12, 129-40.

Mamane, Y., Heylbroeck, C., Génin, P., Algarté, M., Servant, M.J., LePage, C., DeLuca, C., Kwon, H., Lin, R., Hiscott, J. (1999). Interferon regulatory factors: the next generation. *Gene.* 237,1–14.

Marino, N., Marshall, J.C., Steeg, P.S. (2011). Protein-protein interactions: a mechanism regulating the anti-metastatic properties of Nm23-H1. *Naunyn. Schmiedebergs. Arch. Pharmacol.* 384, 351-62.

Martínez-Alvarez, C., Bonelli, R., Tudela, C., Gato, A., Mena, J., O'Kane, S., Ferguson, M. W. (2000). Bulging medial edge epithelial cells and palatal fusion. *Int. J. Dev. Biol.* 44,331-5.

McGrath, J.A., Duijf, P.H., Doetsch, V., Irvine, A.D., de Waal, R., Vanmolkot, K.R., Wessagowit, V., Kelly, A., Atherton, D.J., Griffiths, W.A., Orlow, S.J., van Haeringen, A., Ausems, M.G., Yang, A., McKeon, F., Bamshad M.A., Brunner, H.G., Hamel, B.C., van Bokhoven, H. (2001). Hay-Wells syndrome is caused by heterozygous missense mutations in the SAM domain of p63. *Hum. Mol. Genet.* 10,221-9.

McGurk, L., Morrison, H., Keegan, L.P., Sharpe, J., O'Connell, M.A. (2007). Three dimensional imaging of Drosophila melanogaster. *PLoS. ONE*. 2,e834.

Meng, W., Mushika, Y., Ichii, T., Takeichi, M. (2008). Anchorage of microtubule minus ends to adherens junctions regulates epithelial cell-cell contacts. *Cell.* 135, 948-59.

Melki, R., Lascu, I., Carlier, M.F., Véron, M. (1992) Nucleoside diphosphate kinase does not directly interact with tubulin nor microtubules. *Biochem. Biophys. Res. Commun.* 187, 65-72.

Meraro D, Hashmueli S, Koren B, Azriel A, Oumard A, Kirchhoff S, Hauser H, Nagulapalli S, Atchison ML, Levi BZ. (1999). Protein-protein and DNA-protein interactions affect the activity of lymphoid-specific IFN regulatory factors. *J. Immunol.* 163,6468-6478.

Mertens, A.E., T.P. Rygiel, C. Olivo, R. van der Kammen, and J.G. Collard. (2005). The Rac activator Tiam1 controls tight junction biogenesis in keratinocytes through binding to and activation of the Par polarity complex. *J. Cell. Biol.* 170,1029–1037.

Mertens, A.E., Pegtel, D.M., Collard, J.G. (2006) Tiam1 takes PARt in cell polarity. Trends. *Cell. Biol.* 16, 308-16.

Miller, S.F., Summerhurst, K., Runker, A.E., Kerjan, G., Friedel, R.H., Chedotal, A., Murphy, P., Mitchell, K.J. (2007). Expression of Plxdc2/TEM7R in the developing nervous system of the mouse. *Gene. Expr. Patterns.* 7,635–644.

Mills, A.A., Zheng, B., Wang, X.J., Vogel, H., Roop, D.R., Bradley, A. (1999). p63 is a p53 homologue required for limb and epidermal morphogenesis. *Nature*. 22, 708-13.

Mimori-Kiyosue Y, Tsukita S."Search-and-capture" of microtubules through plus-end-binding proteins (+TIPs). *J. Biochem.* 2003 Sep;134(3):321-6

Mitchell, K.A., Gallagher, B.C., Szabo, G., De S. Otero, A. (2004). NDP kinase moves into developing primary cilia. *Cell. Motil. Cytoskeleton.* 59, 62-73.

Momose, T., Tonegawa, A., Takeuchi, J., Ogawa, H., Umesono, K., Yasuda, K. (1999). Efficient targeting of gene expression in chick embryos by microelectroporation. *Dev, Growth. Differ*. 41,335-44.

Mogensen, M.M. (1999). Microtubule release and capture in epithelial cells. *Biol. Cell.* 91,331-41.

Moretti F, Marinari B, Lo Iacono N, Botti E, Giunta A, Spallone G, Garaffo G, Vernersson-Lindahl E, Merlo G, Mills AA, Ballarò C, Alemà S, Chimenti S, Guerrini L, Costanzo A. (2010). A regulatory feedback loop involving p63 and IRF6 links the pathogenesis of 2 genetically different human ectodermal dysplasias. *J. Clin. Invest.* 120,1570-7.

Munier, A., Serres, C., Kann, M.L, Boissan, M., Lesaffre, C., Capeau, J., Fouquet, J.P., Lacombe, M.L. (2003). Nm23/NDP kinases in human male germ cells: role in spermiogenesis and sperm motility? *Exp. Cell. Res.* 289, 295–306.

Muramatsu, T., Mizutani, Y., Ohmori, Y., Okumura, J. (1997). Comparison of three nonviral transfection methods for foreign gene expression in early chicken embryos in ovo. Biochem. *Biophys. Res. Commun.* 230,376-80.

Murray, J, (2000). Meeting Report. . WHO Meeting: International collaborative research on craniofacial anomalies. Geneva, Switzerland

Murray, J.C. (2002). Gene/environment causes of cleft lip and/or palate. Clin. Genet. 61, 248-56.

Muramatsu, T., Shibata, O., Ryoki, S., Ohmori, Y., Okumura, J. (1997b). Foreign gene expression in the mouse testis by localized in vivo gene transfer. *Biochem. Biophys. Res. Commun.* 233,45-9.

Niessen, C.M. (2007). Tight Junctions/Adherens Junctions: Basic structure and function. *Journal of Investigative Dermatology.* 127, 2525–2532.

Otsuki, Y., Tanaka, M., Yoshii, S., Kawazoe, N., Nakaya, K., Sugimura, H. (2001) Tumor metastasis suppressor nm23H1 regulates Rac1 GTPase by interaction with Tiam1*. Proc. Natl. Acad. Sci*. 98, 4385-90.

Ozato, K., Tailor, P., Kubota, T. (2007). The interferon regulatory factor family in host defense: mechanism of action. *J. Biol. Chem.* 282, 20065-9.

Paddison, P.J., Caudy, A.A., Bernstein, E., Hannon, G.J., Conklin, D.S. (2002). Short hairpin RNAs (shRNAs) induce sequence-specific silencing in mammalian cells. *Genes. Dev.* 16, 948-958.

Paun, A., Pitha, P.M. (2007). The IRF family, revisited. *Biochimie.* 89, 744-53.

Pieters, T., van Hengel, J., van Roy, F. (2012). Functions of p120ctn in development and disease. *Front Biosci.* 17, 760-83.

Pinon VP, Millot G, Munier A, Vassy J, Linares-Cruz G, Capeau J, Calvo F, Lacombe ML. (1999). Cytoskeletal association of the A and B nucleoside diphosphate kinases of interphasic but not mitotic human carcinoma cell lines: specific nuclear localization of the B subunit. *Exp. Cell. Res.* 246, 355-67.

Polette, M., Mestdagt, M., Bindels, S., Nawrocki-Raby, B., Hunziker, W., Foidart, J.M., Birembaut, P., Gilles, C. (2007). Beta-catenin and ZO-1: shuttle molecules involved in tumor invasion-associated epithelial-mesenchymal transition processes. *Cells. Tissues. Organs.* 185, 61-5.

Postel, E.H., Berberich, S.J., Flint, S.J., Ferrone, C.A. (1993). Human c-myc transcription factor PuF identified as nm23-H2 nucleoside diphosphate kinase, a candidate suppressor of tumor metastasis. *Science*. 261, 478-80.

Postel, E.H. (1998). NM23-NDP kinase. *Int. J. Biochem. Cell. Biol.* 30, 1291-5.

Postel EH, Berberich SJ, Rooney JW, Kaetzel DM. (2000). Human NM23/nucleoside diphosphate kinase regulates gene expression through DNA binding to nuclease-hypersensitive transcriptional elements. *J. Bioenerg. Biomembr.* 32, 277-84.

Qin, B.Y., Liu, C., Lam, S.S., Srinath, H., Delston, R., Correia, J.J., Derynck, R., Lin, K. (2003). Crystal structure of IRF-3 reveals mechanism of autoinhibition and virus-induced phosphoactivation. *Nat. Struct. Biol.* 10,913-921.

Qin, B.Y., Liu, C., Srinath, H., Lam, S.S., Correia, J.J., Derynck, R., Lin, K. (2005). Crystal structure of IRF-3 in complex with CBP. *Structure.* 13,1269–1277.

Rossman, K.L., Der, C.J., Sondek, J. (2005). GEF means go: turning on RHO GTPases with guanine nucleotide-exchange factors. *Nat. Rev. Mol. Cell. Biol.* 6,167-80.

Renzi, M.J., Wexler, T.L., Raper, J.A. (2000). Olfactory sensory axons expressing a dominant-negative semaphorin receptor enter the CNS early and overshoot their target. *Neuron.* 28,437-447.

Richardson, R.J., Dixon, J., Malhotra, S. et al. (2006). IRF6 is a key determinant of the keratinocyte proliferation-differentiation switch. *Nat. Genet.* 38,1329-1334.

Richardson R. J., Dixon, J., Jiang, R., Dixon, M. J. (2009). Integration of IRF6 and Jagged2 signalling is essential for controlling palatal adhesion and fusion competence. *Hum. Mol. Genet.* 18,2632-2642.

Richman, J.M., Tickle, C. (1989). Epithelia are interchangeable between facial primordia of chick embryos and morphogenesis is controlled by the mesenchyme. *Dev. Biol.* 136, 201-10.

Richman, J.M., Fu K.K., Cox, L.L., Sibbons, J.P., Cox T.C. (2002). Isolation and characterization of the chick orthologue of the Opitz syndrome gene, Mid1, supports a conserved role in vertebrate development. *Int. J. Dev. Biol.* 46,441-448.

Rinne, T., Brunner, H.G., van Bokhoven, H. p63-associated disorders. (2007). *Cell. Cycle.* 6, 262-268.

Rizos, M., Spyropoulos, M.N. Van der Woude syndrome: a review. Cardinal signs, epidemiology, associated features, differential diagnosis, expressivity, genetic counselling and treatment. *Eur. J. Orthod.* (2004) 26,17–24.

Robin, N.H., Opitz, J.M. and Muenke, M. (1996). Opitz G/BBB syndrome: clinical comparisons of families linked to Xp22 and 22q, and a review of the literature. *Am. J. Med. Genet.* 62,305-317.

Ruden, D. M. (1992). Activating regions of yeast transcription factors must have both acidic and hydrophobic amino acids. *Chromosoma.* 101,342–348.

Ruden, D. M., Ma, J., Li, Y., Wood, K. & Ptashne, M. (1991). Generating yeast transcriptional activators containing no yeast protein sequences. *Nature.* 350,250–251.

Sabel, J.L., d'Alençon, C., O'Brien, E.K. et al. (2009). Maternal Interferon Regulatory Factor 6 is required for the differentiation of primary superficial epithelia in Danio and Xenopus embryos. *Dev. Biol.* 325,249-262.

Sander, E.E., van Delft, S., ten Klooster, J.P., Reid, T., van der Kammen, R.A., Michiels, F., Collard, J.G. (1998). Matrix-dependent Tiam1/Rac signaling in epithelial cells promotes either cell-cell adhesion or cell migration and is regulated by phosphatidylinositol 3-kinase. *J. Cell. Biol*.143:1385-98.

Sander, E.E., ten Klooster, J.P., van Delft, S., van der Kammen, R.A., Collard, J.G. (1999). Rac downregulates Rho activity: reciprocal balance between both GTPases determines cellular morphology and migratory behavior. *J. Cell. Biol.* 147, 1009-22.

Sauka-Spengler, T., Barembaum, M. (2008). Gain- and loss-of-function approaches in the chick embryo. *Methods. Cell. Biol.* 87,237-256.

Schock, F., Perrimon, N. (2002). Molecular mechanisms of epithelial morphogenesis. *Annu. Rev. Cell. Dev. Biol.* 18, 463-93.

Szabo-Rogers, H.L., Geetha-Loganathan, P., Nimmagadda, S., Fu, K.K., Richman, J.M. (2008). FGF signals from the nasal pit are necessary for normal facial morphogenesis. *Dev. Biol.* 15, 289-302.

Sperber, G.H., Craniofacial Development. (2001) London: BC Decker.

Scapoli, L., Palmieri, A., Martinelli, M., Pezzetti, F. (2005). Strong evidence of linkage disequilibrium between polymorphisms at the IRF6 locus and nonsyndromic cleft lip with or without cleft palate, in an Italian population. *Am. J. Hum. Genet.* 76,180–183.

Scapoli. L., Palmieri, A., Martinelli, M., Vaccari, C., Marchesini, J., Pezzetti, F., Baciliero, U., Padula, E., Carinci, P., Carinci, F. (2006). Study of the PVRL1 gene in Italian nonsyndromic cleft lip patients with or without cleft palate. *Ann Hum Genet*. 70, 410-3.

Scapoli L., Martinelli M., Arlotti M., Palmieri A., Masiero E., Pezzetti F., Carinci F. (2008). Genes causing clefting syndromes as candidates for non-syndromic cleft lip with or without cleft palate: a family-based association study. *Eur. J. Oral. Sci.* 116, 507-511.

Short, K.M., Hopwood, B., Yi, Z., Cox, T.C. (2002). MID1 and MID2 homo- and heterodimerise to tether the rapamycin-sensitive PP2A regulatory subunit, alpha 4, to microtubules: implications for the clinical variability of X-linked Opitz GBBB syndrome and other developmental disorders. *BMC. Cell. Biol.* 3,1-14

Sozen, M.A., Suzuki, K., Tolarova, M.M., Bustos, T., Fernandez Iglesias, J.E., Spritz, R.A. (2001). Mutation of PVRL1 is associated with sporadic, non-syndromic cleft lip/palate in northern Venezuela. *Nat. Genet.* 29,141-142.

Sharpe, J., Ahlgren, U., Perry, P., Hill, B., Ross, A., Hecksher-Sorensen, J., Baldock, R., Davidson, D. (2002). Optical projection tomography as a tool for 3D microscopy and gene expression studies. *Science*. 296, 541–545.

Sharpe, J. (2003). Optical projection tomography as a new tool for studying embryo anatomy. *J. Anat. 202*, 175–181.

Short, K. M., Cox, T. C. (2006). Subclassification of the RBCC/TRIM superfamily reveals a novel motif necessary for microtubule binding. *J. Biol. Chem.* 281, 8970-80.

Stottmann, R. W., Bjork, B.C., Doyle, J.B., Beier, D, R. (2010a). Identification of a Van der Woude syndrome mutation in the cleft palate 1 mutant mouse. *Genesis.* 48,281.

Stottmann, R. W., Bjork, B.C., Doyle, J.B., Beier, D, R. (2010). Identification of a Van der Woude syndrome mutation in the cleft palate 1 mutant mouse. *Genesis.* 48,303-8.

Suhara W, Yoneyama M, Kitabayashi I, Fujita T. (2002). Direct involvement of CREB-binding protein/p300 in sequence-specific DNA binding of virus-activated interferon regulatory factor-3 holocomplex. *J. Biol. Chem.* 277,22304-22313.

Sun, D., Baur, S., Hay E.D. (2000). Epithelial-mesenchymal transformation is the mechanism for fusion of the craniofacial primordia involved in morphogenesis of the chicken lip. *Dev. Biol.* 228, 337-349.

Summerhurst, K., Stark, M., Sharpe, J., Davidson, D., Murphy, P. (2008). 3D representation of Wnt and Frizzled gene expression patterns in the mouse embryo at embryonic day 11.5 (Ts 19). *Gene. Expr. Patterns*. 8, 331–348.

Suzuki-Hirano, A., Sato, T., Nakamura, H. Regulation of isthmic Fgf8 signal by sprouty2. *Development.* (2005). 132, 257-265.

Suzuki, K., Hu, D., Bustos, T., Zlotogora, J., Richieri-Costa, A., Helms, J.A., Spritz, R.A. Mutations of PVRL1, encoding a cell-cell adhesion molecule/herpesvirus receptor, in cleft lip/palate-ectodermal dysplasia. *Nat. Genet.* (2000). 25, 427-430.

Takaoka, A., Tamura, T., Taniguchi, T. (2008). Interferon regulatory factor family of transcription factors and regulation of oncogenesis. *Cancer Sci.* 99, 467-78.

Tamura, T., Yanai, H., Savitsky, D., Taniguchi, T. (2008). The IRF Family Transcription Factors in Immunity and Oncogenesis. *Annu. Rev. Immunol*. 26, 535–584.

Tanaka, N., Kawakami, T., Taniguchi, T. (1993). Recognition DNA sequences of interferon regulatory factor 1 (IRF-1) and IRF-2, regulators of cell growth and the interferon system. *Mol. Cell. Biol.* 13, 4531-8.

Taniguchi, T, Ogasawara, K, Takaoka, A, Tanaka, N. (2001). IRF family of transcription factors as regulators of host defense. *Annu. Rev. Immunol.* 19, 623–655.

Tsujimura, H., Tamura, T., Kong, H.J., Nishiyama, A., Ishii, K.J., Klinman, D.M., Ozato, K. (2004). Toll-like receptor 9 signaling activates NF-kappaB through IFN regulatory

factor-8/IFN consensus sequence binding protein in dendritic cells. *J. Immunol.* 172, 6820-6827.

Takaishi, K., Sasaki, T., Kotani, H., Nishioka, H., Takai, Y. (1997). Regulation of cell-cell adhesion by rac and rho small G proteins in MDCK cells*. Cell. Biol.* 139, 1047-59.

Takahasi, K., Suzuki, N.N., Horiuchi, M., Mori, M., Suhara, W. (2003). X-ray crystal structure of IRF-3 and its functional implications. *Nat. Struct. Biol.* 10, 922–927.

Thomason, H.A., Zhou, H., Kouwenhoven, E.N., Dotto, G.P., Restivo, G., Nguyen, B.C., Little, H., Dixon, M.J., van Bokhoven, H., Dixon, J. (2010) Cooperation between the transcription factors p63 and IRF6 is essential to prevent cleft palate in mice. *J. Clin. Invest.* 120, 1561–1569.

Trockenbacher, A., Suckow, V., Foerster, J., Winter, J., Krauss, S., Ropers, H.H., Schneider, R., Schweiger, S. (2001). MID1, mutated in Opitz syndrome, encodes an ubiquitin ligase that targets phosphatase 2A for degradation. *Nature.* Genet. 29, 287–294.

Vasioukhin, V., Fuchs, E. (2001). Actin dynamics and cell-cell adhesion in epithelia. *Curr. Opin. Cell. Biol.* 13, 76-84.

Yang, A., Kaghad, M., Wang, Y., Gillett, E., Fleming, M.D., Dotsch, V., Andrews, N.C., Caput, D., McKeon, F. (1998). p63, a p53 homolog at 3q27-29, encodes multiple products with transactivating, death-inducing, and dominant negative activities. *Mol. Cell.* 2, 305–316.

Yang, A., Schweitzer, R., Sun, D., Kaghad, M., Walker, N., Bronson, R.T., Tabin, C., Sharpe, A., Caput, D., Crum, C., McKeon, F. (1999). p63 is essential for regenerative proliferation in limb, craniofacial and epithelial development. *Nature.* 398, 7147–7148.

Yasue, A., Tao, H., Nohno, T., Moriyama, K., Noji, S., Ohuchi, H. (2001). Cloning and expression of the chick p63 gene. *Mech. Dev.* 100, 105-108.

Yasugi, S., Nakamura, H. (2000). Gene transfer into chicken embryos as an effective system of analysis in developmental biology. *Dev. Growth. Differ.* 42,195-7.

Yee, G.W., Abbott, U.K. (1978). Facial development in normal and mutant chick embryos. I. Scanning electron microscopy of primary palate formation. *J. Exp. Zool.* 206, 307-21.

Young, D.L., Schneider, R.A., Hu, D., Helms, J.A. (2000). Genetic and teratogenic approaches to craniofacial development. *Crit. Rev. Oral. Biol. Med*. 11, 304-317.

Wittmann, T., Waterman-Storer, C. M. (2001). Cell motility: can Rho GTPases and microtubules point the way?. *J. Cell. Sci.* 114, 3795-803.

Washbourne, B.J. and Cox, T.C. (2006). Expression profiles of cIRF6, cLHX6 and cLHX7 in the facial primordia suggest specific roles during primary palatogenesis. *BMC Developmental Biology.* 6,18.

Wedden, S.E. (1987). Epithelial-mesenchymal interactions in the development of chick facial primordia and the target of retinoid action. Development. 99, 341-51.

Webb, P.A., Perisic, O., Mendola, C.E., Backer, J.M., Williams, R.L. (1995). The crystal structure of a human nucleoside diphosphate kinase, NM23-H2. *J. Mol. Biol.* 25, 574-87.

Welten, M.C., de Haan, S.B., van den Boogert, N., Noordermeer, J.N., Lamers, G.E., Spaink, H.P., Meijer, A.H., Verbeek, F.J. (2006). Zebrafish: Fluorescent in situ hybridization protocol and 3D imaging of gene expression patterns. *Zebrafish*. 3, 465–476.

Werner S, Peters KG, Longaker MT, Fuller-Pace F, Banda MJ, Williams LT. (1992). Large induction of keratinocyte growth factor expression in the dermis during wound healing. *Proc. Natl. Acad. Sci*. 89, 6896-900.

Whiting, J. (1997). Craniofacial abnormalities induced by the ectopic expression of homeobox genes. *Mutat. Res*. 396, 97-112.

Willers J, Häffner A, Zepter K, Storz M, Urosevic M, Burg G, Dummer R. (2001). The interferon inhibiting cytokine IK is overexpressed in cutaneous T cell lymphoma derived tumor cells that fail to upregulate major histocompatibility complex class II upon interferon-gamma stimulation. *J. Invest. Dermatol.* 116, 874-9.

Willers, J., Häffner, A., Zepter, K., Storz, M., Urosevic, M., Burg, G., Dummer, R. (2001b). The interferon inhibiting cytokine IK is overexpressed in cutaneous T cell lymphoma derived tumor cells that fail to upregulate major histocompatibility complex class II upon interferon-gamma stimulation*. J. Invest. Dermatol.* 116, 874-9.

Wiater, A., Hulanicka, D., and Klopotowski, T. (1971). Structural requirements for inhibition of yeast imidazoleglycerol phosphate dehydratase by triazole and anion inhibitors. *Acta. Biochim. Pol.* 18, 289-297.

Woolworth, J.A., Nallamothu, G., Hsu, T. (2009). The Drosophila metastasis suppressor gene Nm23 homolog, awd, regulates epithelial integrity during oogenesis. *Mol. Cell. Biol*. 29, 4679-90.

Wu, P., Jiang, T.X., Suksaweang, S., Widelitz, R.B., Chuong, C.M. (2004). Molecular shaping of the beak. *Science*. 3, 1465-6.

Zhang, M., Magit, D., Botteri, F., Shi, H. Y., He, K., Li, M., Furth, P. and Sager, R. (1999). Maspin plays an important role in mammary gland development. *Dev Biol*. 215, 278–287.

Zou, Z., Anisowicz, A., Hendrix, M. J., Thor, A., Neveu, M., Sheng, S., Rafidi, K., Seftor, E. and Sager, R. (1994). Maspin, a Serpin with tumor-suppressing activity in human mammary epithelial cells. *Science*. 263, 526–529.

Zhou, B., Liu, Y., Kahn, M., Ann, D.K., Han, A., Wang, H., Nguyen, C., Flodby, P., Zhong, Q., Krishnaveni, M.S., Liebler, J.M., Minoo, P, Crandall, E.D., Borok, Z. (2012). Interactions between β-catenin and transforming growth factor-β signaling pathways mediate epithelial-mesenchymal transition and are dependent on the transcriptional co-activator cAMP-response element-binding protein (CREB)-binding protein (CBP). *J. Biol. Chem*. 287, 7026-38.

Zucchero, T.M., Cooper, M.E., Maher, B.S. et al. (2004). Interferon regulatory factor 6 (IRF6) gene variants and the risk of isolated cleft lip or palate. *N. Engl. J. Med.* 351, 769-780.

VITA

Monica was born in Ibague, Colombia on September 25th. She grew up in Ibague, and then moved to the capital city Bogota, where she earned her DDS degree at the Universidad Javeriana. Upon graduation, she worked as general dentist, after which point she decided to join the School of Dentistry at the Universidad de Antioquia as a faculty member.

Monica joined the laboratory of Dr. Timothy Cox in 2006 as a graduate student. In 2012, she earned a Doctor of Philosophy at the University of Washington in the discipline of Oral Biology.